

QATAR UNIVERSITY  
COLLEGE OF ENGINEERING  
DEVELOPMENT AND PERFORMANCE TEST OF CHOLINE CHLORIDE  
BASED NATURAL DEEP EUTECTIC SOLVENT FOR SEPARATION OF  
COLLOIDAL SUSPENSIONS

BY

DANA IZZAT ALRESHEQ

A Thesis Submitted to  
the College of Engineering  
in Partial Fulfillment of the Requirements for the Degree of  
Masters of Science in Environmental Engineering

June 2021

© 2021. Dana Al-Resheq. All Rights Reserved.

## COMMITTEE PAGE

The members of the Committee approve the Thesis of

Dana Al-Resheq defended on 13/04/2021.

---

Prof. Hazim Qiblawey

Thesis Supervisor/ Chair Committe

---

Dr. Mustafa Nasser

Thesis Co-Supervisor/ Chair Committe

---

Prof. Fares Almomani

Internal Examinar

Approved:

---

Khalid Kamal Naji, Dean, College of Engineering

## ABSTRACT

AL-RESHEQ, DANA, I., Masters : June : [2021],

Masters of Science in Environmental Engineering

Title: Development and Performance Test of Choline Chloride Based Natural Deep Eutectic Solvent for Separation of Colloidal Suspensions

Supervisor of Thesis: Hazim, Qiblawey; Mustafa S. Nasser.

Clay minerals such as bentonite are considered as a valuable raw material for a variety of industrial applications including drilling fluids for oil and gas industries, cosmetics, papermaking, paint and dyes, pharmaceutical, cement, and water treatment. As a result, large volumes of wastewater contaminated with clay minerals are generated continuously. The presence of clay minerals in water demonstrates a serious problem due to their stability and separation difficulty raising the complexity of the treatment process. Therefore, the development and enhancement of the separation processes are of great interest in the academic and industrial fields. Among the available technologies, coagulation/ flocculation is the most utilized method for the separation of colloids because of its high-performance efficiency, simplicity, and economical properties. Inorganic coagulants like aluminum sulfate and ferric chloride are commonly used destabilizing agents for colloidal particles. However, due to the high dosage requirement, low efficiency, and toxicity, their use in wastewater treatment follows strict regulations. Hence, there has been an increasing need to find more suitable, efficient, and green alternatives for the traditional coagulants.

Therefore, the main purpose of this research study was to introduce the novel application of choline chloride (ChCl) based natural deep eutectic solvents (NADESs)

as a green coagulant for highly stable colloidal particles in suspension. The influence of ChCl-based NADES on the stability of bentonite suspension in terms of its electrokinetics properties, rheological behavior, and dewaterability was investigated. Furthermore, it analyzed the effect of the constituent components as coagulants of the suspension to determine the role of each component on the destabilization process. Consequently, the influence of water on the NADES interactions and hence on its destabilization efficiency were determined. The impact of each coagulant was illustrated in the floc size, zeta potential, turbidity removal, and the settling and rheological behavior of the produced flocs. And finally, the electrokinetic properties including the floc size, zeta potential, and pH of the system were employed to determine the optimum operating conditions in terms of the coagulant dosage and the bentonite concentration.

## DEDICATION

*This work is wholeheartedly dedicated to my beloved parents Izzat Al-Risheq and Nuha Al-Hammouri, my sister Sarah, and my brothers for their continuous support and motivation in my journey of exploring myself and pursuing my dreams. I also extend my dedication to my supervisors whom their guidance made it possible to accomplish this dissertation.*

## ACKNOWLEDGMENTS

First and foremost, thanks to Allah, Almighty for giving me the strength and the ability to accomplish this research study successfully. I would like to express my sincerest gratitude to my supervisor Prof. Hazim Qiblawey and co-supervisor Dr. Mustafa Nasser for imparting their seasoned knowledge and experience, without reservation, at my dispense and to allow me to work on this exceptional research topic. Their proficient mentorship, motivation, patience, and valuable critiques helped me to complete my thesis study along with improving my academic research skills.

I would like to extend my appreciation to Prof. Ibnelwaleed Hussien and Dr. Muneer Babbaad for their valuable contribution to my research study. My work would have not been perfected without their help. Also, I would like to thank technician Dan Corts and Eng. Mohamed Shamlooh from Gas Processing Center (GPC) and technician Amal Ibrahim from Environmental Science Center (ESC) at Qatar University for their assistance and help with my experimental work and for sharing their knowledge and proficiency with me.

A special thanks goes to my grandparents, parents, siblings, other family members, and friends for their never-ending prayers and encouragement through my graduate study journey. Their magnanimous attitude and moral support made it possible for me to achieve my goals, improve myself, and be the person I am today.

## TABLE OF CONTENTS

DEDICATION .....	v
ACKNOWLEDGMENTS .....	vi
LIST OF TABLES .....	xi
LIST OF FIGURES .....	xiii
1. INTRODUCTION .....	1
1.1. Research Overview .....	1
1.2. Tangible Objectives.....	9
1.3. Research Contribution.....	11
1.4. Thesis structure .....	12
1.5. Research Outcomes (Publications).....	13
2. LITERATURE REVIEW .....	14
2.1. Clay minerals and their industrial significance .....	14
2.1.1. Bentonite .....	18
2.2. Colloidal particles stability.....	21
2.2.1. Electrical double layer and zeta potential .....	22
2.2.2. Van Der Waals interaction.....	24
2.2.3. Electrical double layer repulsion .....	24
2.2.4. Brownian motion .....	25
2.2.5. DLVO theory .....	25

2.3.	Coagulation and Flocculation.....	27
2.3.1.	Mechanisms .....	27
2.3.2.	Coagulants and Flocculants .....	31
2.3.3.	Experimental methods used to evaluate coagulation-flocculation.....	39
2.3.4.	Factors affecting the coagulation/ flocculation process.....	49
2.4.	Deep Eutectic Solvents.....	72
2.4.1.	Background.....	72
2.4.2.	Definition .....	72
2.4.3.	Natural deep eutectic solvents .....	75
2.4.4.	Applications .....	79
3.	MATERIALS AND METHODS .....	81
3.1.	Materials.....	81
3.2.	Methods.....	83
3.2.1.	Synthesis of NADES.....	83
3.2.2.	Density measurements .....	85
3.2.3.	Thermogravimetric Analysis (TGA).....	86
3.2.4.	FT-IR Spectroscopy .....	87
3.2.5.	Coagulant preparation.....	88
3.2.6.	Jar Test.....	89
3.2.7.	Zeta potential and turbidity .....	91



3.2.8.	Particle size distribution.....	92
3.2.9.	Settling Test .....	93
3.2.10.	Response surface methodology .....	94
3.2.11.	Rheological Measurements .....	97
3.2.12.	Capillary suction time (CST) .....	99
4.	RESULTS AND DISCUSSION.....	102
4.1.	Characterization of Choline Chloride Based Natural Deep Eutectic Solvents 102	
4.1.1.	Introduction.....	102
4.1.2.	Density Measurements.....	102
4.1.3.	Thermal Stability .....	103
4.1.4.	FT-IR Analysis.....	105
4.1.5.	Conclusions.....	109
4.2.	Choline Chloride Based Natural Deep Eutectic Solvent for Destabilization and Separation of Stable Colloidal Dispersions.....	111
4.2.1.	Introduction.....	111
4.2.2.	pH dependence of Zeta and Turbidity Measurements .....	111
4.2.3.	Zeta and Turbidity Results of Bentonite .....	112
4.2.4.	Floc size distribution.....	120
4.2.5.	Settling Behavior .....	125

4.2.6.	Conclusions.....	127
4.3.	Destabilization of Stable Bentonite Colloidal Suspension Using Choline Chloride Based Deep Eutectic Solvent: Optimization Study.....	129
4.3.1.	Introduction.....	129
4.3.2.	Performance analysis .....	130
4.3.3.	Statistical Analysis.....	136
4.3.4.	Conclusions.....	149
4.4.	Influence of Choline Chloride Based Natural Deep Eutectic Solvent on the Rheological Behavior of Bentonite Suspension.....	151
4.4.1.	Introduction.....	151
4.4.2.	Effect of the coagulant concentration on the destabilization degree ...	152
4.4.3.	Effect of the destabilization process on the rheological behavior of bentonite suspension.....	157
4.4.4.	Destabilization degree vs. rheological behavior of treated bentonite suspension.....	168
4.4.5.	Conclusions.....	174
5.	CONCLUSIONS AND FUTURE PROSPECTS .....	176
5.1.	Conclusions.....	176
5.2.	Future Prospects.....	180
	References.....	181

## LIST OF TABLES

Table 2.1: Rheological models for non-Newtonian fluids [1,13,161] .....	46
Table 2.2: Review of the coagulants/ flocculants efficiency for destabilization of clay minerals.....	58
Table 2.3: Review of some of the available choline chloride based NADES in the literature .....	77
Table 2.4: Applications of choline chloride based deep eutectic solvents .....	79
Table 3.1: Chemicals specifications .....	81
Table 3.2: Chemical composition of Bentonite [67].....	82
Table 3.3: Specification and synthesis conditions of the prepared NADES systems ..	84
Table 3.4: Experimental Ranges and levels of the independent variables.....	95
Table 3.5: Experimental design run order and conditions. ....	97
Table 4.1: Concentration of Coagulant Required to Achieve Turbidity $\leq 5$ NTU .....	119
Table 4.2: Coagulant Dosage with Corresponding Median Floc Diameter.....	121
Table 4.3: RSM Experimental results of the four studied responses.....	136
Table 4.4: Significance results of the studied responses.....	137
Table 4.5: Significance of the models' variables in Equations 4.1 and 4.2 for zeta potential and pH in terms of the P-value. ....	139
Table 4.6: Significance of the models' variables in Equations 4.3 and 4.4 for $D_{50}$ and $D_{90}$ in terms of the P-value.....	144
Table 4.7: Experimental confirmation of the designed models .....	149
Table 4.8: Measured parameters of the coagulated bentonite suspension .....	154
Table 4.9: Initial and equilibrium viscosities of untreated and treated bentonite suspension with NADES and ChCl-LA.....	163

Table 4.10: Elastic/ storage modulus and loss modulus for untreated and treated bentonite suspension with NADES and ChCl-LA at three different concentrations. 165

## LIST OF FIGURES

Figure 1.1: Chemical structure of cationic polyacrylamide.....	5
Figure 1.2: Schematic Binary Phase Diagram of a Eutectic System with Dual Components [43].....	7
Figure 2.1: (a) Octahedral aluminum sheet and (b) tetrahedral silicate sheet [1].....	15
Figure 2.2: Clay minerals classifications [1] .....	17
Figure 2.3: Bentonite Structure [1] .....	20
Figure 2.4: Typical size range of particulate matter [87].....	22
Figure 2.5: Electric double layer and zeta potential [67].....	24
Figure 2.6: Potential energy diagram [19] .....	26
Figure 2.7:Coagulation by Sweep Mechanism (Redrawn from [105]).....	28
Figure 2.8:Coagulation by Electrostatic Patch Mechanism (Redrawn from [107]) ....	29
Figure 2.9:Flocculation by Bridging Mechanism with high molecular weight polymer [36].....	30
Figure 2.10: Chemical structure of Chitosan [127] .....	34
Figure 2.11: Chemical structure of PolyDADMAC .....	35
Figure 2.12: Illustration of sediment bed formed from (a) small particles and (b) aggregated particles [149].....	44
Figure 2.13: Effect of initial pH values on the stability of bentonite suspension [17]	57
Figure 2.14: Similarities and differences between ionic liquids and deep eutectic solvents [195].....	73
Figure 2.15: chemical structure of typical halide salts (hydrogen bond acceptor)and hydrogen bond donors for the synthesis of DES [38].....	74
Figure 2.16: Molecular structure of choline chloride: lactic acid NADES with a molar	

ratio of 1:1 .....	76
Figure 3.1: Heidolph rotatory evaporator .....	84
Figure 3.2: Anton Par densitometer .....	85
Figure 3.3: Thermogravimetric analysis instrument .....	86
Figure 3.4: NICOLET iS10 Thermo Scientific FTIR spectrometer. ....	87
Figure 3.5: Thermo Scientific Finnpipette F2.....	88
Figure 3.6: Stuart jar test apparatus .....	89
Figure 3.7: The coagulation test steps of (a) NADES, ChCl, and LA and (b) ChCl-LA mixture coagulants. ....	90
Figure 3.8: HACH 2100 Turbidimeter.....	91
Figure 3.9: (a) Malvern Instruments Ltd. Zetasizer ZEN3600 (b) measuring cell .....	92
Figure 3.10: Malvern Instruments Ltd. Mastersizer 2000 .....	93
Figure 3.11: Setup for the settling test .....	94
Figure 3.12: (a) Anton Par rheometer model MCR 302 and (b) cup and bob measuring geometry. ....	99
Figure 3.13: (a) Triton 319 Multi-purpose CST (Triton Electronics Limited, UK) and (b) schematic diagram of the CST apparatus [149]. ....	101
Figure 4.1: Density profile of ChCl:LA, ChCl:MA, and ChCl:CA NADES systems. .....	103
Figure 4.2: weight loss curve of ChCl:LA, ChCl:MA, and ChCl:CA NADES systems .....	104
Figure 4.3: FT-IR spectrums for (a) ChCl, (b) LA, (c) ChCl:LA .....	106
Figure 4.4: FT-IR spectrums for (a) ChCl, (b) MA, (c) ChCl:MA.....	108
Figure 4.5: FT-IR spectrums for (a) ChCl, (b) CA, (c) ChCl:CA .....	109

Figure 4.6: Effect of pH on the turbidity and zeta potential of bentonite suspension. .....	112
Figure 4.7: Turbidity and Zeta Potential of Bentonite Suspension as a function of (a) ChCl, (b) ChCl-LA, (c) ChCl:LA NADES, and (d) LA concentrations.....	114
Figure 4.8: Chemical Structure of (a) Choline Chloride and (b) Cationic Polyacrylamide [67].....	116
Figure 4.9: Flocculation through bridging mechanism using cationic polymer (PAM) .....	117
Figure 4.10: Coagulation through electrostatic patch mechanism using ChCl based NADES .....	118
Figure 4.11: Turbidity of Bentonite suspension as a function of concentration for all tested coagulants .....	120
Figure 4.12: Floc size of bentonite suspension treated with ChCl, ChCl-LA, and NADES at different concentrations .....	123
Figure 4.13: Floc size distribution of bentonite suspension treated with 3 coagulants at a concentration of $6.76 \times 10^{-2} \text{ M}$ .....	124
Figure 4.14: Floc size distribution of bentonite suspension treated with NADES at different concentrations. ....	125
Figure 4.15: Settling Behavior of Bentonite Suspension Treated with 3 coagulants at (a) $3.48 \times 10^{-2} \text{ M}$ and (b) $6.76 \times 10^{-2} \text{ M}$ . The onsets display a closer look for the first 5 minutes. ....	127
Figure 4.16: Turbidity as a function of the concentration for bentonite suspension treated with ChCl:LA, ChCl:MA, and ChCl:CA.....	132
Figure 4.17: Zeta potential as a function of the concentration for bentonite suspension	

treated with ChCl:LA, ChCl:MA, and ChCl:CA.....	133
Figure 4.18: Floc size of treated suspensions using ChCl:LA, ChCl:MA, and ChCl:CA at concentrations of $3.48 \times 10^{-2} M$ and $6.76 \times 10^{-2} M$ .....	135
Figure 4.19: Surface graph of the (a) zeta potential and (b) pH as a function of the ChCl:LA dosage ( $x_1$ ) and the bentonite concentration ( $x_2$ ).....	141
Figure 4.20: Graphical verification of the regression models for zeta potential (a) and pH (b).....	142
Figure 4.21: Surface graph of the floc size (a) $D_{50}$ and (b) $D_{90}$ as a function of the ChCl:LA dosage ( $x_1$ ) and the bentonite concentration ( $x_2$ ).....	145
Figure 4.22: Graphical verification of the regression models for the floc size (a) $D_{50}$ and (b) $D_{90}$ .....	146
Figure 4.23: Overlaid contour plot of the optimal region.....	148
Figure 4.24: Turbidity and Zeta Potential of Bentonite Suspension as a function of the coagulant type and concentrations (a) NADES, and (b) ChCl-LA.....	153
Figure 4.25: Particle size distribution for treated bentonite suspension with NADES at three different concentrations.....	155
Figure 4.26: Particle size distribution for bentonite suspension treated with NADES or ChCl-LA at different concentrations.....	156
Figure 4.27: Variation in viscosity with shear rate for bentonite suspension treated with NADES and ChCl-LA at different concentrations.....	159
Figure 4.28: Bingham and Casson parameters for viscoelastic behavior in treated bentonite suspension.....	160
Figure 4.29: Variation in viscosity with time for bentonite suspension treated with NADES or ChCl-LA at a constant shear rate of (a) $1 \text{ s}^{-1}$ at different concentrations and	



(b) $10 \text{ s}^{-1}$ for at $6.76 \times 10^2 \text{ M}$ . .....	162
Figure 4.30: (a) Elastic modulus and (b) viscous modulus for treated bentonite suspension with NADES and ChCl-LA at three different concentrations.....	167
Figure 4.31: (a) Elastic modulus, (b) Bingham yield stress, and (c) viscosity of treated bentonite suspension as a function of zeta potential at different concentrations.....	170
Figure 4.32: (a) Elastic modulus, (b) Bingham yield stress, and (c) viscosity of treated bentonite suspension as a function of $D_{50}$ at different concentrations.....	172
Figure 4.33: (a) Elastic modulus, (b) Bingham yield stress, and (c) viscosity of treated bentonite suspension as a function of CST at different concentrations. ....	174

# 1. INTRODUCTION

## 1.1. Research Overview

Clay minerals are phyllosilicate minerals composed of very fine particles with a median diameter  $\leq 2\mu m$  and a layered structure [1]. Clay minerals occur naturally through low-temperature hydrothermal processes on aluminosilicates [2]. They can be found in nature in most soil, marine sediments, oceans, and argillaceous rocks like mudstones, siltstones, and argillites. According to their composition and structure, clay minerals can be classified into different categories including kaolinite, smectites, and micas. Clay minerals such as bentonite and kaolinite have attracted the attention of several industries, especially in the engineering field due to their desirable physical and chemical properties. These properties include their cation exchange capacity, large surface area to mass ratio, surface charge, sorption ability, viscosity, thixotropy, dispersibility, and plasticity [3]. Moreover, they are considered as budget friendly and abundant industrial materials. Wastewater treatment, drilling fluids, constructions, soil treatment, and landfill applications are some of the engineering industries that involve clay minerals in their processes [4–8]. Furthermore, they have been adopted in other industrial fields such as paper making, and pharmaceutical industries in addition to the synthesis and fabrication of nanomaterial [9–12].

Bentonite is a smectite clay mineral known as hydrated aluminum silicate with the chemical formula of  $(Na)_{0.7} (Al_{3.3} Mg_{0.7}) Si_8O_{20}(OH)_4.nH_2O$ . The formation of bentonite can occur naturally as a result of the hydrolysis of volcanic ash and tuff under elevated temperature. Bentonite is composed of montmorillonite in addition to illite, quartz, pyrite, and other minerals [13]. The mineralogical properties of bentonite may vary according to its type and composition, making it suitable for a variety of applications [14]. Bentonite is characterized by having a negative net charge and hence,

a negative zeta potential due to the isomorphic substitution between aluminum ions with magnesium and iron ions ( $Mg^{+2}$  and  $Fe^{+2}$ ) in addition to the substitution between silicon ions with  $Al^{+3}$  that occurs in the octahedral and tetrahedral layers, respectively [15]. Furthermore, bentonite has very fine platelet-like particles with a very small median diameter ( $D_{50}$ ) resulting in a very large surface area. Therefore, when dispersed in water, bentonite forms a highly stable colloidal suspension with the help of Brownian motion as a result of two factors: the negative zeta potential ( $\zeta < -35mV$ ) and the particle size ( $D_{50} < 5\mu m$ ) [16].

Bentonite particles comprise surfaces and edges, the surfaces possess a permanent negative charge while the charge of the edges relies on the pH of the surrounding. Therefore, the structure and the degree of flocculation of bentonite suspension strongly depend on the pH of the environment [17]. In aqueous media, colloidal particles develop an electrical double layer (EDL) around the particle's surface. The EDL consists of two chief layers: the stern and the diffused layer [18,19]. The difference in the electrical potential between the inner stern layer and the outer diffused layer is known as the zeta potential ( $\zeta$  – potential).  $\zeta$  – potential is an essential parameter in investigating the colloidal stability as it provides an indication on the magnitude of the repulsive forces between the particles. A highly positive or a highly negative zeta potential ( $\zeta < -30 mV$  or  $\zeta > +30 mV$ ) implies greater repulsive between the colloidal particles and hence, more stable suspension [15]. As the  $\zeta$  – potential values approach zero, the repulsive forces decrease reducing the stability of the system. When in water, bentonite particles develop a net negative charge resulting in highly negative zeta potential. As a result, a highly stable suspension with treatment difficulties due to the micro-sized particles with repulsive forces between them hindering their ability to settle is formed [20].

Bentonite has outstanding properties including its non-toxicity, high ion exchange capacity, swelling ability, and large surface area promoting high adsorption capacity [21]. Furthermore, it may be utilized directly in its natural form or it may be treated prior to using it with heating, ion exchange, and acid or soda activation [22]. The composition and desirable properties of bentonite clay minerals resulted in its popularity as a raw material in the industrial sector for a wide variety of applications. The commercial significance of bentonite and other types of clay in the industrial sector led to the generation of wastewater containing a large amount of very fine colloidal clay particles. As a result, highly persistent and stable colloidal suspensions are formed that require the implementation of treatment methods for the destabilization, aggregation, and separation of the colloidal particles from water [9]. The treatment processes of this type of wastewater is a challenging task due to the contaminants separation difficulties in addition to their high expenses and environmental problems. Furthermore, the techniques applied for solid-liquid treatment processes lead to the formation of sludge in large quantities with handling and dewatering problems [23]. Nevertheless, direct discharge of stable colloidal suspension into water bodies is prohibited as it causes a significant increase in turbidity resulting in severe problems for aquatic life. Thus, it is of great importance to properly treat the produced wastewater prior to discharging it into water bodies [9,24].

Treatment of colloidal suspensions requires the implementation of physical or chemical solid-liquid separation methods. Several technologies are available for the treatment of colloidal wastewater such as electrocoagulation, membranes filtration, electro-osmosis, and thermo-mechanical dewatering [25–28]. However, these techniques are energy-intensive and of a high cost [29]. Coagulation-flocculation is among the most used processes for the treatment of water and wastewater, especially

for the removal of suspended colloidal particles as they are highly efficient, economical, and have low cost and energy requirements [1,30,31]. Reduction of the particles' net negative charge and promoting van der Waals attractive forces between them is the key principle in the coagulation and flocculation processes [1]. Coagulation mainly aims for the destabilization of the colloidal particle and the formation of micro-aggregates. On the other hand, during the flocculation process, further aggregation of the particles is exhibited to promote the formation of larger and stiffer flocs [1]. Consequently, the formed aggregates will settle by gravity leading to a relatively clear supernatant. Different types of chemicals were used as destabilizing agents for coagulation and flocculation of colloidal suspension including metal salts and polyelectrolytes, respectively [32]. Aluminum sulfate and ferric and aluminum chlorides are common coagulants used in the industry as they are of low cost and easy to use [30]. However, due to their low removal efficiency and environmental and health concerns represented in the presence of residual metal in the supernatant and formation of toxic sediment, coagulants are not popular. In addition, difficulties in handling it due to the low shear resistivity of the formed aggregates. All mentioned factors raised public concerns and limited their use for water treatment [29,30]. Therefore, there is a continuous search for an environmental friendly and economical alternative coagulants.

In recent years, the use of polyelectrolytes as a flocculant has become a common practice due to their efficiency in treating colloidal suspension through bridging mechanism [1]. Polyelectrolyte such as polyacrylamide (PAM) has been widely used for the separation of colloidal particles from industrial wastewater [20,33–35]. Flocculation of fine colloidal particles using polyelectrolytes such as polyacrylamide (PAM) may occur through different mechanisms such as polymer adsorption and bridging, charge neutralization, particle- surface complex formation and depletion

flocculation, or by a combination of these mechanisms [36]. Cationic polyacrylamide (CPAM) as a flocculant has been widely used for the destabilization and separation of stable colloidal suspension. The destabilization process using CPAM (Figure 1.1) occurs through the adsorption of the cationic polymer chains via hydrogen bonding interactions between the particle surface and polymer's primary amide functional groups. Thus, charge neutralization becomes a major mechanism, where CPAM will locally reverse the particle surface charge [1]. The chief characteristic of CPAM responsible for its function as a destabilizing agent defined in the presence of the quaternary ammonium salt carrying a positive charge is also observed in choline chloride ( $C_5H_{13}OHCl^-N^+$ ). Choline chloride (ChCl) is among the main components utilized as a hydrogen bond acceptors (HBA) in the synthesis of the green solvents known as deep eutectic solvents [37,38].

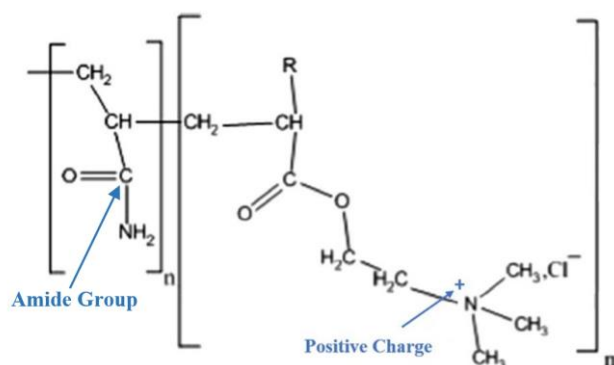


Figure 1.1: Chemical structure of cationic polyacrylamide

Deep eutectic solvents (DES) were reported for the first time in 2003 by Abbot et. al. [39] as a possible alternative for ionic liquids (IL). DESs are described as a

combination of two components at least are mixed under controlled conditions of temperature and rotational speed and a specified molar ratio leading to the formation of a eutectic mixture. Commonly, the constituent components forming a DES are defined as hydrogen bond donor (HBD) and acceptor (HBA). Hence, they associate together through the formation of intermolecular hydrogen bonds [37,40]. The term “deep” in DES comes from the deep depression exhibited in the melting point of solvent compared to its elemental components leading to the formation of a liquid mixture at room temperature [38,41,42]. DES has a very simple preparation technique that depends on continuously heating the components at moderate temperatures coupled with vigorous mixing until a clear homogenous liquid is formed.

A binary eutectic system is defined as a mixture of two components that inhibit the crystallization process of each other at certain molar ratios. As a result, the formed system exhibit a melting point lower than either of its components. The formation of a eutectic system occurs when both constituent components are completely miscible in each other in the liquid phase while immiscible in the solid phase. The phased diagram of a binary eutectic system formed from X and Y is illustrated in Figure 1.2. Lines AB and BC demonstrate the temperatures after which the homogeneous mixture of X and Y starts to solidify. The region above these lines is defined as the liquidus region where the system is liquid at any composition. In contrast, line DBE represents the temperatures at which the system begins to melt and the system is completely crystalline at the solidus region below this line. In regions ABD and CBE, the mixture comprises of two phases: a liquid mixture of X and Y with solid Y and a liquid mixture of X and Y with solid X, respectively. Point B where lines AB, BC, and DBE meet is identified as the eutectic point indicating the temperature and composition at which a eutectic mixture is formed [43].

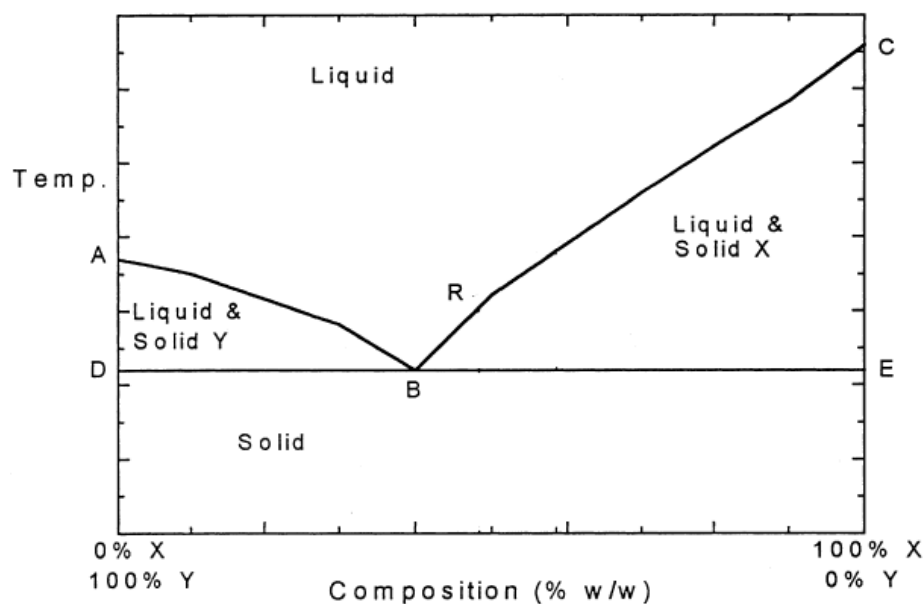


Figure 1.2: Schematic Binary Phase Diagram of a Eutectic System with Dual Components [43]

When DES is formed from natural components mainly primary metabolites such as organic acids, sugars, amino acids, choline salts, and alcohols the resultant DES is defined as natural deep eutectic solvents (NADES) [44]. NADESs have favorable characteristics, as they are stable chemically and thermally, non-toxic, environmental friendly, biodegradable, biocompatible, and composed from widely and naturally abundant components. Additionally, the synthesis process of such solvents is very simple, time-efficient, and economical making them a potential green alternative for some industrial solvents [45,46]. NADESs are distinguished for possessing tunable properties through the manipulation of their composition by varying the molar ratio and water content. Consequently, they become suitable industrial solvents for a wide variety of applications such as gas absorption ( $\text{CO}_2$  and  $\text{SO}_2$ ), lead removal, fuel purification, and nanoparticle fabrication [41,47–52]. Furthermore, DESs can be used in the removal of metal oxides and heavy metals in addition to the preparation, production, and



purification of biodiesel [53–57].

## 1.2. Tangible Objectives

The study aims to achieve the following objectives:

- i. Investigate the destabilization and separation degree of bentonite colloidal suspension using choline chloride (ChCl) based natural deep eutectic solvents (NADES). This objective can be achieved through analysis of the electrokinetic properties, floc size, and settling behavior.
- ii. Determine the impact of water on the NADES efficiency as a coagulant considering the interaction between the hydrogen bond donor and hydrogen bond acceptor. This can be executed by investigating the coagulation efficiency of the constituent components (i.e., HBD and HDA) in addition to a mixture of two components and compare it with the efficiency of the synthesized NADES.
- iii. Examine the role of varying the coagulant' concentration in the suspension on the destabilization and separation processes.
- iv. Test the effect of ChCl based NADES with different hydrogen bond donors including lactic acid, malic acid, and citric acid on the destabilization degree of bentonite suspension.
- v. Investigate the influence of the bentonite concentration and the coagulant dosage on the coagulation degree of the suspension. Furthermore, find the optimum operating conditions under which the treatment efficiency is maximized using response surface methodology (RSM).
- vi. Evaluate the effect of the best performed NADES studies in part iv (ChCl:LA) on the rheological behavior of bentonite suspension. This can be accomplished by conducting a flow and viscoelastic behavior analysis. Moreover, determine the performance of NADES in comparison with the rheological behavior of suspensions treated with ChCl-LA mixture.

- vii. Investigate the influence of NADES and ChCl-LA on the destabilization degree with respect to the rheological behavior of bentonite suspension.

### **1.3. Research Contribution**

Over the past decade, natural deep eutectic solvents (NADESs) have emerged as an environmental friendly and economical solvent with a wide variety of potential applications. In the literature, a large number of research papers studying the use of NADES for different applications including gas adsorption, extraction processes, and fuel purification [49,51,58]. Similarly, numerous studies are focusing on the destabilization and separation processes of colloidal clay particles using traditional coagulants/ flocculants such as metal salts and polyelectrolyte are available in the literature. Such studies mainly highlight the effect of the utilized coagulant/ flocculant on the colloidal suspension in terms of its electrokinetics and rheological behavior [1,59]. However, and to the best of our knowledge, the application of choline chloride (ChCl) based natural deep eutectic solvent as a destabilizing agent for clay suspension has never been investigated before. Therefore, this thesis provides a comprehensive overview of the destabilization process of clay minerals in wastewater in terms of the mechanisms, the available agents, and the factors affecting the process. It also highlights the key experimental parameters in the destabilization processes including zeta potential, turbidity measurements, floc size distribution, and rheological measurements represented in the flow and viscoelastic behaviors.

The current research study investigates for the first time the use of ChCl based NADES as a destabilizing agent for highly stable bentonite suspension. Consequently, it delivers a comprehensive analysis of the influence of ChCl based NADES on electrokinetic properties and rheological behavior of bentonite suspensions. The analysis is conducted through zeta potential and turbidity measurements, floc size, settling behavior, viscosity measurements, and viscous and elastic behaviors of the treated suspensions. Furthermore, it aims to provide the optimum operating conditions

for the process that achieves the desired outcomes.

#### **1.4. Thesis structure**

The structure of the following thesis concerning the influence of choline chloride based natural deep eutectic solvents on the electrokinetic and rheological behavior of bentonite dispersion starts with a comprehensive overview of the main concepts of NADES and the destabilizing process in chapter 2. The chapter focuses on demonstrating the principles of the colloidal systems and the coagulation/ flocculation process represented in the mechanisms, coagulants/ flocculants types, the factors influencing the process, and the experimental methods employed to evaluate its efficiency. Furthermore, a review of some of the available coagulation/flocculation studies in the literature is provided describing the utilized methods to conduct the research study and the obtained outcomes. Additionally, an explanation of the deep eutectic systems, their types, properties, and most common applications is included. Most importantly, the chapter shed light on the existing gap in the application of DES generally and NADES specifically in the wastewater treatment field.

Following that, chapter 3 provides the required materials and apparatus to perform the experimental study. In addition, it describes in detail the followed methodology to achieve the targeted objectives stated in section 1.2.

In chapter 4, the results of the conducted experimental analysis are demonstrated in four sections. Section 4.1 displays the characterization results of the three choline chloride (ChCl) based natural deep eutectic solvents (NADES) in terms of thermogravimetric and FT-IR analysis and density measurements. In Sections 4.1 to 4.4, the influence of ChCl based NADES on the electrokinetic properties of bentonite suspensions, optimization study through response surface methodology of the destabilization process, and the rheological behavior of treated bentonite suspension

with ChCl based NADES are presented, respectively.

Lastly, chapter 5 delivers a comprehensive conclusion of all the obtained results and outcomes from the conducted research study. Moreover, it proposes additional prospect work to further enhance and develop the research topic.

### **1.5. Research Outcomes (Publications)**

- i. **Al-Risheq, Dana I.**, Nasser, M.S, Qiblawey, Hazim, A. Hussein, Ibnelwaleed, Benamor Abdelbaki (2020) ‘Destabilization and Separation of High Stable Colloids’ USA Patent office, **Filled, US 16/883,484**
- ii. **D.I.M. Al-Risheq**, M.S. Nasser, H. Qiblawey, A. Benamor, I.A. Hussein, Destabilization and Separation of High Stable Colloidal Dispersions Using Choline Chloride Based Natural Deep Eutectic Solvent, Sep. Purif. Technol. 255 (2021).  
(Separation and Purification Technology, IF: 5.774)
- iii. **D.I.M. Al-Risheq**, M.S. Nasser, H. Qiblawey, M.M. Ba-abbad, A. Benamor, I.A. Hussein, Destabilization of stable bentonite colloidal suspension using choline chloride based deep eutectic solvent: Optimization study, J. Water Process Eng. 40 (2021) 101885.  
(Journal of Water Process Engineering, IF: 3.465)
- iv. **D.I.M. Al-Risheq**, M.S. Nasser, H. Qiblawey, I.A. Hussein, A. Benamor, Influence of choline chloride based natural deep eutectic solvent on the separation and rheological behavior of stable bentonite suspension, Sep. Purif. Technol. 270 (2021) 118799.  
(Separation and Purification Technology, IF: 5.774)

## 2. LITERATURE REVIEW

### 2.1. Clay minerals and their industrial significance

Clay minerals can be found in nature in most soil, marine sediments, and argillaceous rocks. They are naturally synthesized through low-temperature hydrothermal processes and weathering of aluminosilicates [2]. Furthermore, they can be synthesized in laboratories under a controlled environment for analysis of their structures and properties and industrial application [60]. Clay minerals are a member of the phyllosilicate minerals. They are composed of fine particles with layered structure. The layers are made up of octahedral aluminum (O) sheet with one or two tetrahedral silica (T) sheets. Each particle consists of numerous numbers of stacked layers of T and O sheets. T sheets shown in **Error! Reference source not found.a** are comprised of units made up of four oxygen atoms with silicon atom at the center ( $SiO_4$ ). On the other hand, units in the O sheets illustrated in **Error! Reference source not found.b** possess a composition of  $Al_2O_6$  with six oxygen atoms in an octahedral arrangement surround a central atom of aluminum [2,61]. *Al* atoms occupy only two-third of the available positions in the unit. Therefore, it may be replaced by magnesium (*Mg*) or iron (*Fe*) atoms may replace it due isomorphic substitutions occupying all available positions [1]. Layers of clay minerals may have three sheets TOT (2:1) or two sheets TO (1:1) arrangements: one octahedral sheet bonded with two tetrahedral sheets or one tetrahedral and one octahedral sheet, respectively.

The particles of clay minerals usually comprise three different surfaces identified as inner surface, outer surface, and edges. Cations in the inner and outer surface on the particle are susceptible to isomorphous substitution which is the primary source of the surface net negative or positive charge. A negative charge is gained from the substitution between higher valence and lower valence cation. For example,

replacement of the silicon ion ( $Si^{4+}$ ) in the tetrahedral sheet with the aluminum ion ( $Al^{3+}$ ). Consequently, the substitution from lower valence (i.e.  $Fe^{2+}$ ) to higher valence cations (i.e.  $Fe^{3+}$ ) leads to gaining a positive charge [62]. The surface net charge of clay particles relies on balancing the total electrons gained or lost in the substitution process. However, most of the isomorphous substitution processes in clay minerals yield a net negative charge. Alteration of cations between the particle's layers can occur through ion exchange and adsorption.

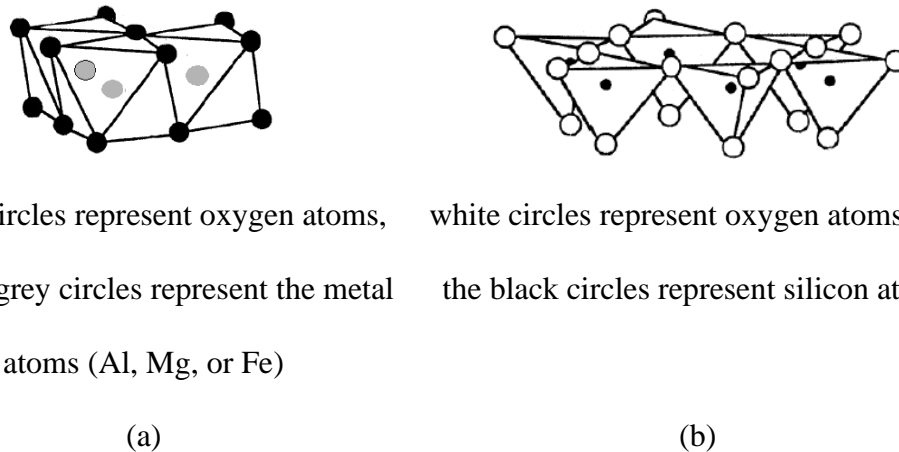


Figure 2.1: (a) Octahedral aluminum sheet and (b) tetrahedral silicate sheet [1]

Depending on the number of tetrahedral and octahedral sheets, presence of exchangeable ions, type of metal ions in the octahedral sheets (Al, Mg, or Fe), crystalline structure, and presence of interlayer water molecules; clay minerals are classified into seven different phyllosilicate groups as shown in **Error! Reference source not found.** [1,63]. Clay minerals impart unique physical, surface, and rheological properties making them of great interest for a wide variety of industries. Surface properties include surface area and charge, cation exchange capacity (CEC), sorption,



and dispersibility. Rheological properties such as viscosity, plasticity, and time dependence (thixotropy). Physical properties as the particles' shape and size, color, opacity, and reflectance [3]. While clay minerals may differ in their surface and rheological properties. However, their physical characteristics especially the shape and size are very similar. Therefore, several techniques can be utilized to distinguish between their different types including infrared spectroscopy (IR), scanning electron microscopy (SEM), differential thermal analysis, X-ray Fluorescence (XRF), and X-ray diffraction (XRD) [64].

Due to their very fine, micro-size particles and high surface area, clay minerals form highly stable colloidal suspensions when found in aqueous media. Their stability in suspension is dependent on several structural and external factors including clay mineral type, surface and edge charges, cation exchange capacity (CEC), pH and salinity of the suspension, and type and concentration of the utilized surfactant [64]. Ion exchange capacity is one of the most fundamental characteristics of clay minerals. It is defined as the amount of cations or anions replacing others on the clay particles' surface expressed in meq/100g of dry clay [61]. Ion exchange occurs due to the clay's tendency to absorb some of the ions (i.e. cation or anions) available in the surrounding media and their ability to retain them. Ion exchange happens in the interlayer space of clay particles without affecting the structure of the silica-alumina sheets. In addition, it may take place on the particles' edges or surface. the capacity or the reactivity of the particle's surface is a function of the available exchangeable ions, ionic sites, surface area, and the surface and edges charge [1,64,65]. Therefore, the determination of the ion exchange capacity for any clay mineral should be done under neutral conditions ( $pH = 7$ ) as acid or alkaline environment alternate the net charge on the surface and edges [61].

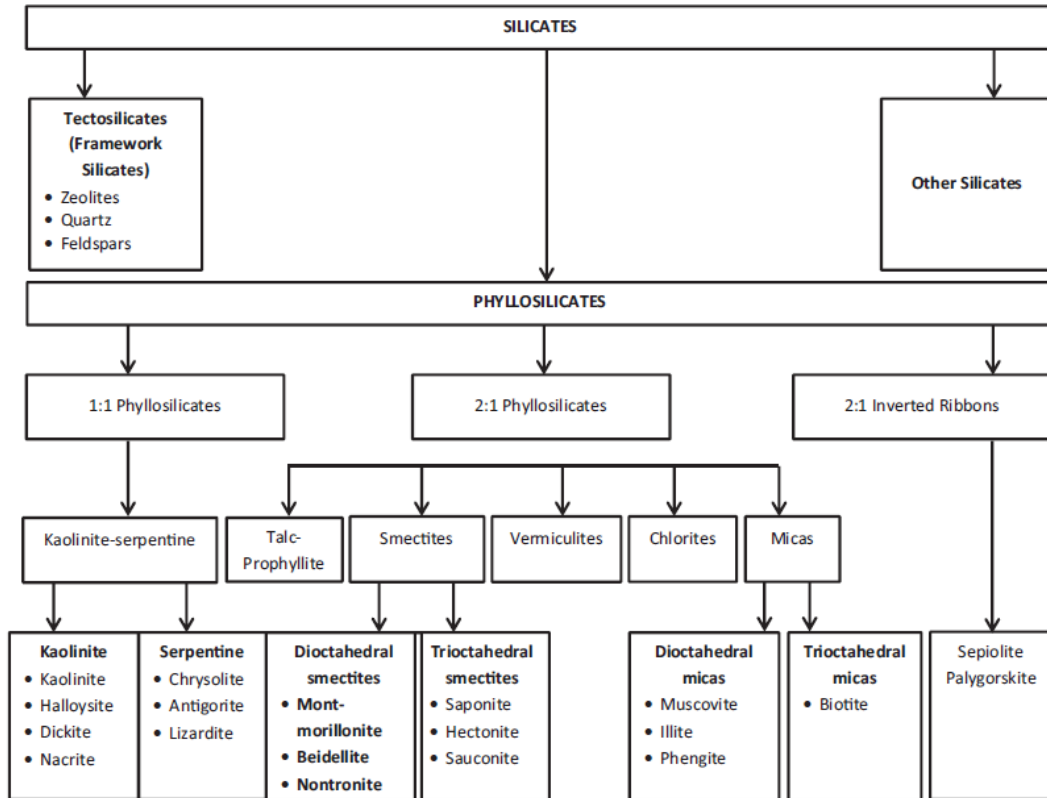


Figure 2.2: Clay minerals classifications [1]

Another important feature of some clay minerals such as smectite is their swelling ability. Swelling is known as the adsorption of solvent molecules usually water resulting in the expansion on the interlayer space until it reaches a maximum limit known as the maximum equilibrium separation [66]. Generally, it occurs due to the presence of stronger attractive forces between the adsorbing molecules and the exchangeable ions than the forces between exchangeable ions and the surface net charge [61]. The particle size of the clays increases as a result of swelling leading to an increase in the volume as well. Furthermore, particles swelling play an important role in determining the rheological behavior of the suspension as it significantly increases its viscosity [67]. The particles size and shape, their charge density, and the exchangeable ions charge are all factors that influence the swelling ability. In addition,

the salinity of the aqueous media has a significant effect on the swelling behavior of the clay. Higher salt concentration in the system reduces the swelling ability of the clay [68].

### 2.1.1. Bentonite

Bentonite is an aluminum phyllosilicate clay mineral classified among smectite clay group with a composition of  $(Na_{0.7})(Al_{3.3}Mg_{0.7})Si_8O_{20}(OH)_4.H_2O$ . It is composed mainly of montmorillonite (80 – 90 wt%) with the remaining as a mixture of impurities, the most common includes biotite, kaolinite, calcite, nontronite, and feldspar [69,70]. Generally, bentonite is naturally formed from weathering and alteration of volcanic ashes under the presence of water. As illustrated in Figure 2.3, bentonite has 2:1 structure with one octahedral aluminum sheet surrounded by two tetrahedral silica sheets [22]. The negative net charge possessed by bentonite particles arises from the isomorphic substitution of the aluminum ion ( $Al^{3+}$ ) in the octahedral sheet with other metal ions such as iron ( $Fe^{2+}$ ), magnesium ( $Mg^{2+}$ ). Furthermore, isomorphic substitution taking place in the tetrahedral sheet (i.e.  $Si^{4+}$  with  $Al^{3+}$ ) influence the charge of the particles. The surface net negative charge resulted from the isomorphic substitution can be balanced by exchangeable cations such as sodium ( $Na^+$ ), calcium ( $Ca^{2+}$ ), and potassium ( $K^+$ ) [22,65,69,71].

Bentonite possesses special physical and chemical properties making it one of the most valuable raw material for a wide range of industrial applications. It is characterized by its crystalline structure, porosity, particles' shape and size, high surface area in a range of 760 – 810  $m^2/g$ , plasticity, high swelling ability, thixotropy, and high cation exchange capacity (80 – 150  $meq/100g$ ) [72–74]. The properties of bentonite may vary depending on its origin, composition, impurities and organic content, surface area, type and amount of the exchangeable ions, and the chemical substitution degree [3,69].

The nature of the industrial application of bentonite relies greatly on its composition and exchangeable cations. Commercially, Ca-bentonite and Na-bentonite are the most common grades utilized in the industrial field. The main difference between the two grades is their swelling behavior as the latter shows considerably higher swelling abilities [3]. According to the industrial application need, bentonite may be used naturally or may be treated by ion exchange, acid or soda activation, or thermally treated before usage [22]. Bentonite is extensively used as a filler in the papermaking industry to enhance the quality of the produced paper [75,76]. Furthermore, due to its high swelling capacity and dispersivity, bentonite is commonly utilized as an agent for water-base drilling fluids in the oil and gas industry to enhance their rheological characteristics [77]. In the pharmaceutical industry, bentonite is used to enhance the entrapment and sustained-release of the drugs. In addition, it is utilized in hydrophobic drugs to enhance their dissolution rate and bioavailability [78]. Bentonite has versatile applications in the food industry, paint and dyes, cosmetics, construction, agriculture applications, and in wastewater treatment for the removal of organic matter and nutrients and sludge dewatering [4,5,80,81,6–12,79]. Moreover, it can be used for the production of nanocomposites, and in catalyst synthesis [5,78,82].

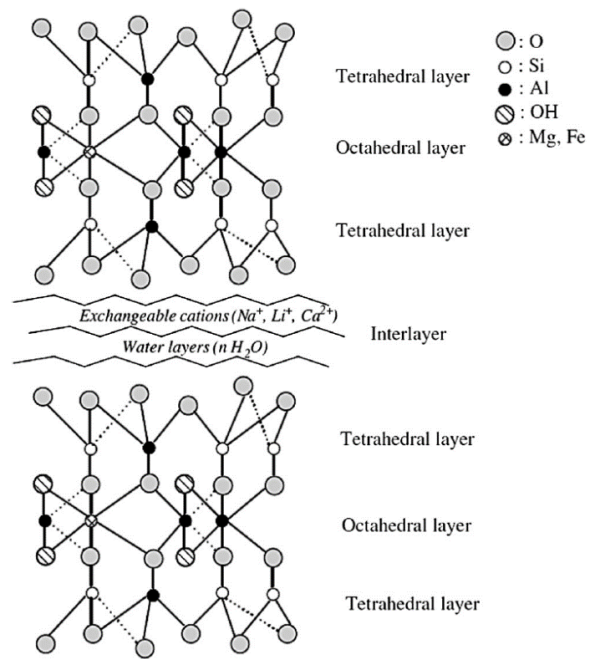


Figure 2.3: Bentonite Structure [1]

## 2.2. Colloidal particles stability

Contaminates in wastewater can be classified into three main categories: suspended solids such as sand and gravel, dissolved solids which include organic and inorganic compounds (calcium, magnesium, and bicarbonate), and colloidal particles such as clays [83]. As illustrated in Figure 2.4, colloids are very fine particles with a median diameter varying between  $10^{-9} m$  and  $10^{-6} m$ . Typically, colloids are large compared to molecules and atom, however, they are still not visible to the naked eye. As a consequence of their micrometric nature, they exhibit extremely large surface area compared to its mass giving a very small mass to surface area ratio. Thus, gravitational forces are negligible while surface phenomena predominant [84].

Colloids are widely available in nature and are utilized in many engineering processes. They gain their stability as a result of the repulsion forces between the similarly charged surfaces. Therefore, the stability can be assessed by evaluating the dominant interaction forces between the particles in a system. If repulsion forces are dominant, the system is highly stable, and the particles will remain in suspension for a long time. On the other hand, if attractive forces are dominant, then the system is destabilized, and aggregation will occur. Colloids can be classified according to the dispersion medium and the dispersion phase to emulsions (liquid-liquid), dispersions (liquid-solid), foams (liquid-gas), gels (solid-liquid), and aerosols (gas-liquid/ solid) [85,86]. When placed in water, colloids develop a negative surface charge forming a very stable suspension which is attributed to the domination of repulsion forces between the particles [87]. Counter ions available in water will be attracted to the colloidal particles neutralizing the surface charge and resulting in the formation of an electrical double layer [84].

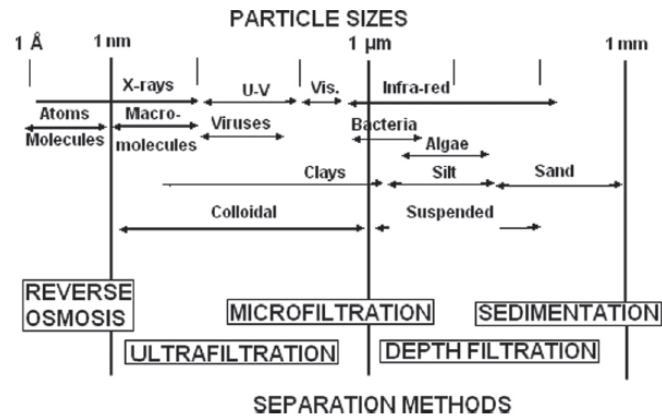


Figure 2.4: Typical size range of particulate matter [87]

### 2.2.1. Electrical double layer and zeta potential

The development of an electrical double layer may occur as a result of ionization, ion dissolution, and ion adsorption [1]. The electrical double layer shown in Figure 2.5 consists of two chief layers: the inner stern layer and the outer diffused layer. The Stern layer represents the inner rigid region, and it can be divided into two subregions: the inner Helmholtz plane (IHP) and outer Helmholtz plane (OHP). IHP contains only counter ions tightly packed on the surface of the colloidal particle, while OHP comprises both co and counter ions. The rigidity and high ion density in the Stern lead to a movement restriction and high electrical potential [1]. On the other hand, ions in the outer diffused layer are dispersed and free to move due to the diffusion forces. The slipping plan or also known as the shear surface is the interaction surface between the stagnant medium in the Stern layer and the mobile medium in the diffused layer

The maximum potential, which is known as the Nernst potential is exhibited at the surface of the colloidal particle. The potential decreases across the Stern layer as a result of the presence of counter ions until it reaches the slipping plan where it is known as the zeta potential [87]. Zeta potential ( $\zeta$  – *potential*) is defined as the potential

difference between the inner Stern layer and the outer diffused layer. It is considered as the main reason for colloidal stability as its magnitude indicates the interaction forces between the particles [88]. The high magnitude of zeta potential indicates the presence of repulsion forces between the particles, the higher the potential the greater the repulsion. Highly positive ( $\geq +30 \text{ mV}$ ) or highly negative ( $\leq -30 \text{ mV}$ ) zeta potential values interpret a more stable colloidal suspension. Reducing the stability of the suspension can be achieved by the addition of a destabilizing agent known as a coagulant or a flocculant through which the zeta potential will decrease due to the reduction in similar repulsive surface charge. Moving away from the slipping plan, both the ion concentration and the potential decrease gradually until the potential reaches electrical neutrality in the surrounding media [89].



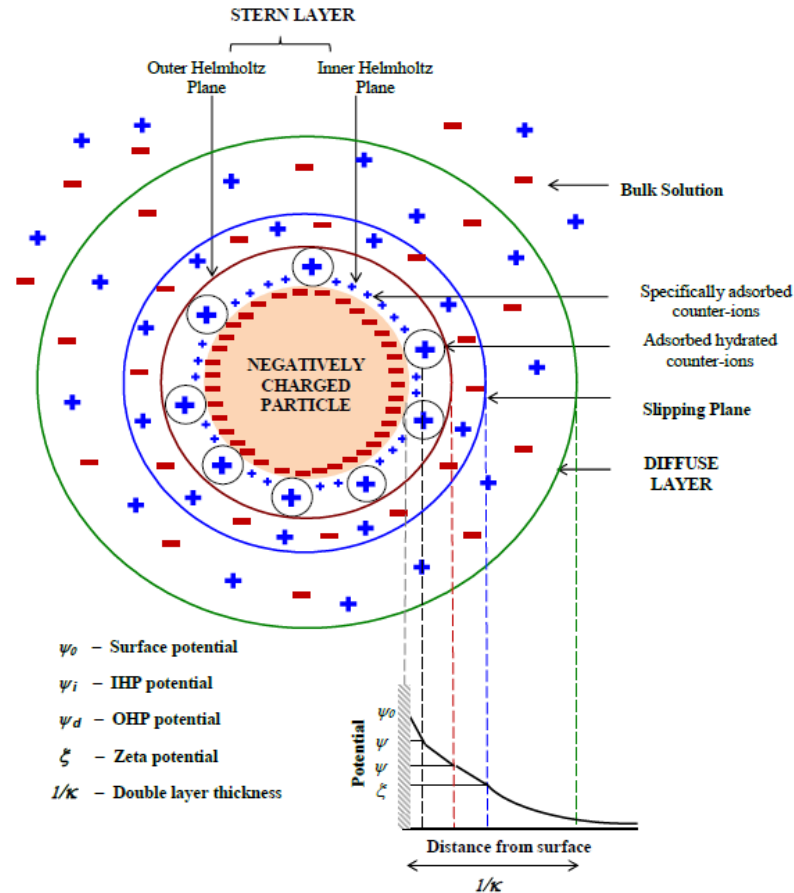


Figure 2.5: Electric double layer and zeta potential [67]

### 2.2.2. Van Der Waals interaction

Van der Waals forces are intermolecular attractive forces between molecules and atoms. There are three types of Van der Waals forces: dipole-dipole interaction; induced dipole-dipole interaction, and dispersion forces which are attractive forces between non-polar molecules. These forces play a unique role in colloids and surface chemistry in determining their properties and behavior [90].

### 2.2.3. Electrical double layer repulsion

When two particles in suspension move closer to each other due to Brownian motion, overlapping of the two double layers will occur. Ions distribution around the

particles is altered hence increasing the free energy of the system. Bringing the particles to a closer distance from each other and changing the distribution of the surrounding ions need a certain amount of work known as repulsive energy [90,91].

#### **2.2.4. Brownian motion**

Brownian motion is defined as the random and uncontrolled motion of particles or molecules in a fluid (i.e. liquid or gas) as a result of their continuous collision with each other. In colloidal systems, the Brownian motion arises from the continuous collision between the colloids and the water molecules [92]. It is considered one of the main characteristics of colloidal dispersion that accounts for their stability [93,94].

#### **2.2.5. DLVO theory**

The DLVO theory was established in the 1940s by Derjaguin Landau and Verwey Overbeek research groups to explain the stability of colloidal dispersion. It takes into consideration the main two forces acting on the dispersed particles: attractive van der Waals and electrostatic repulsion due to the presence of an electrical double layer [95]. According to the DLVO theory, colloidal stability in the dispersion is estimated by balancing the forces (attraction and repulsion) between the particles. The negative surface charge of the colloidal particles is balanced out by ions in the solution resulting in the accumulation of positive charges around the particle and hence, the formation of an electrical double layer and electrostatic repulsion. Overlapping between the double layer of two particles result in the electrostatic double layer interaction ( $V_t$ ). As shown in Figure 2.6, the total interaction ( $V_t$ ) is a function of the distance ( $x$ ) between two particles and is defined as the algebraic sum of the attractive van der Waals ( $V_A$ ) and the electrostatic repulsion ( $V_R$ ) forces [96]. The attractive van der Waals energy  $V_A$  is inversely proportional  $x$ ; it decreases as the distance between the two particles increases. Consequently, the repulsion interaction energy shows an exponential

relationship with the distance, therefore, changes in  $V_R$  takes longer time [19]. Thus, at medium to large separation the repulsion forces dominant (stable system) while at small separation the van der Waals attraction outweigh repulsion forces resulting in an unstable system (attraction instability) [85,97].

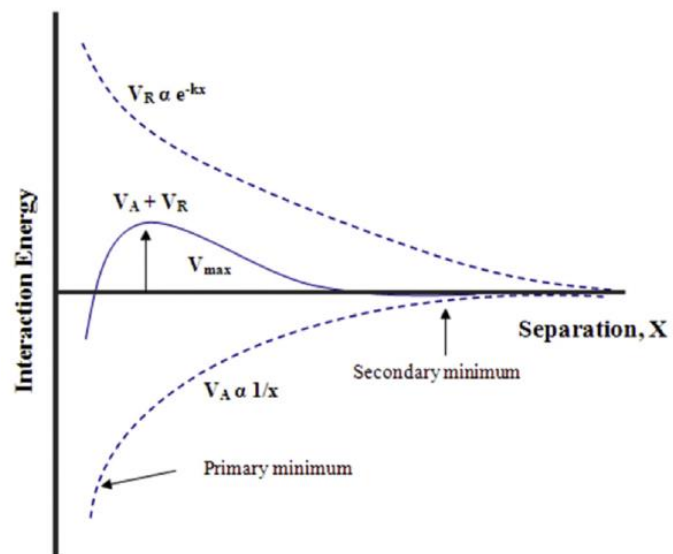


Figure 2.6: Potential energy diagram [19]

## **2.3. Coagulation and Flocculation**

Coagulation and flocculation are two interdependent processes. They are conventional physicochemical wastewater treatment methods that represent the backbone for any wastewater treatment plant (WWTP) [89]. Mainly, they concern with the treatment of persistent suspension through overcoming the stabilizing forces between the colloids and suspended particles [98,99]. Coagulation is the first step that involves the addition of organic or inorganic coagulant and destabilization of the suspension to initiate the aggregation of particles. It is also known as the rapid mixing stage to uniformly distributed the coagulant in the system [1]. The resultant flocs are relatively small and fragile and may break upon force application [30]. On the other hand, flocculation represents the further aggregation of the particles by the addition of a flocculant, usually a polymer, and the formation of larger and stronger flocs that can settle under the influence of gravitational forces giving clear suspension. Flocculation involves a slow mixing stage over a longer period of time in order to enhance the interaction between the particles and hence, larger flocs [1].

### **2.3.1. Mechanisms**

#### **2.3.1.1. Sweep coagulation**

Sweep coagulation (Figure 2.7) is exhibited when a metal salt such as aluminum ‘alum’ sulfate and ferric chloride are used to coagulate turbid suspension. Sweep coagulation depends on the hydrolysis of metal salts to form solid metal hydroxide. The addition of metal salts to the water in high concentration promotes the formation of amorphous metal hydroxide as aluminum or iron hydroxide ( $Al(OH)_3/ Fe(OH)_3$ ) which will precipitate. Colloidal particles in the system are enmeshed or swept out by the metal hydroxide precipitation [100–102]. Sweep coagulation is usually encountered during the treatment of a system with relatively low turbidity [103]. The produced flocs

are weak with a loose structure and can easily break [104].

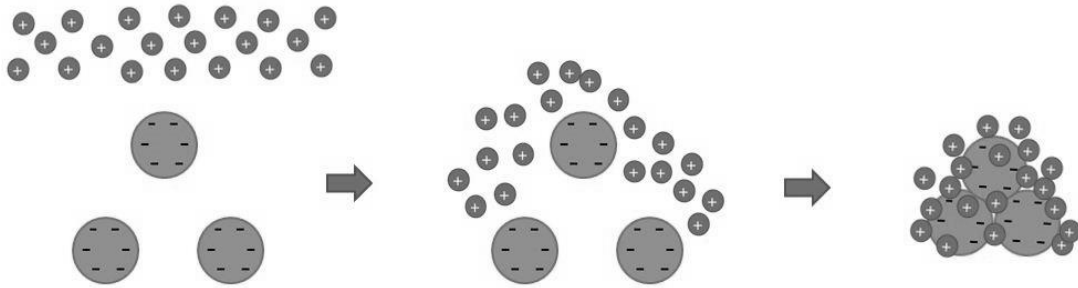


Figure 2.7:Coagulation by Sweep Mechanism (Redrawn from [105])

### 2.3.1.2. Electrostatic patch coagulation (EPC)

EPC occurs when the used coagulant cannot fully neutralize the negative surface charge of the colloidal particles. Accordingly, two areas can be distinguished on the particles' surface: the covered areas where the cationic coagulant is adsorbed and the uncovered negatively charged areas as illustrated in Figure 2.8. As a result of the presence of two oppositely charged areas, a positively charged patch on one particle attracts a negatively charged surface on another particle due to electrostatic interaction between them. Thus, increasing the collision rate between the particles and consequently promote particle aggregation. According to this mechanism, high turbidity removal can be achieved without the need to fully neutralize the negative surfaces [106,107]. The EPC mechanism was proposed for the first time by Gregory to explain the high reduction in turbidity with relatively high zeta potential [108,109]. Furthermore, the high turbidity removal ( $< 10$  NTU) of kaolin suspension with poly-

aluminum chloride ( $PACl_{22}$ ,  $PACl_{25}$ , and  $PACl - E$ ) at a zeta potential greater than  $-15\text{ mV}$  was interpreted with EPC mechanism [31,107].

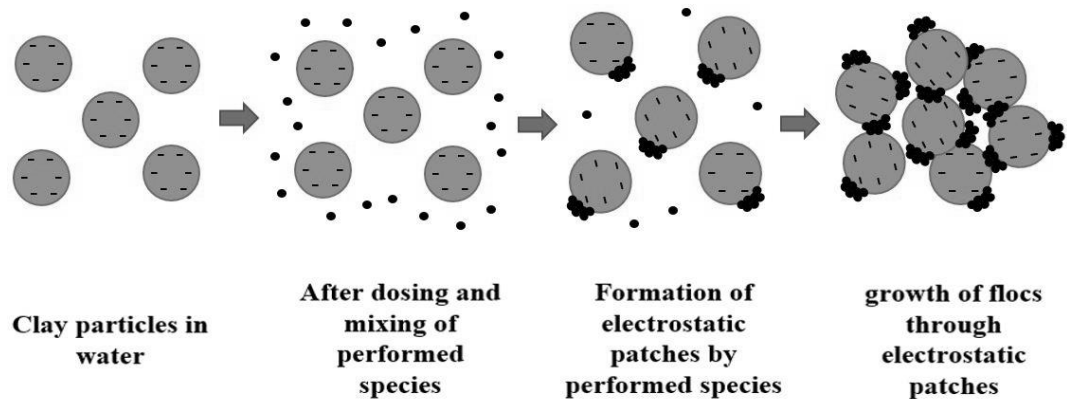


Figure 2.8:Coagulation by Electrostatic Patch Mechanism (Redrawn from [107])

### 2.3.1.3. Charge neutralization

Charge neutralization arises from the utilization of a coagulant or a flocculant with a high positive charge to destabilize negatively charged particles in suspension. The cationic destabilizing agent will adsorb to the particles' surface as a result of electrostatic interaction between them. Therefore, the negative charge on the particles will be reduced or completely neutralized enabling them to move closer to each other forming larger flocs that will settle under the force of gravity [105,110]. Destabilization via cationic polymers such as polyacrylamide usually occurs through charge neutralization. Monitoring and controlling the applied dosage is an essential step as overdosing can cause a charge reversal due to the saturation of the surface of the particles with positive charges and thus, reaggregation and stabilization of the suspension [102].

#### 2.3.1.4. Bridging

Flocculation of fine particles through bridging mechanism takes place when a long-chain polymer with high molecular weight is utilized [36,111,112]. The mechanism demonstrated in Figure 2.9 can be described by three steps: polymer addition and mixing, adsorption on the particles' surface, and lastly aggregation and flocs growth. The charge density and the molecular weight of the polymer are the two main factors that influence destabilization through bridging. For bridging to occur, the polymer chain must be adsorbed on the surface by few attachment points only while the bulk of the chain is stretch out to the surrounding to enable other particles to adhere to the polymer chain. Thus, the same particle may get attached to more than one polymer chain leading to the formation of a larger flocs network [36]. However, high adsorption affinity to the surface and high dosage are undesirable as they may result in a 'hairball effect' where the particle surface will be completely coated with the polymer which prevents bridging and restabilizes the system [99].

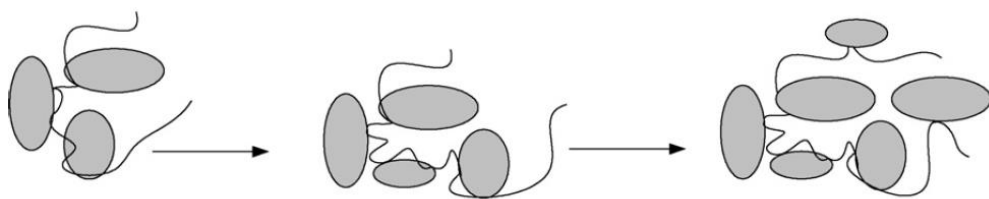


Figure 2.9:Flocculation by Bridging Mechanism with high molecular weight polymer [36]

### **2.3.1.5. Compression of the electric double layer**

Colloidal stability is mainly attributed to the repulsion between the electrical double layers. Destabilization of colloidal dispersion through compression of the electrical double layer occurs when an electrolyte with oppositely charged ions is introduced to the system at high concentrations [1]. The penetration of the counter-ions into the outer diffused layer compresses the layer giving a denser, thinner, and smaller volume outer layer. Consequently, the net repulsion forces between the particles will decrease allowing them to come closer to each other, and hence, destabilization and agglomeration occur. The reduction degree of the repulsion forces depends on the type of the added ions: monovalent, divalent, or trivalent. Addition of higher valent ions such as  $Al^{3+}$  results in steeper potential gradient across the Stern layer in addition to rapid neutralization over a shorter distance in the solution compared to divalent and monovalent ions as  $Mg^{2+}$  and  $Na^+$ , respectively [87].

### **2.3.2. Coagulants and Flocculants**

Coagulants and flocculants are chemical substances used in water and wastewater treatment to enhance the separation between the solid phase and the liquid phase. The solid phase is usually presented as very fine particles (colloids) dispersed in water [113]. As a result, a highly stable suspension with little or no tendency for sedimentation and agglomeration is formed. Therefore, in order to promote agglomeration and sedimentation, reducing the stability of the system is a must. This can be achieved by the addition of coagulants, flocculants, or a combination of both as destabilizing agents.

#### **2.3.2.1. Coagulants**

Coagulants mainly concern with the reduction of the electric charge on the particles' surface and hence decreasing the electrical repulsion between them. They can



be classified into two categories: inorganic coagulants such as metal salts and organic coagulants such as polyDADMAC.

**Inorganic coagulants:**

Metal salts are considered the most popular inorganic coagulants. They can be classified into two main categories: aluminum-based and iron-based. Their popularity arises from their effectiveness for a wide variety of water and wastewater treatment. In addition, they are readily available and cost-effective materials [114]. However, inorganic coagulants have some disadvantages as they show high sensitivity toward the pH and produce larger sludge volume compared to other destabilizing agents [113].

- Aluminum sulfate ( $Al_2(SO_4)_3$ ): also known as Alum is the most common metal salt for water treatment processes [115]. It is widely used for the removal of suspended colloids due to its high efficiency, availability, and cheap prices [116]. However, the low water quality produced as a result of the presence of significant aluminum content, large sludge volume, and its adverse effect on human health limited its use in some applications [117,118]. When added to water, aluminum hydroxides are formed and precipitate with the suspended solids found in water. The formation of aluminum hydroxide occurs through the reaction between the acidic coagulant and the water alkalinity represented in calcium carbonate ( $CaCO_3$ ). As a result, the pH of the treated water will be reduced [119].
- Ferric chloride ( $FeCl_3$ ): is an iron-based coagulant utilized to prevent the health impacts associated with aluminum sulfate. It is primarily used for the reduction of turbidity formed from suspended colloids in wastewater [115]. Ferric chloride has a similar destabilization mechanism to aluminum sulfate; however, iron hydroxide precipitate is formed. Consequently, a significant reduction in the pH of the system

is obtained due to the consumption of water's alkalinity to the formation of the iron hydroxide [119].

- Poly aluminum chloride (PAC): is pre-polymerized aluminum salts with a chemical formula of  $(Al_m(OH)_n(Cl)_{(3n-m)})_x$  usually obtained from hydrolyzing  $AlCl_3$  [113,120]. It has been extensively applied during the last decade for wastewater treatment instead of aluminum sulfate and ferric chloride [121]. Compared to the conventional coagulants, PAC has higher performance efficiency at a lower dosage, over a wider pH range, and at lower temperatures. In addition, utilization of PAC results in lower sludge volume, aluminum residue in water, and effect on the pH of water [122]. The degree of polymerization of PACI influences its basicity. According to Zouboulis et. al. [123], utilizing PACI with higher basicity and aluminum content as a coagulant result in enhanced performance through charge neutralization.

### **Organic coagulants:**

Organic coagulants are usually polymers of low to medium molecular weight. They can be classified into two main categories: natural such as chitosan and synthetic as (Poly-diallyl-dimethylammonium chloride) polyDADMAC. Compared to inorganic coagulants, they are safer, require a lower dosage, and produce lower sludge volume. Moreover, the efficiency of organic coagulants is less affected by the pH of the solution.

- Chitosan: is a cationic linear amino polysaccharide polymer with nontoxic, biodegradable, antimicrobial, and biocompatible properties (Figure 2.10). It is considered the second most abundant polysaccharide-based polymer after cellulose. Chitosan is derived from chitin found in the exoskeleton of shellfish such as crawfish, crabs, and shrimps [124,125]. Its production occurs through the alkaline deacetylation process where the acetyl group is removed from chitin by

treating it with a strong alkali such as NaOH [126,127]. Due to its desirable properties in addition to its unique physicochemical characteristics as a result of the amino group and high content of nitrogen, chitosan has been utilized in a variety of applications [128,129]. Consequently, chitosan has been used widely as a coagulant in the last two decades for wastewater treatment due to its high charge density and long-chain (medium molecular weight) [95,99]. The coagulation process with chitosan is influenced by several factors: the molecular weight, the degree of deacetylation, and the pH as it affects the charge density [110].

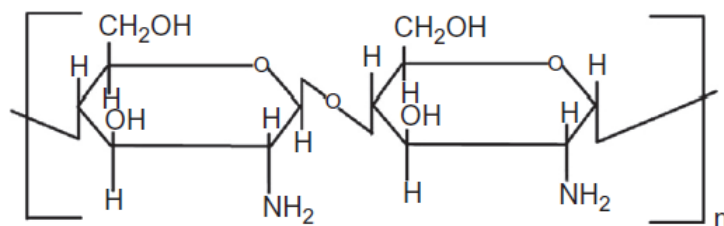


Figure 2.10: Chemical structure of Chitosan [127]

- PolyDADMAC: is a synthetic linear polymer used extensively in water treatment industries [130]. It is synthesized by free-radical initiated addition polymerization of diallyl-dimethylammonium chloride (DADMAC) monomer with the presence of organic peroxide as a catalyst. It is a water-soluble polymer with a molecular weight in the low to medium range [110]. As illustrated in Figure 2.11, PolyDADMAC comprises repeating pyrrolidine rings forming the backbone of the polymer [131]. It is classified as a cationic polyelectrolyte (ionic polymer) due

to the presence of a positive charge in its structure from the amine group. Furthermore, it is characterized by high charge density making it suitable as a coagulant [132].

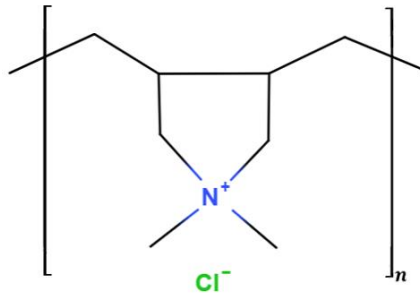


Figure 2.11: Chemical structure of PolyDADMAC

### 2.3.2.2. Flocculants

Flocculants play a key role in further reducing the repulsion forces and connecting the colloidal particles to form large flocs with a high tendency to settle. They are water-soluble polymers of natural or synthetic origins. Polymeric flocculant can be classified according to their molecular weight (MW) or ionic properties. Three polymers categories arise from the variation in the MW: low with MW less than  $< 10^5 \text{ g/mol}$ , moderate with MW values ranging between  $10^5$  and  $10^6 \text{ g/mol}$ , and high with MW values greater than  $10^6 \text{ g/mol}$  [110]. On the other hand, polymers can be classified as ionic polymers (polyelectrolytes) and non-ionic polymers depending on their ionic properties [1].

#### **Ionic polymers (Polyelectrolyte):**

Polyelectrolytes are polymers with a charged functional group in their repeating

unit. They can be divided into two classes depending on the charge type to univalent and multivalent polyelectrolytes. Univalent polyelectrolytes are homogeneous in terms of the charge type, they can be cationic or anionic. On the other hand, multivalent or amphoteric polyelectrolytes comprise repeating units with negatively and positively charged functional groups [1]. The charge density (CD) is considered an important parameter in the flocculation process with polyelectrolytes. It can be determined through experimental methods such as colloids titration and usually expressed in terms of *mol%* or *meq/g* [110].

- **Cationic Polyelectrolytes:** are polymers with a positively charged functional group. The majority of such polymers obtain their positive charge from the presence of quaternary ammonium groups in their structure [110]. Cationic polyacrylamide (CPAM) and Epichlorohydrin/ dimethylamine (EPI/ DMA) polymers are examples of synthetic flocculants possessing quaternary ammonium groups. CPAM is prepared by polymerization of acrylamide with chloromethylated monomer [1]. It possesses a linear chain structure, however, modification methods can be employed to give highly branched chains to enhance its flocculation performance for clay suspensions [133]. Its major application is in the field of wastewater and potable water treatment in addition to sludge conditioning due to its high efficiency as a flocculant and its rapid dissolution [134]. Synthesis of EPI/ DMA polymers occurs through a chemical reaction of EPI with a primary or a secondary amine such as DMA. The produced polyelectrolyte is characterized by a linear chain, low molecular weight, and both hydrophobic and hydrophilic groups (methyl group and quaternary ammonium, respectively) [110,135]. EPI/ DMA can be used for the removal of suspended

and colloidal particles from wastewater through charge neutralization and bridging mechanisms [135,136].

- **Anionic Polyelectrolytes:** are polymers with a negatively charged functional group, usually carboxylic acid ( $R - COOH$ ) or sulfonic acid ( $R - S(=O)_2 - OH$ ) in their structure [137]. Unlike cationic polyelectrolytes, the charge density of anionic polyelectrolytes is dependent on the pH value of the media [110]. Poly(acrylic acid) and poly(styrene-sulfonic acid) are examples of the most common anionic flocculants. Additionally, anionic PAM (APAM) with high molecular weight and low charge density represent a good flocculant for wastewater treatment. It is synthesized through the polymerization reaction between acrylamide and acrylic acid which impart the negative charge to the polymer. The removal of suspended and colloidal particle with APAM occurs through steric interactions, covalent, or hydrogen bonding [138]. Generally, anionic polyelectrolyte has been widely applied in the field of water and wastewater treatment especially in papermaking, mining, and oil exploring industries. They play an important role in the treatment of water-containing metal ions and sludge conditioning/ dewatering [138]. Moreover, they are efficient as a thickening agent in textile and cosmetic industries [1].
- **Amphoteric Polyelectrolytes:** also known as polyampholytes are polymers with both negative and positive charged functional groups among their carbon chain. Factors such as charge density, ionizable groups, and charge balance affect their solubility in water [139]. Amphoteric polyelectrolytes have been utilized in various applications like drilling fluids, papermaking industry, and wastewater treatment. Due to the presence of cationic and anionic charges, they were found to be efficient flocculants for the removal of colloids such as clay minerals

dispersed in water [140,141]. Their flocculation efficiency depends upon the ratio between the cationic and anionic functional groups. The flocculation may occur through charge neutralization, bridging, or adsorption [140]. The most known polyampholytes are amphoteric PAM which is synthesized through the free radical polymerization of acrylamide monomer with other functional groups such as carboxylic acid, sulfonic acid, or vinyl group [1,141].

### **Non-ionic Polymers:**

Unlike polyelectrolytes, non-ionic polymers do not bear any charged functional groups in their structure. They can be naturally occurring polymers or synthetic polymers produced through homo-polymerization. Usually, synthetic polymers occupy 1 – 3% of negatively charged functional groups. Polyacrylamide (PAM) is a non-ionic polymer synthesized from acrylamide monomers with less than 1% anionic groups under controlled conditions of pH, concentration (i.e. monomers and initiator), and temperature [110]. On the other hand, natural non-ionic polymers include starch, cellulose, and galactomannans. They are biodegradable, non-toxic, and widely available substances [110,139]. In general, non-ionic polymers serve as good flocculant municipal and industrial wastewater [1].

### **2.3.3. Experimental methods used to evaluate coagulation-flocculation**

Evaluation of coagulants and flocculants efficiency in the treatment of wastewater containing colloidal particles can be conducted through several experimental methods including analysis of the physicochemical properties such as turbidity removal, reduction in negative zeta potential, and the size and settling velocity of the formed flocs. Furthermore, the performance of the destabilizing agent can be assessed by evaluating the strength of the produced sediments through rheological measurements.

#### **2.3.3.1. Turbidity and Zeta potential**

The turbidity of a system is an optical characteristic defined as the measure of the reduction in water transparency due to the presence of colloidal and suspended particles. A large amount of colloidal and suspended particles in water leads to higher turbidity and hence, lower transparency [142]. Turbidity measurements are conducted through an electronic device using the light scattering method known as a turbidimeter. A white light beam is directed to the water sample and passes through it. The intensity of the scattered light is measured through a photometer at a 90° angle to the direction in which the light beam passes the sample. The amount of scattered light is directly proportional to the turbidity of the water sample measured in nephelometric turbidity units (NTU) [143].

Turbid water is usually associated with an increase in temperature and a reduction in the photosynthesis rate. This is attributed to the heat adsorption and sunlight scattering by the colloidal particles. As a result, the level of dissolved oxygen (DO) in water decreases. Furthermore, the presence of colloids in water may cause filter clogging, prevent disinfection via UV radiation, and interfere with chemical disinfectants. Additionally, it affects the water aesthetic as it is unsafe and unappealing



for consumers to use turbid water [142,143]. Therefore, turbidity reduction is considered as one of the main targets for wastewater treatment plants especially for effluent discharged into water bodies or effluents reused in agriculture or domestic applications [144]. According to the world health organization (WHO), the maximum acceptable turbidity limit for agriculture and drinking water is 5 *NTU*. However, turbidity of 1 *NTU* or less is preferred to ensure effective disinfection of water [145,146].

Turbidity reduction is always associated with a change in the zeta potential of the colloids in suspension. The magnitude of the zeta potential indicates the stability degree of particles in the system. Consequently, it is an important method to evaluate the performance of coagulation and flocculation processes. Zeta potential analysis provides an insight into the particles' surface charge density and the adsorption affinity of the destabilizing agent to the particles' surface. In the treatment process via coagulation and flocculation, a reduction in the negative value of zeta potential to approach the zero point of charge (ZPC) is desirable [1,17]. Various studies examined the effect of different coagulants and flocculants on the turbidity and zeta potential of the studied systems. Al-Risheq et. al. [147] and Alshaikh et. al. [17] studied NADES and cationic PAM, respectively of bentonite suspension with a solid concentration of 1 *g/L*. NADES and cationic PAM have the same positively charged functional group ( $NR_4^+$ ), however, PAM have large molecular weight and longer chains. Consequently, the studies followed the same operating conditions for the jar test and settling time. At the optimum dosage for each destabilizing agent, both achieved similar residual turbidity of 0.65 *NTU* and 0.53 *NTU* for NADES and CPAM, respectively. However, significant variation the zeta potential is observed as the suspension treated with NADES had a zeta potential value of  $-18.8$  *mV* while a positive zeta potential of

3.79 *mV* was obtained for the treated suspension with CPAM. The difference in the potential values is attributed to the structural difference between the two destabilizing agent and their mechanism. Destabilization of bentonite with CPAM occurred through charge neutralization and bridging [17]. On the other hand, the electrostatic patch mechanism was used to describe the destabilization mechanism of NADES where only patches on the clay surface are neutralized [147].

### 2.3.3.2. Floc size

Usually, the effectiveness of the coagulation/ flocculation process is primarily measured by the reduction of the supernatant turbidity and negative zeta potential. However, the type of information provided from these parameters is not sufficient for the following treatment steps [103]. The size and the strength of the produced flocs are among the chief characteristics that determine the efficiency of the coagulant/ flocculent in the treatment process [32]. Floc size is usually evaluated through particle size distribution (PSD) which can be conducted via multiple techniques. However, laser diffraction is the most utilized method due to its precision and accuracy over a wide range. PDS is usually described by the D-values represented in  $D_{10}$ ,  $D_{50}$ , and  $D_{90}$ .  $D_{10}$ ,  $D_{50}$ , and  $D_{90}$  provide the floc diameter at 10%, 50%, and 90% in the cumulative floc size distribution, respectively. The  $D_{50}$  values are used to describe the median diameter of the flocs in any system. Additionally, the number average or first moment ( $D_n$ ) and the weight average or second moment ( $D_w$ ) defined by Eq. 2.1 and Eq. 2.2, respectively can be employed to analyze the changes in the floc size [66].

$$D_n = \sum \frac{N_i \times D_i}{N_i} \dots \text{ (Eq. 2.1)}$$

$$D_w = \sum \frac{N_i \times D_i^2}{N_i \times D_i} \dots \text{ (Eq. 2.2)}$$

Where  $N_i$  is the occurrence frequency while  $D_i$  is the particle size in  $\mu m$ . The  $D_w$  takes

into consideration the effect of both large and small flocs unlike the  $D_n$  which describes the number average particle size (ordinary arithmetic mean) without giving more weight to larger particles. Hence, for quantifying coagulation/ flocculation, the weight average ( $D_w$ ) is more relevant as it accounts for the weight rather than only the number of the particles [17,66].

The characteristics of the produced flocs including the size, strength, and structure are dependent on the type of the employed coagulant and its destabilization mechanism. Metal salts are one of the most utilized inorganic coagulants in the treatment process, however, destabilization through the sweep mechanism, which depends on the initial pH and the formed precipitate, results in relatively small and fragile flocs [30]. In contrast, the charge neutralization mechanism exhibited by organic coagulants and polyelectrolytes has an advantage over inorganic coagulants in terms of the size and strength of the formed flocs. However, the bridging mechanism associated with high molecular weight polyelectrolytes is the most remarkable for producing the largest flocs with high shear resistance [148]. Li et. al. [103] studied the influence of three destabilization mechanisms (i.e. charge neutralization, sweep coagulation, and bridging) on the strength of the resultant flocs. It was found that the variation of floc strength was in the following hierarchy: bridging > charge neutralization > sweep coagulation. Another study was conducted to analyze the performance difference between ferric chloride and polyDADMAC in terms of the floc size and strength for bentonite suspension with a solid concentration of 1 g/L [32]. The study revealed that at the same coagulation conditions, polyDADMAC gives larger, denser, and more shear resistance flocs compared to ferric chloride. The obtained results are in good agreement with the observations found by Li et. al. [103] as destabilization with polyDADMAC occurs via charge neutralization while destabilization with ferric chloride occurs

through sweep coagulation.

#### **2.3.3.3. Capillary suction time**

Capillary suction time (CST) is a simple method that measures the required time to filter out the free water, not chemically bonded to solids, in the sediment volume under the influence of the capillary suction pressure [149]. The wastewater treatment process results in the formation of sediment/ sludge with water representing more than 90% of its volume [150,151]. Therefore, CST was established to determine the water filterability rate required to reduce the sediment volume. Water filterability rate depends mainly on two factors: the permeability of the sediment layer and the solid capacity for holding water [149]. As illustrated in Figure 2.12, sediment bed formed from relatively small and dense flocs with high compactness has small pores. Therefore, a longer time is required for the removal of free water resulting in high CST values, hence, low filterability rates. On the other hand, large and less compacted aggregates result in wider capillaries (interstices). As a result, the water flow more easily and radially. As a result, shorter CST associated with faster filtration rate are achieved [152,153].

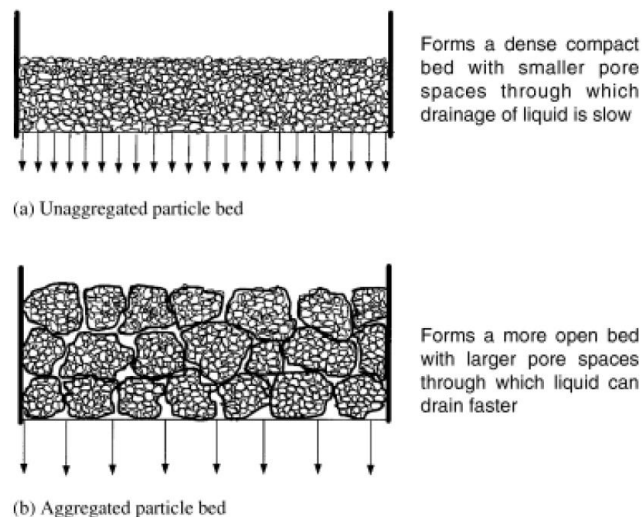


Figure 2.12: Illustration of sediment bed formed from (a) small particles and (b) aggregated particles [149]

Reducing the required CST and energy for sludge dewatering is an essential step to reduce the cost of sludge disposal which accounts for 40 – 50% of any wastewater treatment plant [154]. Therefore, chemical conditioning of the sludge using coagulants or flocculants was found to enhance the stability of sludge and increase its filtration rate. Several studies investigated the influence of the coagulation/ flocculation process on the dewaterability of the sludge. The influence of polyDADMAC on the dewaterability of industrial membrane bioreactor sludge was investigated by Yousefi et. al. [23]. Upon the addition of polyDADMAC with an optimum dosage of 40 mg/L, the dewaterability of the sludge decreased from 15 s to 7 s. This decrease was associated with an increase in the floc size from 17  $\mu\text{m}$  to 65  $\mu\text{m}$ . the coagulant/ flocculent dosage plays a major role in enhancing the filterability of the sludge. In a study conducted by Pambou et. al. [155], the CST curve decreased upon increasing the polymer dosage. However, after a certain dosage, the CST values started to increase again illustrating an overdosing followed by re-stabilization of the sludge.

#### 2.3.3.4. Rheological Measurements

Rheology is defined as the science that studies the matter behavior of flow and deformation upon force application [156]. It also concerns with the relationship between the shear stress ( $\tau, mPa$ ) and shear rate ( $\dot{\gamma}, s^{-1}$ ) [157]. The ratio of the shear stress to the shear is known as the viscosity ( $\mu, mPa \cdot s$ ) of the system (Eq. 2.3).

$$\mu = \frac{\tau}{\dot{\gamma}} \dots \text{Eq. 2.3}$$

According to the behavior of fluids upon shearing, they can be classified into two different categories: Newtonian and non-Newtonian. When the viscosity is independent of the shear rate, the fluid is described as a Newtonian fluid having an ideal viscous flow behavior. In this case, the fluid does not exhibit yield stress. On the other hand, if the viscosity varies upon shearing, the fluid is a non-Newtonian fluid. Four types can be distinguished in non-Newtonian fluids; shear-thinning (pseudoplastic), shear thickening (dilatant), thixotropic, and rheopectic [158,159]. For pseudoplastic materials, the viscosity decreases with shear, while it increases for dilatant. Thixotropic and rheopectic fluids have time-dependent properties; thixotropic fluids exhibit a decrease in viscosity when shear is applied followed by an increase upon reducing or removing the applied force and vice versa for rheopectic fluids [159]. Generally, coagulated/ flocculated as clay suspension demonstrates a time-dependent thixotropic behavior as under a constant shear rate, both the viscosity and yield stress of the system decrease with time [90]. This behavior can be explained by analyzing the influence of the shear rate on the interactions between the formed aggregates. With time, the interaction strength weakens and the aggregates breakdown into smaller constituents. As a result, the viscosity of the system decreases until an equilibrium viscosity is reached.

The concentration of solids in a suspension system has a great influence on its

rheological behavior. To initiate the flow in systems with high solid concentration, it is required to apply a minimum stress value known as the yield stress. The magnitude of yield stress represents the interaction strength between the solid particles themselves (particle-particle interactions) and in between the solid particle and the fluid in the system (particle-fluid interactions) [1,160]. The rheological behavior of non-Newtonian fluids can be described by several empirical models relating the shear stress with the shear rate including Bingham, Casson, Herschel-Bulkley, and power-law models [159]. **Error! Reference source not found.** summarizes the rheological models with their empirical formula and parameters.

Table 2.1: Rheological models for non-Newtonian fluids [1,13,161]

Model	Equation	Parameters
Bingham	$\tau = \tau_0 + n_{pl}\dot{\gamma} \dots (Eq. 2.4)$	$n_{pl}$ : Bingham plastic viscosity ( $Pa \cdot s$ ) $\tau_0$ : Yield stress ( $Pa$ ) $\dot{\gamma}$ : Shear rate
Power-law	$\tau = k\dot{\gamma}^n \dots (Eq. 2.5)$	For power law: $n < 1$ implies a shear-thinning or pseudoplastic fluid $n > 1$ implies a shear-thickening or dilatant fluid
Casson	$\sqrt{\tau} = \sqrt{\tau_0} + \sqrt{n_{\infty}\dot{\gamma}} \dots (Eq. 2.6)$	$n_{\infty}$ : Infinite rate apparent viscosity ( $Pa \cdot s$ )

Model	Equation	Parameters
Herschel-Bulkley	$\tau = \tau_0 + k\dot{\gamma}^n \dots$ (Eq. 2.7)	<p><math>k</math>: Fluid flow consistency (Pa.s<sup>n</sup>)</p> <p><math>n</math>: Flow-behavior index (–), is a measure of the effective fluid viscosity with respect to <math>\dot{\gamma}</math></p> <p>for Herschel and Bulkley: <math>0 &lt; n &lt; 1</math></p>

The Bingham model defined by Eq. 2.4 is commonly used to describe the behavior of clay suspensions with high solid content [162]. The model indicates that under low shear rates and stresses, the material has a solid-like characteristic. The flow is initiated upon the application of finite stress and a Newtonian behavior is exhibited upon increasing the applied stress. Diluted clay suspensions with pseudoplastic behavior and no yield stress are usually expressed in terms of the power-law model (Eq. 2.5) [67]. Casson and Herschel-Bulkley models defined by Eq. 2.6 and Eq. 2.7, respectively are widely used to describe the behavior of coagulated/flocculated clay suspensions. According to the model, the behavior of the aggregates in the system is a function of the applied shear rate. At low shear rate magnitudes, the system appears to have initial yield stress while at an elevated shear rate a shear-thinning/ pseudoplastic behavior is exhibited. The magnitude of  $\tau_0$  interprets the strength of the formed aggregates in a flocculated suspension. Furthermore, it measures the required stress to obtain a suspension composed of the primary particles only due to breakage of the



flocculated suspension [163]. From Eq. 2.7 describing the Herschel-Bulkley model, it should be mentioned that when  $n = 1$  the equation transforms to the Bingham model and when  $\tau_0 = 0$  the power-law model is attained. In case where both conditions occur (i.e.,  $n = 1$  and  $\tau_0 = 0$ ), the system demonstrates a Newtonian behavior [164]. Several rheological methods are available in the literature to measure and determine the yield stress of a solid-liquid system. The most common method to determine the yield stress is by extrapolating the linear section of the shear stress vs. shear rate curve also known as the flow curve to  $\dot{\gamma} \cong 0 \text{ s}^{-1}$  [165,166].

Alongside the flow behavior, viscoelastic properties represented in the viscous modulus ( $G''$ ), elastic modulus ( $G'$ ), and complex viscosity ( $\eta^*$ ) are employed to evaluate the kinetics of the flocculated suspension [23,36]. These parameters can be obtained by performing an oscillatory test. The elastic and viscous modules describe the status of the studied system during the test. For the elastic modulus, the system stores the energy received due to the applied oscillatory motion, therefore, it is also known as the storage modulus. On the other hand, the viscous modulus is described as the loss modulus as the system will undergo an irreversible deformation resulting in an energy loss [163].  $G'$  and  $G''$  are strain/ stress dependent parameters; however, at low applied magnitude they become independent of strain/stress resulting in a linear region known as the linear viscoelastic region (LVR). For the applied conditions of angular frequency during the oscillatory test, the magnitudes of  $G'$  and  $G''$  in the linear viscoelastic region are of valuable meaning for the system characteristics. When  $G' > G''$  it indicates that the studied sample has a solid-like structure and is identified as a viscoelastic solid. In contrast, when  $G' < G''$  the sample has a liquid-like behavior and is described as a viscoelastic liquid [167].

The interactions between the clay mineral particles and their structures in

suspension are an important factor for several industrial applications. Such information can be attained by studying the viscoelastic properties of the suspension (i.e.,  $G'$  and  $G''$ ) on the suspensions. In clay suspensions, three modes of particle-particle interactions can be observed: edge to edge (EE), face to face (FF), and edge to face (EF). The destabilization degree of the suspension depends greatly on the interaction mode exhibited by the particles [36,168–170]. For example, the produced sediments through EE and EF interaction modes are characterized by their low density and large volume. On the other hand, FF interactions result in more dense aggregates [168,170,171]. In two different studies by Khandal and Tadros [172] and Sohm and Tadros [173], the viscoelastic properties of a bentonite suspension represented in the  $G'$  and  $G''$  measured through dynamic oscillatory measurements were employed to differentiate between cross-linked network structures and isolated flocs. The authors linked the  $G'$  and  $G''$  results to the gelation kinetics of the suspension under study to provide information regarding the gelation mechanism and gel strength of the colloidal suspension.

#### **2.3.4. Factors affecting the coagulation/ flocculation process**

The efficiency of the coagulation/ flocculation process for the treatment of wastewater is primarily dependent on the operating conditions of the process. The coagulant/ flocculant type and dosage, pH, temperature, mixing conditions, in addition to molecular weight and charge density when polyelectrolytes are utilized represent the main factors affecting the destabilization process. Therefore, to ensure achieving the desirable results, understanding the influence of each factor on the destabilization process and optimizing it is essential.

##### **2.3.4.1. Coagulant/ flocculent type and dosage**

The selection of the right destabilizing agent type with the appropriate dosage

has a major influence on the efficiency of the treatment process. Destabilizing agents can be organic or inorganic, natural or synthetic. Consequently, polymeric flocculant can be cationic, anionic, amphoteric, or nonionic. The applied coagulant/ flocculant dosage is the most critical factor in the destabilization process. Optimizing the applied dosage according to the selected coagulant/ flocculant, their properties, water chemistry, and the operating conditions is an essential step to minimize the cost and the amount of sludge produced [174]. Insufficient or excess dosing can significantly reduce the performance efficiency of the coagulant/ flocculant. Generally, the zeta potential value is employed as a measure to determine the optimum coagulant/ flocculant dosage. The concentration at which the zeta potential approaches the zero point charge (ZPC) also known as the isoelectric point is usually designated as the optimum concentration. When excess coagulant/ flocculant dosage is applied, the zeta potential values change from being highly negative to highly positive due to the saturation of particles surface with the destabilizing agent. As a result, the new positively charged particles repel each other's and hence, re-stabilization occurs [175]. In the coagulation process, overdosing may disturb the destabilization and sedimentation process due to the resuspension of the colloidal particles resuspension [176]. Therefore, to avoid excess dosing, identifying the critical coagulation concentration, also known as the inflection point after which no significant changes in the system are observed is a must [177].

Hussain et. al. [178], performed a study to investigate the performance of three aluminum-based coagulants: Alum, PACl, and high-performance PACl for the treatment of surface water. Larger flocs and faster settling times were obtained when high-performance PAC was utilized compared to alum and PACl. In another study by Bazrafshan et. al. [174], the effect of ferric chloride dosage when combined with natural coagulant aid for the treatment of synthetic kaolin suspension was analyzed. The dosage

of  $FeCl_3$  and the natural coagulant aid varied between 2 – 35 mg/L and 0.1 – 5 ml/L, respectively. Increasing the  $FeCl_3$  dosage was found to enhance the turbidity reduction, the highest reduction was achieved with 10 mg/L and 0.4 ml/L of  $FeCl_3$  and natural coagulant, respectively. In addition, it was noticed that lower dosage of natural coagulant is preferred to prevent high organic matter content, microbial growth, increase in turbidity, and undesirable color [174]. Furthermore, depending on the coagulant type and dosage, different coagulation mechanisms may occur. For aluminum sulfate, the coagulation process occurs through sweep coagulation where the amorphous hydroxide precipitation plays the main role [179]. On the other hand, the coagulation mechanism with PACl was a function of the pH, in acidic environment coagulation takes place through charge neutralization while in alkaline environment sweep coagulation is dominant [180].

In the flocculation process, the adsorption affinity of the flocculant to the surface of the particles plays a major role in determining the flocculation efficiency. High adsorption affinity results in saturation of the adsorption sites which prevents bridging to occur and may result in re-stabilization of the particles [29]. The adsorption affinity of the polymeric flocculants can vary according to their type and the dosage. In general, destabilization using polyelectrolytes occurs via adsorption and hydrogen bonding with the colloidal particles. The use of anionic polyelectrolytes such as anionic PAM was found to be more effective for the destabilization of negatively charged particles than cationic polyelectrolytes. This is attributed to the repulsive forces which limit the adsorption of the flocculant to only few active sites on the particles. As a result, particles saturation and re-stabilization is avoided [169]. Several studies were conducted to compare the performance of cationic and anionic polyelectrolytes for flocculation of negative colloids. For example, Nasser et. al. [9] studied the effect of

three polymeric flocculants (i.e. anionic, cationic, and non-ionic) on the destabilization degree of papermaking suspension containing kaolinite clay. Reductions in the residual turbidity and negative zeta potential were enhanced by increasing the dosage of the cationic polyelectrolyte until the optimum dosage was reached. Any excess addition of the flocculant resulted in a reversed effect. Anionic PAM was found to be the most efficient in terms of turbidity reduction at its optimum dosage. In addition, it resulted in larger and less dense floc with an open structure compared to cationic PAM which can be justified by the lack of attractive forces and the formation of loops and tails on APAM. In contrast, at low dosage of non-ionic PAM insignificant turbidity reduction is observed. Slight dosage addition led to an adverse effect on the suspension turbidity due to displacing the counter ions in the interlayer with the non-ionic PAM.

#### **2.3.4.2. Molecular weight and charge density**

When polymers are utilized as coagulants/flocculants for wastewater treatment, their performance is strongly influenced by the molecular weight (MW) and the charge density (CD) [20]. The charge density is described as the percentage of the polymeric chain occupied by ionic functional group. Shaikh et. al [17], investigated the effect of both MW and CD on the destabilization behavior of bentonite suspension. polymers with molecular weight varying between 6 – 15 *million g/mol* and charge densities between 20% – 80% were utilized as flocculation for the treatment of bentonite suspension with solid concentration of 1.5 *g/L*. For the same coagulant type (i.e. cationic), it was found that by increasing the charge density from 20% to 80%, the adsorption isotherm increase from 1.0 *mg/g* bentonite to 1.7 *mg/g* bentonite with no clear steady state at 80% CD indicating strong adsorption. In the same manner, polymer with higher MW (10 – 15 *million g/mol*) exhibited higher adsorption isotherm compared to lower MW (6 – 10 *million g/mol*). The influence of both MW and CD

on the turbidity and zeta potential is very limited. However, at the same MW (i.e. 10 – 15 million *g/mol*), flocculant with CD of 80% was associated with smaller flocs compared to lower CDs. This phenomena is attributed to the strong adsorption affinity of high CD PAMs to the bentonite particles which led to their saturation and limited the bridging mechanism [17].

In the coagulation process where chitosan is used as a destabilizing agent, the deacetylation degree (DD) has an influence on the performance along the MW. Soros et. al [144], examined the effect of the MW, DD, and chitosan dosage on its coagulation efficiency in terms of turbidity for synthetic bentonite and kaolinite suspensions. MW of 5,000, 50,000, 100,000, 600,000, and 1,000,000 *Da* with constant DD of 90% were investigated to analyze the MW effect. On the other hand, to study the DD effect, chitosan with DD of 70%, 75%, 80%, 85%, 90%, and 95% and MW of 50,000 *Da* were utilized as coagulants. For all DD, turbidity reduction of 80% and higher was achieved at low to moderate dosage. At 3 *mg/L* chitosan with DD of 85% was found to achieve the highest reduction of 99.2%. At high coagulant dosage (i.e. 30 *mg/L*), the reduction drops to less than 25% for DD of 70%. However, high dosages appear to have less significant effect on the residual turbidity for chitosan with higher DD hence, overdosing probability is lower. Furthermore, it was found that by increasing the MW the turbidity reduction increases for both bentonite and kaolinite suspensions. For bentonite suspension, increasing the MW from 5,000 *Da* to 100,000 *Da* leads to an increase in the turbidity reduction from 10% to 98.1%, respectively. For MW above 100,000 *Da*, the increase in turbidity reduction is insignificant.

#### **2.3.4.3. Mixing conditions**

Mixing or agitation is an essential step in the coagulation and flocculation processes as it can significantly affect the destabilization degree of the system. The

mixing step can be divided into two regimes: rapid and slow mixing. The rapid mixing stage usually varies from few seconds up to 3 minutes. Its main target is to guarantee the uniform distribution of the destabilizing agent among the system and the formation of a homogeneous solution [181]. BinAhmed et. al. [182], studied the effect of different rapid mixing speeds and times on the destabilization process of highly turbid kaolin suspension in terms of the floc size and strength. the rapid mixing speeds and times were 80, 100, and 120 rpm and 20, 40, and 60 s, respectively. It was found that larger flocs with low compactness (low shear resistance) were formed under a shorter mixing time. In contrast, smaller flocs with higher strength (high shear resistance) were obtained with a longer mixing time. The observed phenomena is attributed to exposure to an extended period of high shear rate resulting in floc breakage and hence, smaller flocs which exhibit lower collision efficiency [183].

On the other hand, the slow mixing is considered as the flocs growth stage and it is a very critical step in the destabilization process. The optimization of the slow mixing stage helps in enhancing the separation efficiency of the formed flocs from the supernatant [121]. Yu et. al. [183], conducted a study to evaluate the influence of the slow mixing speed on the coagulation/ flocculation efficiency. Aluminum sulfate (alum) was utilized as a coagulant at a concentration of 0.2 mM for a diluted kaolin suspension with clay concentration of 0.05 g/L. The jar test was carried at a constant rapid mixing of 200 rpm for 60 sec and variable mixing speeds of 40, 50, 60, 80, and 100 rpm. It was found that before breakage, the slow mixing speed has an inversely proportional relationship with the flocculation index (FI) which gives a precise measure of particle aggregation. As a result, when increasing the slow mixing speed, the flocculation index decreases. After breakage, the FI of the regrowth was found to be similar for all mixing speeds. The obtained results were supported by the particle size

distributions. Both mixing time and speed influence the destabilization process, however, mixing time optimization is more essential as sufficient time enhances the collision efficiency through which the flocs become more compacted and shear resistant. Generally, increasing the rapid mixing speed should be associated with a shorter mixing time. While for slow mixing, increasing the speed may cause floc breakage under a high shear rate due to floc splitting and turbulent drag [184,185].

#### **2.3.4.4. pH**

The pH of the media plays a major role in determining the efficiency of the coagulation/ flocculation process. Polymeric flocculants (i.e. natural and synthetic) are usually not affected by the pH changes [30]. However, the efficiency of inorganic coagulants is highly influenced by the pH of the media. Generally, the determination of the optimum pH range to achieve higher efficiency during the destabilization process is mainly dependent on the type of the utilized coagulants [186]. Consequently, the type and characteristic of the effluent have an influence on the optimum pH range. When the pH of the media is outside the desirable range, the coagulation efficiency decreases significantly. Furthermore, the coagulation mechanism varies according to the selected pH range from charge neutralizing, bridging, double layer compression, or sweep coagulation [177]. However, sweep coagulation is not desirable as it result in the formation of large sediment volume with large amounts of metal precipitation.

Yang et. al. [186], studied the influence of the pH on three aluminum-based coagulants ( $Al_2(SO_4)_3$ ,  $AlCl_3$ , and PAC) for the treatment of kaolin-humic acid synthetic water. The initial pH of the system ranged from 4 – 9 and the effect was recorded in terms of turbidity removal. As the pH increased from acidic to neutral (pH = 6), the turbidity removal gradually increased to more than 90% for all coagulants. A slight increase was observed in the turbidity removal at higher pH values



for  $AlCl_3$  and PAC while the removal percentage decrease for  $Al_2(SO_4)_3$ . The observed trends were attributed to the formation of positive hydrolysate which can neutralize negatively charged kaolin particles at lower pH values while at pH higher than 8 the formed hydrolysates are negatively charged. At an optimum dosage, the optimum pH range was as following: between 5 – 8 for PAC and between 6 – 7 for  $Al_2(SO_4)_3$  and  $AlCl_3$  [186]. Commonly, coagulation using aluminum-based metal salts tends to be most efficient at pH values of 6 or lower as destabilization by the formed positive Al species occurs through charge neutralization rather than adsorption or sweep coagulation. At pH higher than 6, amorphous participate starts forming and destabilization occurs through sweep coagulation which is unfavored [187]. The same trends also apply to destabilization using iron-based coagulants.

Furthermore, initial pH has an influence on the electrokinetic behavior of the effluent. The effect of varying pH on bentonite suspension was analyzed in terms of zeta potential and turbidity as shown in Figure 2.13 [17]. With the addition of  $H^+$  ions to the suspension, the decrease in the pH is associated with a gradual decrease in the negative zeta potential while the turbidity remains constant at pH higher than 2. Once the pH reaches 2, a clear supernatant is formed after a settling time of 5 minutes and the maximum decrease in the negative zeta potential is obtained. The observed phenomena was attributed to the neutralization of part of the negative charges on bentonite surface causing the zeta potential value to reach the zero point of charge (ZPC) [17]. In contrast, increasing the pH value by adding a base such as  $NaOH$  to the system results in negative charge build up which will lead to increase in the negative zeta potential and re-stabilization of the system. Nasser el. al. [9], studied the effect of the initial pH on papermaking suspension containing precipitated calcium carbonate (PCC), a negatively charged colloidal particle. Trends similar to shaikh et. al. [17] were

observed upon the addition of  $H^+$  ions to the suspension. However, the reduction in turbidity did not occur suddenly but in a gradual manner with the decrease in the pH.

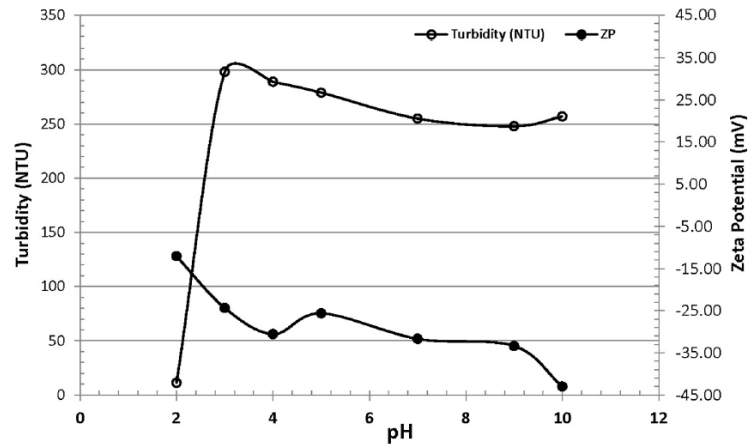


Figure 2.13: Effect of initial pH values on the stability of bentonite suspension [17]

A review of some of the key research papers related to the coagulation/ flocculation process and its influence on the electrokinetic of industrial clay minerals are presented

Table 2.2: Review of the coagulants/ flocculants efficiency for destabilization of clay minerals.

Coagulant	Flocculent	clay mineral	Investigated parameters	Main Observations	Reference
PACl Alum	-	Kaolin	pH Floc growth rate Temperature	<ul style="list-style-type: none"> <li>For Alum and PACl, increasing the aluminum concentration led to a faster destabilization and floc formation rate. This observation is attributed to the increase in the collision-attachment efficiency between the particle and the increase in their volume at higher concentrations.</li> <li>Coagulation performance of PACl was less sensitive to the pH of the media compared to Alum. Therefore, at varying temperature conditions, PACl has an advantage over Alum as the temperature change affect the ion product of water (<math>H^+</math> and <math>OH^-</math>).</li> <li>More rapid destabilization rate was attained in suspension treated with PACl than Alum.</li> </ul>	[188]

Coagulant	Flocculent	Clay mineral	Investigated parameters	Main Observations	Reference
Chitosan		Local	Turbidity removal	<ul style="list-style-type: none"> <li>Utilization of natural coagulant for destabilization of clay suspension was found to be significantly efficient in turbidity removal.</li> <li>The turbidity reduction varied between 90 – 96% with the maximum reduction achieved by chitosan followed by M. oleifera and lastly cactus.</li> <li>Higher turbidity reduction was accomplished with M. oleifera (94.8%) compared to cactus (92.2%). However, the required dosage for M. oleifera was two times higher than that required when cactus is the utilized coagulant.</li> </ul>	[189]
Cactus Opuntia	-	natural			
Moringa Oleifera		clay			

Coagulant	Flocculent	Clay mineral	Investigated parameters	Main Observations	Reference
Chitosan	-	Natural clay	Turbidity removal Settling time pH	<ul style="list-style-type: none"> <li>Over a pH range varying from 4 to 10, the maximum reduction in turbidity using chitosan was obtained at neutral pH value.</li> <li>The utilized chitosan dosage plays an important role in determining the residual turbidity of the supernatant. At neutral media, the maximum removal percentages of 61.9% 84.1%, and 95.30% for wastewater with low, medium, and high initial turbidity, respectively were achieved at a concentration of 1.5 mg/L.</li> </ul>	[190]

Coagulant	Flocculent	clay mineral	Investigated parameters	Main Observations	Reference
Chitosan Alum	-	Natural clay	Turbidity removal Settling time pH	<ul style="list-style-type: none"> <li>Utilization of chitosan as a coagulant aid for aluminum sulfate (Alum) further increased the coagulation efficiency and resulted in the formation of large coarse flocs with a rapid settling rate. The turbidity removal percentage increased to 74.8, 96.7 and 98.2% for water with low, medium and high initial turbidity, respectively.</li> </ul>	[190]
Aluminum sulfate	CPAM (C448,C4 98) APAM (A130,A1 15)	Kaolin	Zeta potential Residual turbidity Floc size	<ul style="list-style-type: none"> <li>The produced flocs using PAMs with higher molecular weight were larger in size than medium molecular weight PAMs.</li> <li>Between cationic and anionic PAMs with similar molecular weight, the larger flocs were formed through the flocculation process with cationic PAM.</li> </ul>	[191]

Coagulant	Flocculent	Clay mineral	Investigated parameters	Main Observations	Reference
Aluminum sulfate	CPAM (C448,C498) APAM (A130,A115)	Kaolin	Zeta potential Residual turbidity Floc size	<ul style="list-style-type: none"> <li>The influence of the molecular weight on the density of the flocs was more apparent for anionic PAMs. Increasing the molecular weight of the utilized PAM was associated with the formation of denser flocs.</li> <li>Stronger and more shear resistance flocs were formed using cationic PAM as a flocculent.</li> <li>The zeta potential of the bentonite suspension treated with aluminum sulfate and cationic PAM increased from <math>-40\text{ mV}</math> to reach the zero point of charge.</li> </ul>	[191]

Coagulant	Flocculent	Clay mineral	Investigated parameters	Main Observations	Reference
-	CPAM APAM Amphoteric PAM	Bentonite	Adsorption Turbidity Zeta potential Floc size	<ul style="list-style-type: none"> <li>The maximum reduction in the supernatant residual turbidity and negative zeta potential was obtained by cationic PAM which demonstrates strong adsorption affinity to the bentonite particles.</li> <li>For zeta potential and residual turbidity, the influence of the polymer's molecular weight was not significant.</li> <li>The floc size of the produced sediments was found to be directly proportional to the molecular weight of the polymers.</li> <li>The influence of the charge density on the floc size varied depending on the type of the polyelectrolytes. With increasing the charge density, the floc size increased for APAMs and decreased for CPAMs.</li> </ul>	[17]



Coagulant	Flocculent	Clay mineral	Investigated parameters	Main Observations	Reference
-	CPAM APAM Amphoteric PAM	Bentonite	Adsorption Turbidity Zeta potential Floc size	<ul style="list-style-type: none"> <li>Between the three tested PAM types, cationic PAM with high molecular weight and charge density (FO 4800 SH) was the most efficient destabilizing agent</li> </ul>	[17]
Rice, Wheat, Corn, and potato starches	-	Kaolin	Turbidity Sludge volume Zeta potential	<ul style="list-style-type: none"> <li>At acidic pH of 4, a 50% reduction in turbidity was attained by rice starch. Combining rice starch with a traditional coagulant through two-steps coagulation process further enhanced the turbidity removal percentage by 30%.</li> </ul>	[192]
Alum PACl			Floc size and density	<ul style="list-style-type: none"> <li>The two-steps coagulation process using traditional and natural coagulant resulted in a reduction of the chemical based sludge volume by 60%.</li> </ul>	

Coagulant	Flocculent	Clay mineral	Investigated parameters	Main Observations	Reference
Rice, Wheat, Corn, and potato starches	-	Kaolin	Turbidity Sludge volume Zeta potential	<ul style="list-style-type: none"> <li>Larger flocs were produced for suspension coagulated with natural coagulants. Furthermore, the flocs produced by rice starch were the largest.</li> <li>The bulk densities of the flocs generated by traditional coagulants were double the densities of the rice starch flocs.</li> </ul>	[192]
Alum PACl	APAM		Floc size and density	<ul style="list-style-type: none"> <li>Single APAM systems showed poor destabilization efficiency for bentonite suspension with slight reduction in the turbidity at lower dosage associated</li> </ul>	
PolyDADMAC (C1) Polyamine (C2)	(F1: Low MW and F2: high MW)	Bentonite	Turbidity Zeta potential Floc size	<ul style="list-style-type: none"> <li>and a steady zeta potential in the region between <math>-30\text{ mV}</math> and <math>-40\text{ mV}</math> depending on the APAM type. In contrast, the single APAM systems were able to achieve large flocs.</li> </ul>	[94]

Coagulant	Flocculent	Clay mineral	Investigated parameters	Main Observations	Reference
PolyDADMAC (C1)	APAM (F1: Low MW and F2: high MW)	Bentonite	Turbidity Zeta potential Floc size	<ul style="list-style-type: none"> <li>Single cationic coagulant systems demonstrated good coagulation performance with residual turbidities of 1.98 <i>NTU</i> and 1.56 <i>NTU</i> at concentrations of 20 <i>mg/L</i> and 30 <i>mg/L</i>. Increasing the concentration above these values led to reversible results verified by the zeta potential values. However, the produced flocs were smaller in size compared to the APAM.</li> <li>Utilization of hybrid system combined the advantages of the cationic coagulant with excellent turbidity reduction and the large flocs of the anionic flocculent. Hence, it provided better destabilization performance.</li> </ul>	[94]

Coagulant	Flocculent	Clay mineral	Investigated parameters	Main Observations	Reference
PolyDADMAC	-	Bentonite	Residual turbidity	<ul style="list-style-type: none"> <li>• Coagulation of bentonite suspension using PolyDADMAC as a coagulant occurred through charge neutralization.</li> <li>• The residual turbidity of the supernatant decreased gradually upon increasing the concentration of the organic coagulant until it reaches a minimum turbidity at a concentration of 0.61 <i>ppm</i>.</li> <li>• Further increase in the concentration led to re-stabilization of the bentonite suspension due to the saturation of the particles with the coagulant resulting in positively charged particles repelling each other.</li> </ul>	[193]

Coagulant	Flocculent	Clay mineral	Investigated parameters	Main Observations	Reference
PACl Polyaluminum- ferric-silicate- chloride (PSiFAC <sub>1.5:10:15</sub> )	-	Kaolin	Residual Turbidity Residual Al concentration	<ul style="list-style-type: none"> <li>PSiFAC<sub>1.5:10:15</sub> coagulant formed through copolymerization method achieved a reduction in the supernatant turbidity to below 1 NTU with minimum dosage of 1.5 – 2 mg/L while the required dosage of PACl to achieve similar reduction was higher than 3 mg/L.</li> <li>The lowest residual aluminum concentration of 135 µg/L (below the legalization limit 200 µg/L) was attained by using PSiFAC<sub>1.5:10:15</sub> with a dosage of 2 mg/L.</li> </ul>	[194]

Coagulant	Flocculent	Clay mineral	Investigated parameters	Main Observations	Reference
PolyDADMAC (C591 and C595)  FeCl <sub>3</sub>	-	Bentonite	Turbidity Removal Floc size and strength	<ul style="list-style-type: none"> <li>Both organic and inorganic coagulants achieved remarkable turbidity removal varying from 70% to 99%. However, the organic coagulants showed lower residual turbidity and faster settling rate compared to ferric chloride.</li> <li>Depending on the type and concentration of the utilized PolyDADMAC, the produced flocs ranged in size from 400 <math>\mu m</math> to 500 <math>\mu m</math>. On the other hand, smaller flocs were produced with ferric chloride (350 <math>\mu m</math> at optimum concentration)</li> <li>Larger, more compactable, and more shear resistance flocs were formed through coagulation with PolyDADMAC compared to ferric chloride.</li> </ul>	[32]

Coagulant	Flocculent	Clay mineral	Investigated parameters	Main Observations	Reference
-	CPAM (C446, C496, C492) APAM (A130 LMW, A130, A100)	Kaolinite	Adsorption Turbidity Zeta potential Floc size Settling test	<ul style="list-style-type: none"> <li>Higher reduction in the negative zeta potential was accomplished with cationic PAM than anionic PAM.</li> <li>Increasing the concentration of the cationic PAM after the zero point of charge caused charge reversal and re-stabilization of the suspension.</li> <li>The required dosage to neutralize the surface charge is inversely proportional to the charge density of the polymer</li> <li>For cationic PAMs, the settling rate was found to be directly proportional to the molecular weight and inversely proportional to the charge density of the polymer.</li> </ul>	[36]

Coagulant	Flocculent	Clay mineral	Investigated parameters	Main Observations	Reference
-	CPAM (C446, C496, C492) APAM (A130 LMW, A130, A100)	Kaolinite	Adsorption Turbidity Zeta potential Floc size Settling test	<ul style="list-style-type: none"> <li>Anionic PAMs resulted in a more rapid settling rate compared to cationic PAMs. While cationic PAMs were more efficient in turbidity removal.</li> <li>Flocs produced from anionic PAMs were larger flocs than cationic PAM.</li> </ul>	[36]



## **2.4. Deep Eutectic Solvents**

### **2.4.1. Background**

For decades, ionic liquids (ILs) have been considered as green solvents and thus, utilized in a variety of industrial sectors because of their remarkable physical and chemical properties including low vapor pressure and volatility, and high thermal stability. Moreover, ILs are identified as designer solvents as they are characterized by their tailorable properties through the utilization of different cations and anions combinations [40]. Hence, they have become a promising alternative for chemical solvents. However, in recent years, labeling ILs as green solvents has been questioned as more in-depth studies have shown that they are toxic, unstable, and flammable [195]. In addition, they possess undesirable properties including poor biodegradability, non-biocompatibility, high viscosity, and the high cost of the required materials and large-scale production [195,196]. Furthermore, their high sensitivities to impurities limited their widespread in the industrial sector [197]. Therefore, to overcome the drawbacks and limitations of the traditional ILs, a new class of green solvents known as deep eutectic solvents (DESs) has been designed.

### **2.4.2. Definition**

Deep eutectic solvents (DESs) are descended from the ionic liquids family. However, as illustrated in Figure 2.14, they are safer for the environment, cheaper, and possess a simpler synthesis method. In some studies, different terms are employed to refer to a DES such as low transition temperature mixtures (LTTM) and low melting mixtures (LMM) [198,199]. DESs are liquid systems composed of two or three nontoxic and inexpensive components that are able to associate together through hydrogen bond interactions. The constituent components of a DES are usually defined as hydrogen bond

donor (HBD) and hydrogen bond acceptor (HBA). Through a simple procedure of continuous mixing and heating, a eutectic mixture with a melting point lower than that of the constituent components is formed [200]. Hence, DESs are liquid at temperatures ranging from room temperature up to 150°C [201]. The deep depression in the freezing point exhibited by the DES systems upon their synthesis is attributed to the charge delocalization happening on the proton in the HBD and the halide ion such as  $Cl^-$  and  $Br^-$  in the HBA [37].

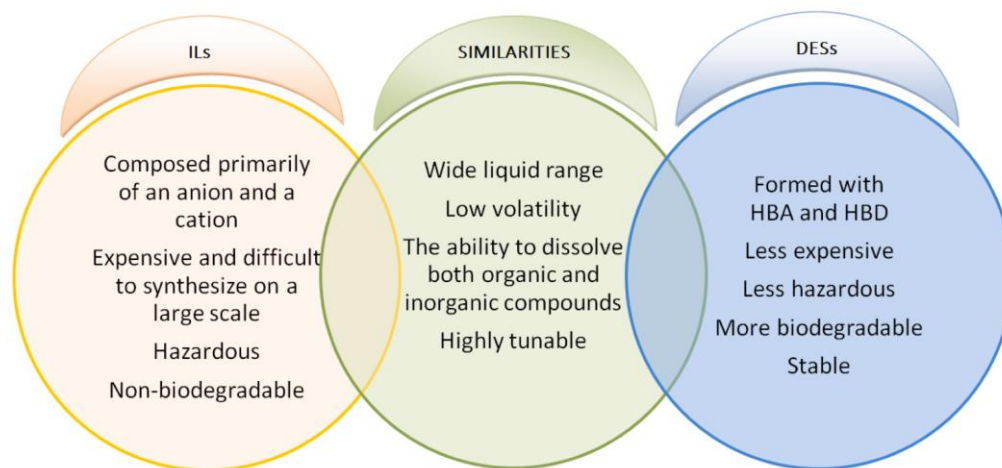


Figure 2.14: Similarities and differences between ionic liquids and deep eutectic solvents [195]

The first DES reported in the literature in a study by Abbott et. al. [39] in 2003 was synthesized from quaternary ammonium salt with urea at an adequate molar ratio resulting in a mixture with unique eutectic properties. The possible combinations of HBA and HBD

to form DES are extremely larger and a numerous number of combinations have been reported in the literature. Figure 2.15 shows some of the available HBD and HBA for the synthesis of DES. As a result of combination variety, four different DES types classified according to the constituent components can be distinguished: type 1 from quaternary salt with metal halide, type 2 from quaternary salt with hydrated metal halide, type 3 from quaternary salt with hydrogen bond donor, and type 4 from metal halide with hydrogen bond donor [37,202–204].

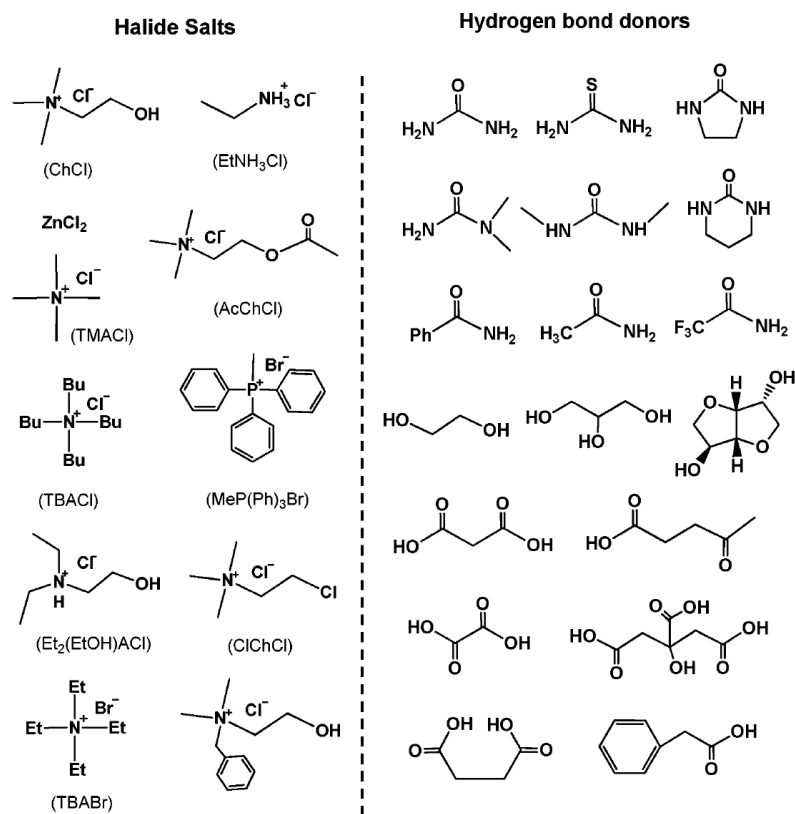


Figure 2.15: chemical structure of typical halide salts (hydrogen bond acceptor) and hydrogen bond donors for the synthesis of DES [38].

### **2.4.3. Natural deep eutectic solvents**

DES produced from a combination of naturally abundant metabolites such as choline chloride, sugars, carboxylic acids, and amino acids at a defined molar ratio is known as natural deep eutectic solvent (NADES) [205]. NADES was reported in the literature for the first time as a new DES class by Choi et. al. [206] in 2011. They fall within type III of the DES classifications as they are produced from quaternary ammonium with a HBD (Figure 2.16). Choline chloride (ChCl), a quaternary ammonium salt, is a green material and widely used in various applications including animal feed, human nutrition, and the pharmaceutical industry. Animal feed (poultry, swine, ruminant) is the largest end-product user with around 94% of the total annual production. ChCl is used as an additive to animal feed as it helps in the development and accelerating the growth rate [207,208]. Owing to its remarkable characteristics represented in nontoxicity, availability, low cost, and biodegradability, ChCl is among the most utilized quaternary ammonium salt for the synthesis of NADES. Generally, this class of DES is known for its simple preparation method, the abundance and low cost of its raw materials, and biodegradability [37]. Furthermore, NADESs are environmental friendly solvents, easy to handle, nonvolatile, nonflammable, and do not require any additional purification process. Consequently, their storage and large-scale application are feasible.

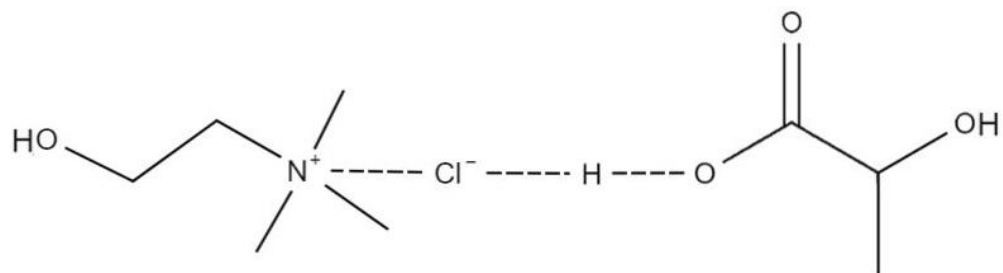
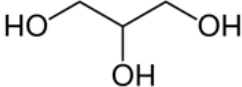
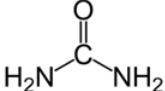
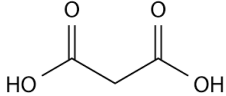
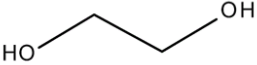
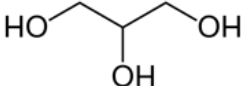
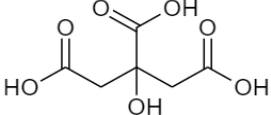
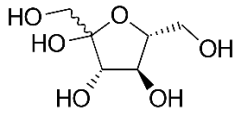
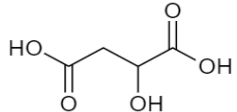
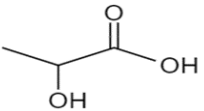
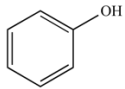
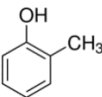


Figure 2.16: Molecular structure of choline chloride: lactic acid NADES with a molar ratio of 1:1

Similar to DES, NADESs are designer solvents as their properties can be tuned according to the targeted application by manipulating the utilized hydrogen bond donor and molar ratio [37]. Furthermore, they are known for their biocompatibility with enzymes and ability to solvate different species of transition metal [37,201]. As a result, they are designated as versatile solvents with a wide range of possible applications such as biodiesel purification from glycerol [209], metal oxides processing [56], and the synthesis of cellulose derivatives [210]. Additionally, NADESs qualify as an alternative of ionic liquids and traditional solvents in a variety of processes including gas adsorption [41,211], and metal ions extraction [212]. Table 2.3 presents some of the choline chloride based natural deep eutectic solvents available in the literature with their physicochemical properties.

Table 2.3: Review of some of the available choline chloride based NADES in the literature

Hydrogen Bond Donor	Molecular Structure	HBA:HBD	Melting	Density	Viscosity	Reference
		Molar Ratio	Point (°C)	(g/cm <sup>3</sup> )	(mPa.s) @ 25°C	
Glycerol		1:2	-40	1.18	259	[213]
Urea		1:2	12	1.25	750	[39,213,214]
Malonic Acid		1:1	10	1.25	1,124	[213,215]
Ethylene Glycol		1:2	-66	1.12	37	[213,216]
Glycerol		1:3	-32.65	1.20	450	[217]
Citric Acid		1:1	43	—	1,003,100	[41]

Hydrogen Bond Donor	Molecular Structure	HBA:HBD	Melting	Density	Viscosity	Reference
		Molar Ratio	Point (°C)	(g/cm <sup>3</sup> )	(mPa.s) @ 25°C	
Fructose		1:1	—	1.23	625	[41]
Malic Acid		1:1	—	1.28	4,4079	[41]
Lactic Acid		1:1	—	1.16	412	[41]
Phenol		1:3	—	1.095	58.8	[218]
O-cresol		1:3	-	1.071	77.6	[218]

#### 2.4.4. Applications

Because of their green properties and remarkable characteristics, DESs are attracting attention as an alternative solvent for a wide variety of applications. Several research studies available in the literature reported the use of DES as a solvent for metal processing, surface fabrication, and coating [219–224]. Furthermore, it has been utilized as a media for the synthesis of polymers, organics, and zeolite analogs [225–228]. A review paper by Alonso et. al. [229], reported the use of DES for the synthesis reaction of more than fifty organic. Additionally, DESs can be employed in electrochemical applications [230], preparation of carbon-carbon nanotube composite [231], leather processing [232], pretreatment of wood cellulose for nano-fibrillation [233], and drug solubilization [234]. Table 2.4 summarize some of the most popular application of choline chloride based DES.

Table 2.4: Applications of choline chloride based deep eutectic solvents

Application	References
CO <sub>2</sub> Capture	[41,235–242]
SO <sub>2</sub> Removal	[49,211,243,244]
Lead Removal	[50]
Denitrification	[245,246]
Polyphenolic Extraction	[247]
Bio-diesel Preparation and Purification	[55]
Removal of Heavy Metal	[53,54]
Removal of Metal oxide	[56]



Application	References
Bio-diesel Production	[57]
Nanoparticle Fabrication	[248–251]

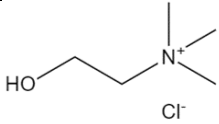
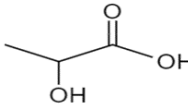
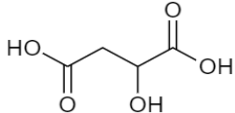
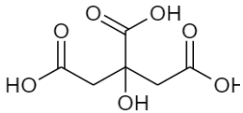
Reflecting on Table 2.4 above, it is worth mentioning that there is no previous application of DES generally or ChCl based NADES specifically in the wastewater treatment and colloidal destabilization field. Therefore, in the upcoming sections, an extensive study on the influence of choline chloride based natural deep eutectic solvents on the electrokinetic properties and rheological behavior of bentonite colloidal dispersion will be conducted.

### 3. MATERIALS AND METHODS

#### 3.1. Materials

All chemicals used in this study for the NADES synthesis were purchased from Sigma Aldrich. Table 3.1 shows the utilized chemicals with their specification including the structure, phase, purity, molecular weight, melting/ boiling point, and their CAS Number.

Table 3.1: Chemicals specifications

Name	Structure	Phase	Purity	Molecular Weight ( $gmol^{-1}$ )	Melting/ boiling Point ( $^{\circ}C$ )	CAS No.
Choline chloride		Solid	98.0%	139.62	302-305	67-48-1
Lactic acid		Liquid	85.0%	90.08	122	50-21-5
Malic acid		Solid	99.0%	134.09	131-133	6915-15-7
Citric acid		Solid	99.5%	192.12	153-159	77-92-9

Bentonite (CAS Number 1302-78-9) purchased from Sigma Aldrich was used with deionized water at room temperature of 25°C to prepare the bentonite suspension. The detailed composition of the bentonite is presented in Table 3.2 as per described by AlShaikh [67]. The Silica gel (CAT No. 297-011-020R) utilized to keep ChCl under dried conditions was purchased from Grifiin & George with a regeneration temperature of 150°C – 175°C. Lastly, hydrochloric acid (CAS Number 7647-01-0) was purchased from Fisher Scientific.

Table 3.2: Chemical composition of Bentonite [67]

Composition	Weight Percent (%)
$Na_2O$	2.43
$K_2O$	0.26
$Fe_2O_3$	3.25
$MgO$	2.67
$Al_2O_3$	24.05
$SiO_2$	58.02
$CaO$	0.75
$FeO$	0.31

## 3.2. Methods

The obtained experimental results in this study were replicated a minimum of three times and the average value was taken for each measurement. The results were reproducible with an experimental error of 5% or less.

### 3.2.1. Synthesis of NADES

In this study, three choline chloride (ChCl) based NADESs were used as coagulants for destabilization and separation of highly stable bentonite colloidal suspension. NADESs were synthesized by mixing ChCl as the HBA with lactic acid (LA), malic acid (MA), or citric acid (CA) as the HBD with a molar ratio of 1:1. ChCl is a hygroscopic substance meaning it tends to absorb moisture from the surrounding environment. Therefore, it was placed in a glass desiccator with silica gel for at least 48 hours prior to its use to remove any water content. Furthermore, a 1000 mL Heidolph rounded flask was dried in a DRY-Line oven at 90°C for 10 minutes to ensure the removal of any water droplets and prevent the absorption of water by ChCl. The molar ratio of the HBA to the HBD was scaled down to 0.25 M for simplicity (i.e., 13.54 g of ChCl and 22.52 g of LA). The required amount of the HBA and HBD were measured using an ISOLAB analytical balance with 0.0001g precision and placed in the flask. The flask was attached to the Heidolph 2 G3 Hei-VAP Precision rotatory evaporator shown in Figure 3.1. The NADES systems were synthesized in an oil bath under atmospheric pressure with continuous heating and mixing at a constant rotational speed till a clear transparent liquid was formed. The synthesis conditions and specification of each system are described in Table 3.3. The liquid NADES was transferred to a 100 mL SCHOTT glass container and stored under dried conditions at room temperature.



Figure 3.1: Heidolph rotatory evaporator

Table 3.3: Specification and synthesis conditions of the prepared NADES systems

HBA	HBD	Molar ratio	Mixing temperature (°C)	Rotational speed (RPM)	Mixing time (hr)	Remarks
ChCl	LA	1:1	80	200	1	Liquid at room temperature
ChCl	MA	1:1	80	200	2-3	Viscous fluid Highly viscous at room temperature
ChCl	CA	1:1	90	200	24	temperature, needs heating to flow

### 3.2.2. Density measurements

Density measurements for the three ChCl-based NADES systems were performed using Anton Paar DMA 4500M densitometer shown in Figure 3.2 which employs the U-tube oscillating principle and provides measurements with 5-digits accuracy ( $\pm 0.00005 \text{ g.cm}^{-3}$ ) [252]. Calibration of the densitometer was performed using water's density as a reference -obtained from Wagner and Pruss fundamental equation of state- to ensure the measurement accuracy of the instrument. The density profiles of ChCl:LA and ChCl:MA NADESs were obtained over a temperature range from 20°C to 80°C at atmospheric pressure of 1 bar. On the other hand, ChCl:CA NADES density profile was attained over a smaller temperature range varying from 45°C to 65°C due to its high viscosity at lower temperatures.



Figure 3.2: Anton Par densitometer

### 3.2.3. Thermogravimetric Analysis (TGA)

Thermogravimetric analysis (TGA) was performed on the synthesized NADES using PerkinElmer Pyris 6 TGA instrument shown in Figure 3.3. TGA instrument was calibrated to verify their performance by running a weight loss experiment of a calcium oxalate sample. The TGA was conducted to obtain the decomposition and onset temperatures of ChCl:LA, ChCl:MA, and ChCl:CA NADES and to analyze their thermal stability. NADES systems were heated from 30°C to 700 °C with an increment of 5 °C per minute under a dried atmosphere using nitrogen gas to generate a weight loss curve.



Figure 3.3: Thermogravimetric analysis instrument

### 3.2.4. FT-IR Spectroscopy

Fourier transform infrared (FT-IR) spectrum is considered as the material fingerprint as no two unique compounds have the same spectrum. Therefore, it can be employed to identify the composition and the bonds of the compound. When IR radiation passes through the sample, part of the radiation gets absorbed while the other is transmitted. The spectrum is created by measuring the energy absorbed by the samples at different wavelengths [253]. NICOLET iS10 Thermo Scientific FT-IR spectrometer shown in Figure 3.4 was used to create the FT-IR spectrums for all raw components (ChCl, LA, MA, and CA) in addition to the spectrum of the three synthesized NADESs (ChCl:LA, ChCl:MA, and ChCl:CA). The spectrums were generated by running 24 scans for each sample over a wavenumber between  $400\text{ cm}^{-1}$  and  $4000\text{ cm}^{-1}$  and a resolution of  $16\text{ cm}^{-1}$ . OMNIC software was employed to process and display the generated FT-IR spectrum.



Figure 3.4: NICOLET iS10 Thermo Scientific FTIR spectrometer.



### 3.2.5. Coagulant preparation

Three different NADES systems were tested as destabilizing agents for bentonite suspension, which are: ChCl:LA, ChCl:MA, and ChCl:CA. In addition, the performance of the constituent components of ChCl:LA NADES (i.e., ChCl and LA) and a binary mixture of ChCl and LA (ChCl-LA) as coagulants were evaluated to assess the influence of each component of the suspension stability. Furthermore, coagulation with the constituent components was performed to analyze the difference. A stock solution with a concentration of 1.2 M was prepared for each coagulant. For ChCl, LA, and the NADES systems, the specified amount of each was mixed with deionized water to prepare the stock solutions. For the coagulation test, a wide range of concentrations ranging from  $2.98 \times 10^{-3} M$  to  $6.76 \times 10^{-2} M$  (0.25 to 6.0 %v/v) was selected to analyze the impact of varying the concentration on bentonite suspension. The coagulant volume required to be added to the suspension was calculated using Eq. 3.1. The required volume was measured using the Thermo Scientific FinnpiPETTE F2 shown in Figure 3.5.

$$\begin{aligned} & \text{coagulant concentration in suspension} \\ &= \frac{\text{coagulant}_{\text{concentration}} \left( \frac{\text{mol}}{\text{mL}} \right) \times \text{coagulant}_{\text{volume}} (\text{mL})}{\left( \frac{\text{coagulant}_{\text{volume}} + \text{suspension}_{\text{volume}}}{1000} \right) (\text{L})} \dots \text{Eq. 3.1} \end{aligned}$$



Figure 3.5: Thermo Scientific FinnpiPETTE F2.

### 3.2.6. Jar Test

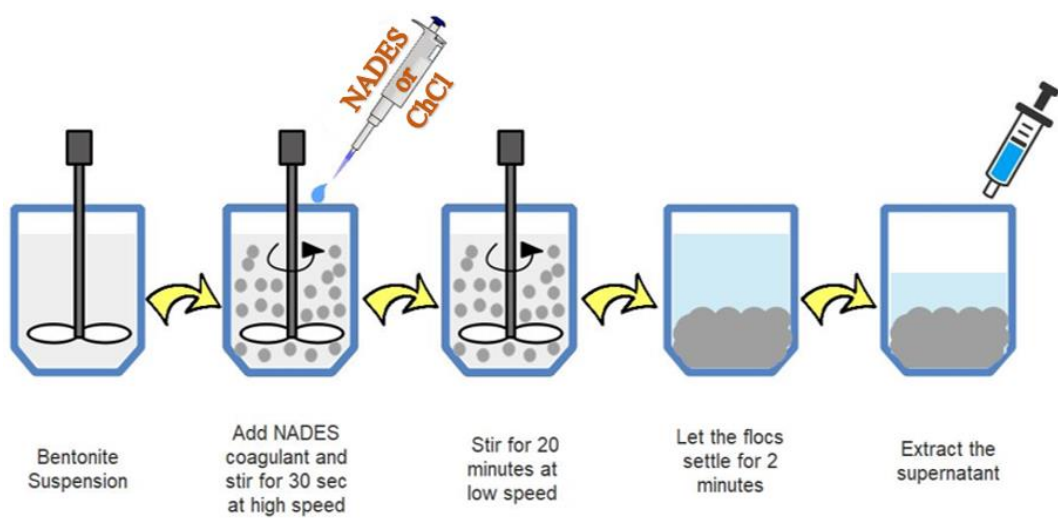
The coagulation test was carried in a Stuart Flocculator SW6 jar test apparatus that consists of six compartments with rectangular paddles (Figure 3.6). The standard coagulation/ flocculation procedure as described in the literature was followed [9,17,171,254]. The coagulation test began with rapid mixing at 180 rpm for 30-60 seconds of the prepared bentonite suspension while simultaneously adding the required coagulant volume followed by a slow mixing stage at 50 rpm for 20 minutes.



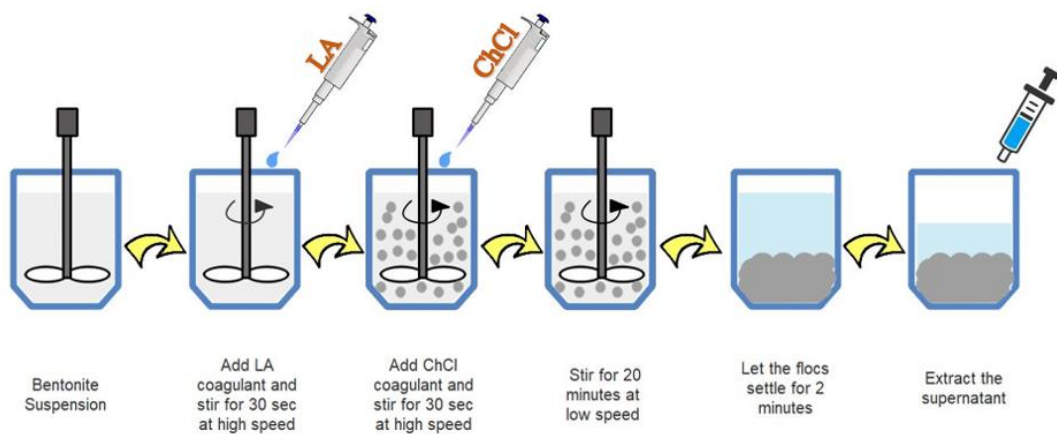
Figure 3.6: Stuart jar test apparatus

Figure 3.7 demonstrates schematically the addition steps of the each coagulant during the coagulation test. Figure 3.7b explains the addition mechanism of the binary ChCl-LA mixture. Equal parts of LA and ChCl coagulants were used in the destabilization process. The required volume of the LA stock solution was added to the bentonite suspension and mixed well at high speed for 30 seconds. Then, the same volume of ChCl stock solution was added to the suspension followed by continuous mixing for 30 seconds. The addition of LA followed by ChCl was found to be better

than adding ChCl followed by LA as the addition of LA at first helps in preparing the media by reducing its pH to around three which promotes destabilization of the system and floc formation. On the other hand, when adding ChCl at first the obtained results in terms of turbidity removal and floc size were found to be very similar to coagulated suspension with ChCl only and the only difference was in the pH value.



(a)



(b)

Figure 3.7: The coagulation test steps of (a) NADES, ChCl, and LA and (b) ChCl-LA mixture coagulants.

### 3.2.7. Zeta potential and turbidity

The influence of varying the pH on the turbidity and zeta potential of the bentonite suspension was studied by adding hydrochloric acid ( $H^+$  ions) to the suspension a drop at a time. The pH of the suspension was measured using HACH HQ11d pH meter. The pH readings varied from 10 to 2 and the effect of this variation on the turbidity and zeta potential was recorded using a HACH 2100N turbidimeter (Figure 3.8) and a Malvern Instruments Ltd. ZEN3600 Zetasizer (Figure 3.9), respectively. Furthermore, the variation in the turbidity and zeta potential of the bentonite suspension upon coagulant addition at different concentrations were analyzed. Bentonite suspension was prepared by mixing 1.5 g of bentonite in 1 L of deionized water using a Fischer Scientific homogenizer for 5 minutes. After the coagulation test, the formed flocs were allowed to settle for 2 minutes before sampling the supernatant for the turbidity and zeta potential measurements.

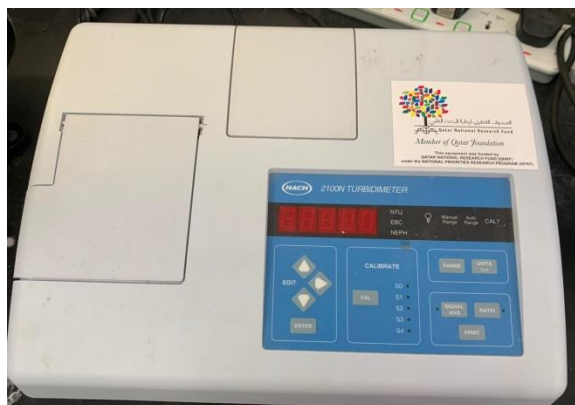


Figure 3.8: HACH 2100 Turbidimeter



(a)

(b)

Figure 3.9: (a) Malvern Instruments Ltd. Zetasizer ZEN3600 (b) measuring cell

### 3.2.8. Particle size distribution

For particle size distribution, bentonite suspension was prepared by mixing 3 g of bentonite in 1 L of deionized water with a Fischer Scientific homogenizer for 5 minutes. The coagulation test was performed following the same procedure as described in section 3.2.6. The particle size distribution was investigated over a wide coagulant concentration ranging from  $2.98 \times 10^{-3} M$  to  $6.76 \times 10^{-2} M$ . The formed flocs were allowed to settle for ten minutes before sampling them for measurements. Samples of the resultant sediments were collected from a fixed position near the bottom of the beaker. The flocs were then analyzed using a Mastersizer 2000 (Malvern Instruments Ltd., UK) shown in Figure 3.10 to study the effect of changing the coagulant type and dosage.



Figure 3.10: Malvern Instruments Ltd. Mastersizer 2000

### 3.2.9. Settling Test

For the settling test, the suspension was prepared by mixing 3 *g* of bentonite in 1 *L* of deionized water with a Fischer Scientific homogenizer for 5 minutes. The prepared suspension was then divided into 200 mL and transferred to graduated cylinders (Figure 3.11). The required coagulant dosage was added to the cylinder and mixed well for 2 minutes using a glass rod. The volume of the interface between the supernatant and the formed flocs was recorded every minute for the first 10 minutes and then every 5 minutes for an hour to generate the settling curve. The final sedimentation volume was recorded after 2 hours.

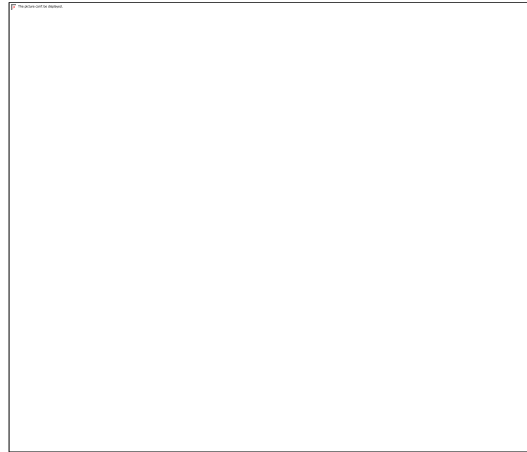


Figure 3.11: Setup for the settling test

### 3.2.10. Response surface methodology

Experimental design and analysis of the obtained data were done through Minitab Software (version 17). The design was generated using response surface methodology (RSM) in combination with the central composite design method (CCD) in order to find the optimum conditions for the coagulation process using ChCl based NADES as a coagulant. Central composite design (CCD) is a sampling design method commonly used in RSM to generate a quadratic (second-order) model by selecting central, axial, and corner points without the need to perform a full factorial design. The bentonite concentration in water and the ChCl:LA dosage were selected as the two dominating variables in the studied process. Therefore, according to Eq. 3.2, the design will have a total of nine experiments: one run at the central point (0,0), four runs at the axial points  $\{(\sqrt{2},0), (-\sqrt{2},0), (0,\sqrt{2}), (0,-\sqrt{2})\}$  and another four runs at the corner points  $\{(1,1), (-1,1), (1,-1), (-1,-1)\}$ .

$$N = 2^k + 2k + 1 \dots \text{Eq. 3.2}$$

Where N is the total experimental runs and k is the number of the studied variables.

However, in CCD designs, additional replicate runs of the central point are required - usually four- resulting in increasing the total number of experiments to exceed “N” [255].

The ranges of both independent variables with the corresponding level for each are presented in Table 3.4. The ranges of the independent variables were selected according to a set of experiments conducted to roughly estimate the operating conditions that maximize the turbidity removal, floc size, and zeta potential reduction separately.

Table 3.4: Experimental Ranges and levels of the independent variables

Variables	Ranges and levels				
	-2	-1	0	1	2
ChCl:LA dosage (mM), $x_1$	2.83	14.0	40.9	67.8	78.9
Bentonite concentration ( $gL^{-1}$ ), $x_2$	0.57	1.5	3.75	6	6.93

Table 3.5 shows the full factorial CCD design (9 experiments) in addition to four replicate experiments for the central points (run number 3, 6, 7, and 11) which are required to estimate the percentage error involved in the developed model [256]. The two independent variables are expressed in terms of their original units in panel B (mM for the ChCl:LA dosage and  $gL^{-1}$  for the bentonite concentration) alongside the design code (panel A). The design code values were as follows: maximum point (2), 1, central point (0), -1, and minimum point (-2). The results of each experiment were



represented in terms of four dependent variables or also known as responses which are zeta potential, turbidity removal percentage, floc size, and pH. The selection of the optimum conditions for the designed process was based on the analyzed data of the four responses and predicted using the second-order quadratic equation illustrated in Equation 3.3 [257]:

$$Y = \beta_0 + \sum_{i=1}^k \beta_i X_i + \sum_{i=1}^k \beta_{ii} X_i^2 + \sum_{i \leq j}^k \sum_j^k \beta_{ij} X_i X_j + \dots + e \dots \text{Eq. 3.3}$$

Where  $i$ ,  $j$ , and  $\beta$  are the linear, the quadratic, and the regression coefficients, respectively. While “ $k$ ” is the number of independent variables of the designed experiment and “ $e$ ” is the random error [258].

The relationship between the two variables and the responses in addition to the significance of the model was evaluated using the P-value with a confidence interval of 95%. Therefore, generated models for each response and model’s terms (i.e.,  $X_i$ ,  $X_i^2$ , and  $X_i X_j$ ) with P-value below 5% (0.05) are identified as significant. On the other hand, when the P-value is higher than 0.05, this indicates that the studied variable or relationship is insignificant and does not have an effect on the process [259]. Furthermore, the quality of the fit of the experimental data to the polynomial model was assessed through the correlation coefficient ( $R^2$  and adjusted  $R^2$ ); the closer the value of  $R^2$  to unity the better the fit of the produced model

Table 3.5: Experimental design run order and conditions.

Run	Panel A		Panel B	
Order	$x_1$	$x_2$	$x_1$ (mM)	$x_2$ (gL <sup>-1</sup> )
1	0	0	40.9	3.75
2	-1	1	14.0	6.00
3	0	0	40.9	3.75
4	0	-2	40.9	0.57
5	-2	0	2.83	3.75
6	0	0	40.9	3.75
7	0	0	40.9	3.75
8	1	1	67.8	6.00
9	2	0	78.9	3.75
10	-1	-1	14.0	1.50
11	0	0	40.9	3.75
12	0	2	40.9	6.93
13	1	-1	67.8	1.50

### 3.2.11. Rheological Measurements

In section 4.4, the rheological and electrokinetic measurements were performed on bentonite suspension with a concentration of 10 g/L. After the completion of the coagulation test, a settling time of 24 hours was given for the treated suspension to settle and stabilize before carefully extracting the supernatant on top. The rheological characteristics of the treated bentonite suspension using ChCl:LA NADES and ChCl-

LA mixture were studied by Anton Paar Rheometer Model MCR 302 using cup and bob measuring geometry presented in Figure 3.12. The prepared bentonite suspensions were mixed gently to create homogenous samples before carefully loading them into the measuring cylinder to avoid disturbing the flocs. Then, an equilibrium time of 3 minutes was given for the samples to stabilize before starting the tests.

The flow behavior of the treated suspensions was examined by studying the viscosity and shear stress as a function of the shear rate which varied between 0.01 to 1000  $s^{-1}$ . Bingham model was used to describe the samples under study which was done through RheoPlus software algorithms to fit the data. Consequently, the viscosity vs. time with a constant shear rate of 1  $s^{-1}$  was conducted in order to examine the thixotropic behavior of formed flocs. In addition, the same test was performed at a higher shear rate of 10  $s^{-1}$  to examine whether the flocs will breakdown to their original state or will maintain their strength even at higher shearing. Furthermore, the elastic and viscous modulus ( $G'$  and  $G''$ ) were studied as functions of the angular frequency in the range of 0.1–500 rad/s and a constant strain of 0.3%. The strain value was selected following a strain sweep test conducted at a constant oscillatory frequency of 6.28 rad/s to ensure that all studied samples fall within the linear viscoelastic region (LVR). All rheological measurements were conducted at a controlled temperature of  $25.0 \pm 0.1^\circ\text{C}$ .

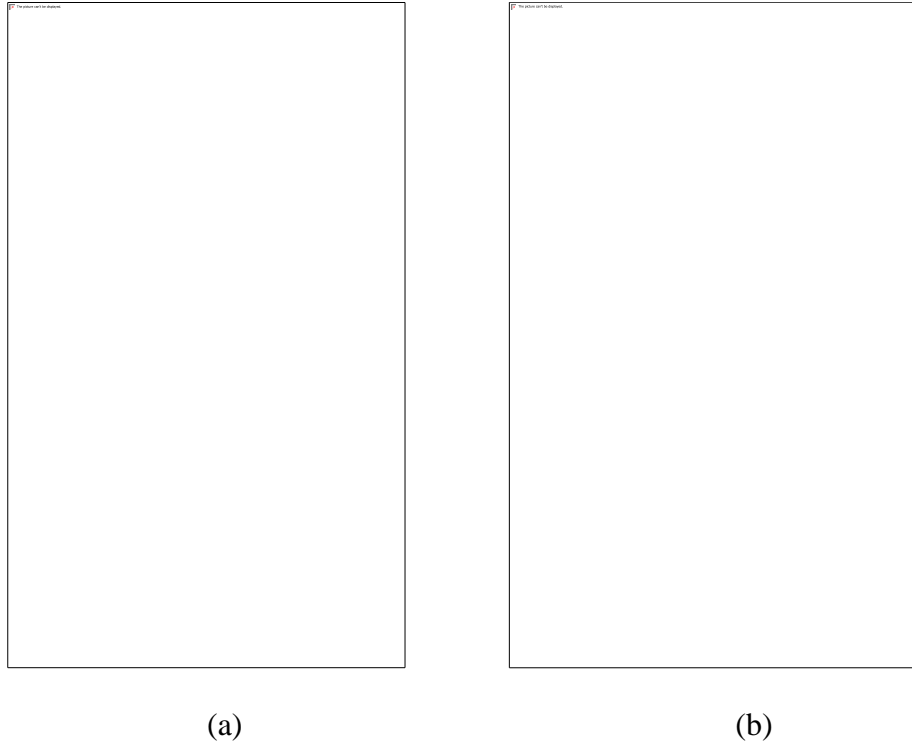


Figure 3.12: (a) Anton Par rheometer model MCR 302 and (b) cup and bob measuring geometry.

### 3.2.12. Capillary suction time (CST)

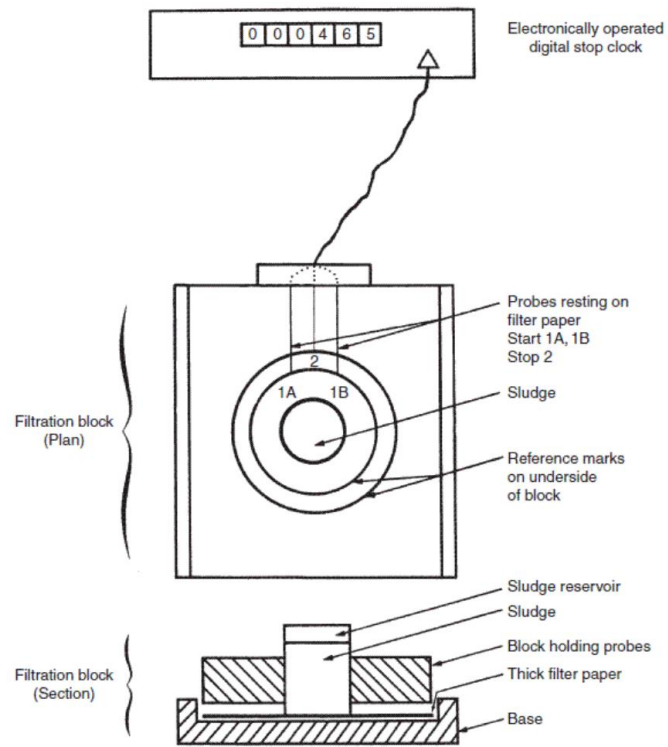
Triton 319 Multi-purpose CST (Triton Electronics Limited, UK) shown in Figure 3.13 was utilized to perform the CST analysis on the treated bentonite suspension. The equipment comprises two Perspex plates with the top one coupled with two-electrode sensors connected to a stopwatch, a filter paper to be placed in between the two plates, and a hollow steel cylinder which represents the filtrate reservoir [153]. The CST values represent the time required for the water within the filtrate in the steel cylinder to move through the filter paper from point 1A where the first electrode sensor is placed to point 1B under the influence of the capillary suction pressure (CSP) (Figure 3.13b). The CSP of the filter paper is around two times the hydrostatic pressure within

the steel cylinder. Hence, the CST is independent of the filtrate volume within the cylinder [260].

CST analysis was conducted on the same bentonite suspension prepared for the rheological measurements in section 3.2.11. The formed sediment was poured into the steel cylinder to the indicated level. The capillary suction pressure acting on the liquid-air interface of the filter paper forces the water from the filtrate to pass through the porous media leaving the sediment cake on top of the filter paper.



(a)



(b)

Figure 3.13: (a) Triton 319 Multi-purpose CST (Triton Electronics Limited, UK) and (b) schematic diagram of the CST apparatus [149].

## 4. RESULTS AND DISCUSSION

### 4.1. Characterization of Choline Chloride Based Natural Deep Eutectic Solvents

#### 4.1.1. Introduction

The following section aims to evaluate the properties of the synthesized NADES (i.e., ChCl:LA, ChCl:MA, and ChCl:CA) in terms of their density profile and thermal stability. Furthermore, analysis of the new interactions formed between the HBD and HBA in each solvent through FT-IR spectroscopy is conducted to confirm the formation of NADES.

#### 4.1.2. Density Measurements

The density profiles of the three NADES systems under study (i.e., ChCl:LA, ChCl:MA, and ChCl:CA) at atmospheric pressure of 1 bar are presented in Figure 4.1. The temperature profile for ChCl:LA and ChCl:MA was performed over a temperature ranging from 25°C – 90°C (298.15K – 363.15K). However, as ChCl:CA exhibits a very high viscosity at room temperature, the density measurements were conducted over a smaller temperature range varying from 42°C – 67°C (315.15K – 340.15K). At a room temperature of 298.15K and atmospheric pressure, the density for ChCl:LA and ChCl:MA were measured to be 1.159 gcm<sup>-3</sup> and 1.278 gcm<sup>-3</sup>, respectively. On the other hand, at a temperature of 318.18 K, the density of the ChCl:CA system was found to be 1.31 gcm<sup>-3</sup>. Furthermore, from Figure 4.1, the density for the systems under study is observed to exhibit a linear decrease with a regression coefficient of 0.99 with increasing the temperature. The reduction in density is attributed to the increase in volume as a result of higher molecular activities in the system. In addition, comparing the overall trend between the three studied systems; ChCl:CA shows the highest density values followed by ChCl:MA and lastly ChCl:LA. The obtained density measurements

show good agreement with the available literature. For example, the thermochemical characteristics of ChCl:LA and ChCl:CA NADESs were investigated in a study conducted by Altamash et. al. [41]. At a temperature of 298.15 K, the density of ChCl:LA was  $1.16 \text{ gcm}^{-3}$ . On the other hand, the density of ChCl:CA was  $1.31 \text{ gcm}^{-3}$  at the same temperature [41].

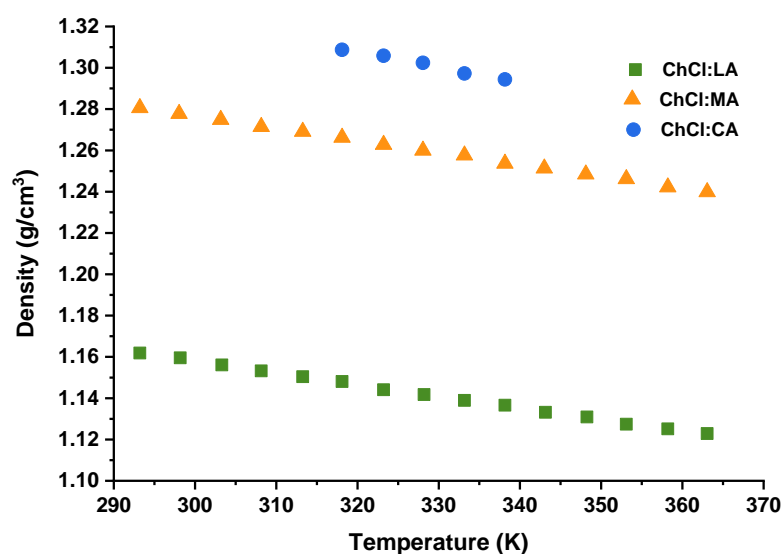


Figure 4.1: Density profile of ChCl:LA, ChCl:MA, and ChCl:CA NADES systems.

### 4.1.3. Thermal Stability

Studying thermal stability for NADESs by performing a TGA analysis is considered a vital step in many applications. Its importance comes from the need to identify the decomposition temperature after which the NADES will start degrading for optimizing the operational temperature of the processes utilizing NADES. The type of HBA and HBD in addition to their molar ratio are the two main factors playing a key role in the thermal stability of NADES. Figure 4.2 illustrates the weight loss curve for



the synthesized NADESs with a molar ratio of 1:1 over a temperature range from 30°C to 500°C (303 K – 773 K). The decomposition process of the systems can be described as a single step degradation with a decomposition temperature ( $T_d$ ) of 460 K, 480 K, and 440 K for ChCl:LA, ChCl:MA, and ChCl:CA, respectively. Multiple studies are available in the literature showing the physiochemical properties of ChCl:LA, ChCl:MA, and ChCl:CA including their thermal stability. Elhamarnah et. al. [42] studied the thermochemical and rheological characteristics of ChCl:MA NADES. The decomposition temperature was measured to be 207 °C (480.15 K). Moreover, Altamash et. al. [41] investigated the properties of several NADES including ChCl:CA and ChCl:LA. The obtained results for the two systems from the thermogravimetric analysis were as follows: ChCl:LA exhibited a decomposition temperature of while ChCl:CA demonstrated a decomposition temperature of 440.15 K. The obtained experimental results for thermal stability and the decomposition temperatures were aligned with values from the literature.

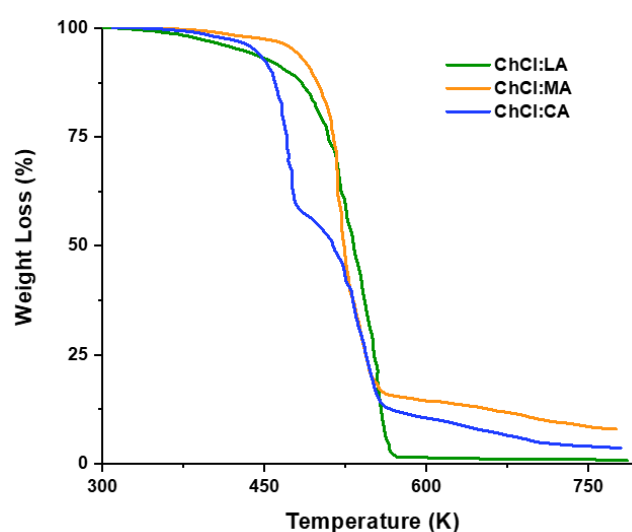


Figure 4.2: weight loss curve of ChCl:LA, ChCl:MA, and ChCl:CA NADES systems

#### 4.1.4. FT-IR Analysis

Figure 4.3, Figure 4.4, and Figure 4.5 show the FT-IR spectrums over a wavenumber ranging from  $400\text{ cm}^{-1}$  to  $4000\text{ cm}^{-1}$  for the constituent components and the three NADES systems i.e., ChCl:LA, ChCl:MA, and ChCl:CA, respectively. Analyzing the functional groups' peaks for each component and comparing them to the peaks in the NADES spectrum is one way to prove the formation of a hydrogen bond between the HBA and HBD which is the reason behind the eutectic characteristics of NADES [261]. From the FT-IR spectrum for ChCl, vibrations at  $3200$ ,  $2850$ ,  $1300 - 1000$ , and  $623\text{ cm}^{-1}$  are observed. The hydroxyl group ( $O - H$  stretching) and the alkane group ( $C - H$  stretching) in the ChCl structure are represented in peaks at  $3200$  and  $2850\text{ cm}^{-1}$ , respectively. Peaks at  $1300 - 1000\text{ cm}^{-1}$  represent the stretching bond between the nitrogen atom in the amine group and the carbon atom in the alkane group ( $C - N$ ) and the stretching carbon oxygen bond in the primary alcohol group [262]. The presence of the chloride ion in the ChCl is illustrated in the vibrational peak at  $623\text{ cm}^{-1}$  [263]. From the LA spectrum in Figure 4.3b, the peak at  $3393\text{ cm}^{-1}$  represents the stretching bond in the hydroxyl group ( $O - H$ ). The trough peak appearance is due to the presence of two hydroxyl group: one from the alcohol group and the other from the carboxylic group. The  $O = C$  in the carboxylic group is shown through the vibrational peak at  $1710\text{ cm}^{-1}$ . The stretching bonds of  $C - O$  and  $C - H$  in addition to the bending bond of  $O - H$  from the hydroxyl and alkane groups in the lactic acid's structure are illustrated in the peaks over a wavenumber from  $1450$  to  $800\text{ cm}^{-1}$ .

A comparison between the three FT-IR spectrums in Figure 4.3 reveals the occurrence of new interactions between ChCl and LA to produce NADES. The shift in the carboxyl group of LA from  $1710\text{ cm}^{-1}$  to  $1741\text{ cm}^{-1}$  in NADES in addition to a

downward shift in the hydroxyl group to  $3290\text{ cm}^{-1}$  and the formation of a wider and flatter peak indicates the formation of a hydrogen bond between the two components ( $O = C - O - H \cdots N$ ). Furthermore, from the NADES spectrum in Figure 4.3c, it can be observed that both components (i.e., ChCl and LA) have retained their structure in the formed solvents. Most of the distinguished peaks in ChCl and LA such as the peaks at  $1710$  and  $1212\text{ cm}^{-1}$  in LA and peaks at  $1150$ ,  $800$ , and  $623\text{ cm}^{-1}$  in ChCl appear in the NADES spectrum as well.

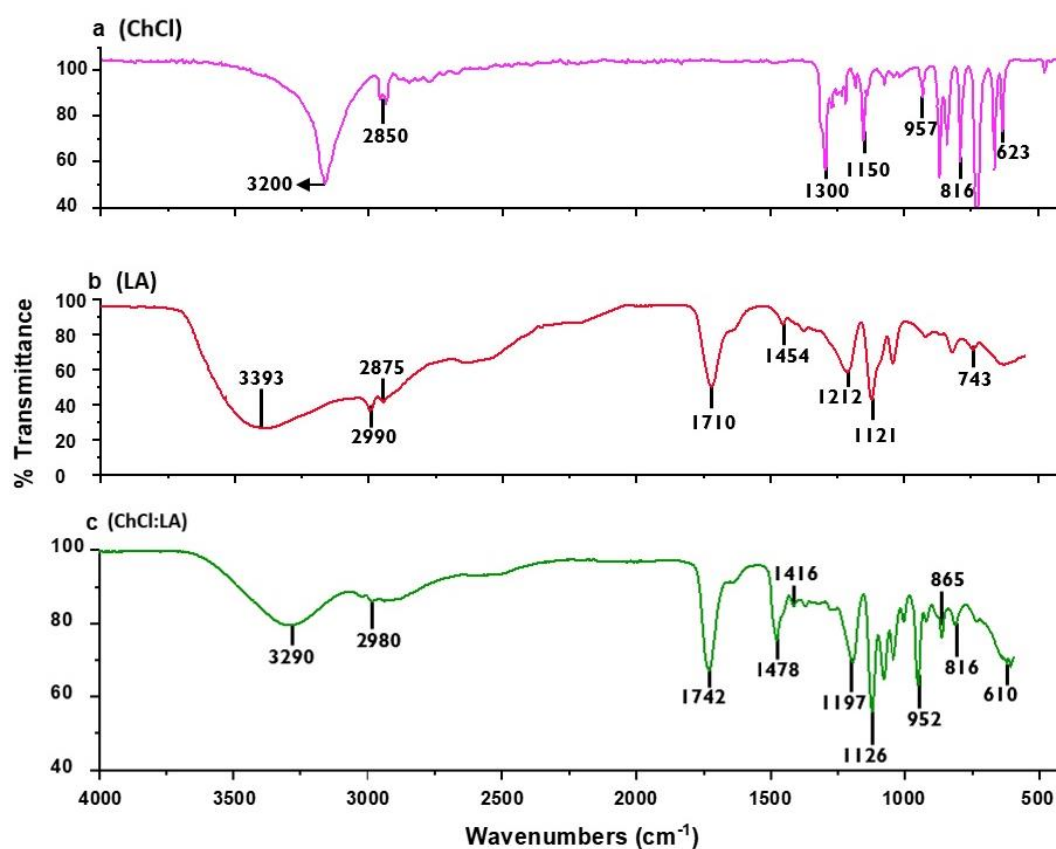


Figure 4.3: FT-IR spectra for (a) ChCl, (b) LA, (c) ChCl:LA

From the FT-IR spectra of MA and CA in Figure 4.4b and Figure 4.5b, respectively, the sharp and the trough peaks ranging between  $3500$  and  $2500\text{ cm}^{-1}$

represent the  $O - H$  stretching in the hydroxyl and carboxyl groups in the acid structures. Furthermore, the peaks at  $1750 - 1690 \text{ cm}^{-1}$  correspond to the carboxylic groups ( $C = O$ ). Multiple peaks are shown in Figure 4.4b and Figure 4.5b due to the presence of more than one  $C = O$  in the structure of MA and CA. The vibrations from  $1450$  to  $800 \text{ cm}^{-1}$  are indication of  $C - O$  stretching,  $O - H$  bending, and  $C - H$  stretching from the hydroxyl and alkane groups in the acids' structures. By comparing the spectrums in Figure 4.4 and Figure 4.5, a shift in peaks of the carboxylic groups from to  $1724 \text{ cm}^{-1}$  and  $1721 \text{ cm}^{-1}$  can be observed in ChCl:MA and ChCl:CA NADESs, respectively. Furthermore, the formation of broader peaks in Figure 4.4c and Figure 4.5c between  $3500$  and  $2500 \text{ cm}^{-1}$  indicates the formation of a hydrogen bond between the nitrogen in the amine group and the hydrogen from the carboxyl group in the acids. Similar to ChCl:LA, by analyzing the FT-IR spectrums for ChCl:MA and ChCl:CA, it can be noticed that both the hydrogen bond donor and acceptor have retained some of their structure as some of the peaks can be observed in both spectrums. For example, the peak at  $623 \text{ cm}^{-1}$  which represents the halogen compound in choline chloride can be observed in all of the NADESs spectrums as well. The obtained results show good agreement with the data available in the literature and prove the formation of the new hydrogen bonding in the synthesized DES in this work [261–266].

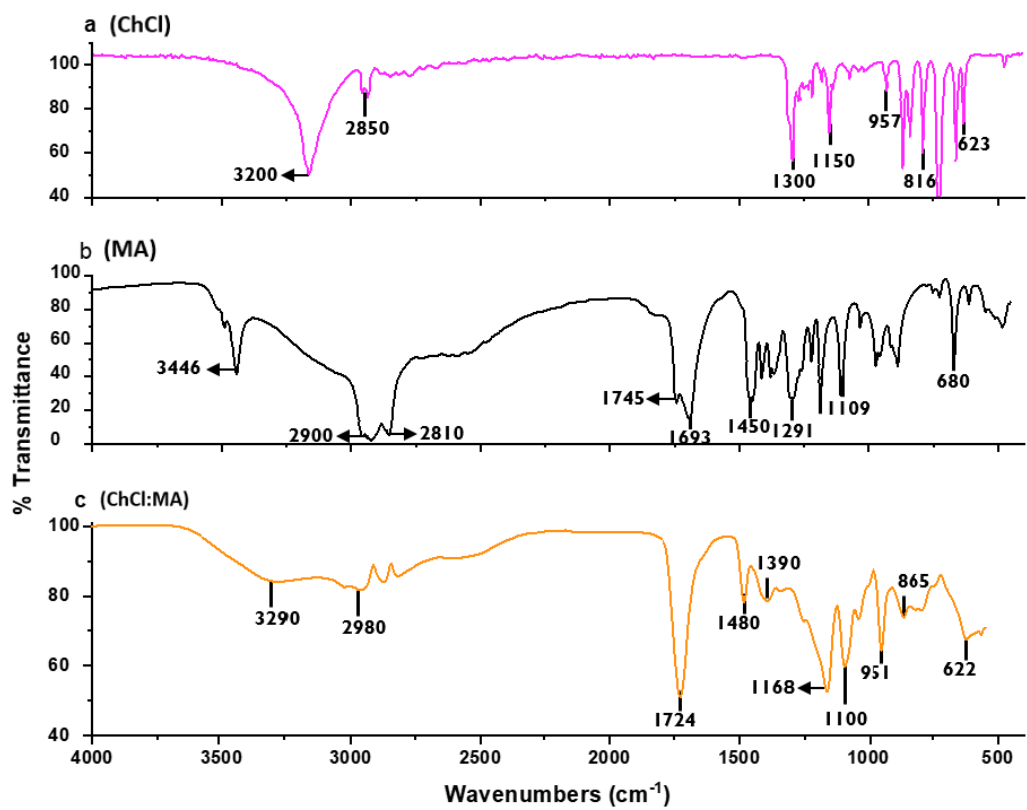


Figure 4.4: FT-IR spectrums for (a) ChCl, (b) MA, (c) ChCl:MA

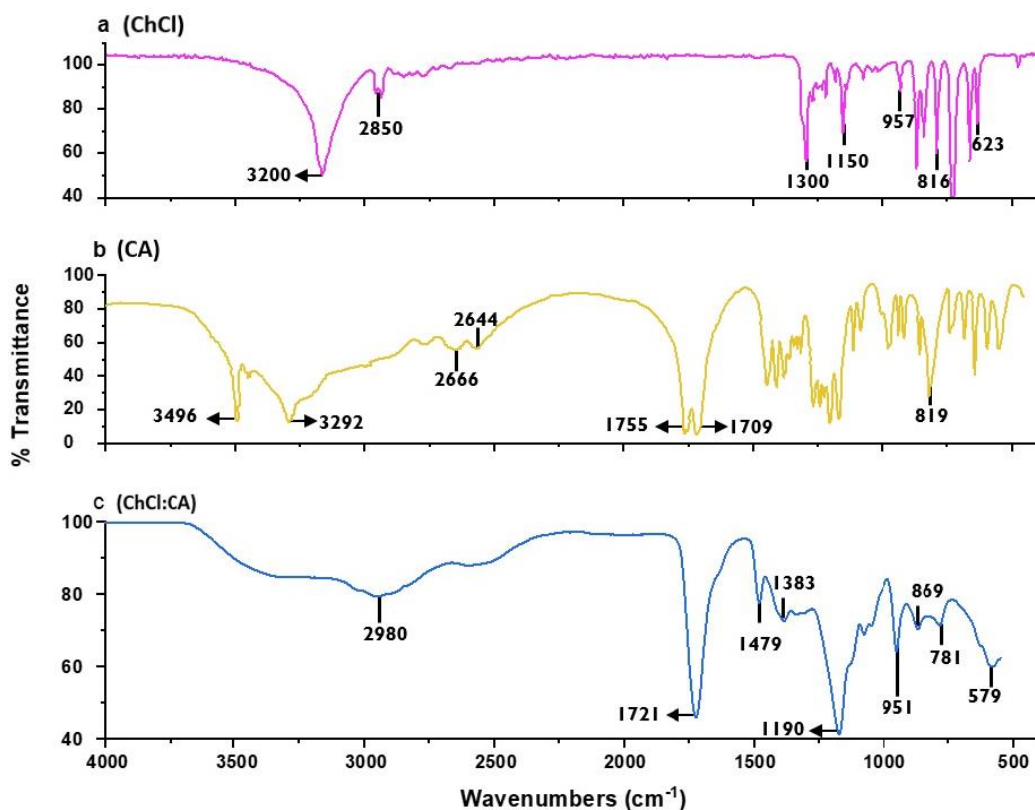


Figure 4.5: FT-IR spectrums for (a) ChCl, (b) CA, (c) ChCl:CA

#### 4.1.5. Conclusions

Some of the physical and thermal properties of the three NADES systems under study including their density and thermal stability were investigated. Furthermore, the FT-IR analysis of the synthesized NADES and their individual components was performed to identify the functional groups in each component and to confirm the formation of new interactions between them. The conducted characterization study revealed the following conclusions:

- The hydrogen bond donor had a significant effect on the analyzed properties for the NADES systems.
- For all three NADES systems under study, the density was found to decrease linearly upon increasing the temperature at a constant pressure.

- The highest density was exhibited by ChCl:CA due to the strong interaction between the components followed by ChCl:MA and ChCl:LA.
- With a decomposition temperature ( $T_d$ ) of 480 K (207°C), ChCl:MA NADES is the most stable system under a wide temperature range followed by ChCl:LA and ChCl:CA.
- From the FT-IR analysis, the formation of a hydrogen bond between the hydrogen atom in the carboxylic group in the acid and the nitrogen atom in the amine group in ChCl was confirmed.
- The obtained results were in good agreement and comparable to the available data in the literature.

## **4.2. Choline Chloride Based Natural Deep Eutectic Solvent for Destabilization and Separation of Stable Colloidal Dispersions**

### **4.2.1. Introduction**

In the following section and for the first time, choline chloride (ChCl) based NADES is introduced as a coagulant for bentonite suspension. The utilized NADES is synthesized from ChCl as the HBA and lactic acid (LA) as the HBD with a 1:1 molar ratio. This study concerns with analyzing the influence of ChCl:LA dosage on the coagulation process of bentonite suspension and determining the destabilization mechanism exhibited by NADES. Furthermore, it evaluates the effect of water on NADES interactions and its performance as a coagulant in comparison to its components. Hence, the influence of ChCl, LA, and a binary mixture of the two components (will be referred to as ChCl-LA) on the stability of bentonite suspension is investigated. The efficiency of each coagulant (i.e., ChCl, LA, ChCl-LA, and NADES) is examined using key experimental parameters for coagulation including turbidity and zeta potential measurements of the supernatant, floc size distribution, settling rate, and final sedimentation volume.

### **4.2.2. pH dependence of Zeta and Turbidity Measurements**

The effect of varying the pH of the bentonite suspension on its turbidity and zeta potential is presented in Figure 4.6. At initial conditions and prior to the hydrochloric acid addition, bentonite suspension represents a basic media with a pH of 10. As a result, both the edges and the faces of bentonite particles possess are negatively charged. Therefore, at a pH of 10, the turbidity and zeta potential of the suspension were 350 NTU and  $-40.4$  mV, respectively. Upon adding the  $H^+$  ions, the pH decreases gradually with no significant change in the turbidity measurements. When the pH reaches 2 a drastic decrease in turbidity from 325 NTU to 11.2 NTU is exhibited



resulting in a relatively clear supernatant. Furthermore, by reducing the pH of the suspension toward more acidic conditions, the zeta potential moves toward a less negative potential gradually. The reduction in the negative zeta potential is due to neutralizing part of the negative charges on the bentonite particles by increasing the concentration of the hydrogen ions in the suspension [17]. Consequently, the repulsive forces between the particles and therefore the stability of the suspension are reduced allowing the edge and faces of the bentonite platelets to come closer together producing an edge-to-face (EF) structure and hence, settle without coagulation [17].

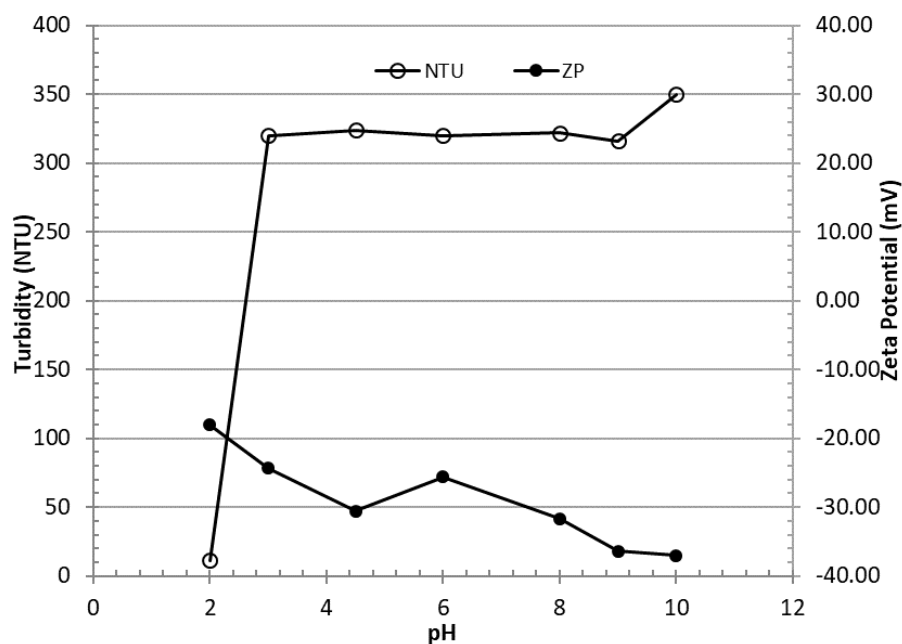


Figure 4.6: Effect of pH on the turbidity and zeta potential of bentonite suspension.

#### 4.2.3. Zeta and Turbidity Results of Bentonite

Turbid systems are very stable and usually associated with a highly positive or highly negative zeta potential. According to the world health organization (WHO), a

turbidity of 5 NTU or below is acceptable for agriculture and drinking water while ideally turbidity of 0.1 NTU is preferred for drinking water [145,267].

Some researchers have shown that deep eutectic solvents dissociate in water at different degrees. According to D'Agostino et. al. [268], the dissociation degree of deep eutectic solvents in water relies on the hydrogen bond donor and acceptor of the synthesized solvent. Furthermore, in a study conducted by Hammond et. al. [269], it was proven that above 42 wt% of water the DES–DES interactions in the studied system start to weaken, and above 52 wt% of water the DES–water interactions become stronger and dominant in the system and it can be described as an aqueous solution of DES components. Therefore, to analyze the effect of water on the prepared ChCl:LA NADES and its efficiency as a destabilizing agent; ChCl, LA, and a mixture of both components (ChCl-LA) were examined as destabilizing agents for bentonite suspension. Figure 4.7 shows the turbidity and zeta potential behavior for coagulated bentonite suspensions with four different additives (a) ChCl, (b) ChCl-LA, (c) ChCl:LA NADES, and (d) LA. Prior to the addition of coagulant, both the edge and face of the bentonite particles were negatively charged with a zeta potential of  $-40.4\text{ mV}$  and turbidity of 350 NTU. Figure 4.7a illustrates the turbidity and zeta potential measurements for bentonite suspension treated with ChCl as a coagulant. A small reduction in the negative zeta potential to around  $-30\text{ mV}$  is obtained at a concentration of  $1.78 \times 10^{-2}\text{ M}$  (1.48 %v/v) due to the presence of a positively charged functional group in the ChCl structure. Furthermore, ChCl was found to be effective in terms of turbidity reduction; achieving a removal percentage of 98%. It is worthy to mention that the pH of the dispersion remains constant at pH of  $\sim 9$  after ChCl addition.

Next, the binary mixture of ChCl and LA (ChCl-LA mixture) was assessed as a coagulant for the same bentonite suspension to further investigate the difference in the

performance with the synthesized NADES. The zeta potential and the turbidity results for suspensions treated with ChCl-LA mixture with variable concentrations are displayed in Figure 4.7b. At a concentration of  $1.78 \times 10^{-2} M$ , a reduction in turbidity and the negative zeta potential to 4.3 NTU (98.8%) and  $-22.5 mV$ , respectively were achieved. Hence, the ChCl-LA mixture performance is very similar to the ChCl and the effect of LA was observed in a further reduction in the negative zeta potential only.

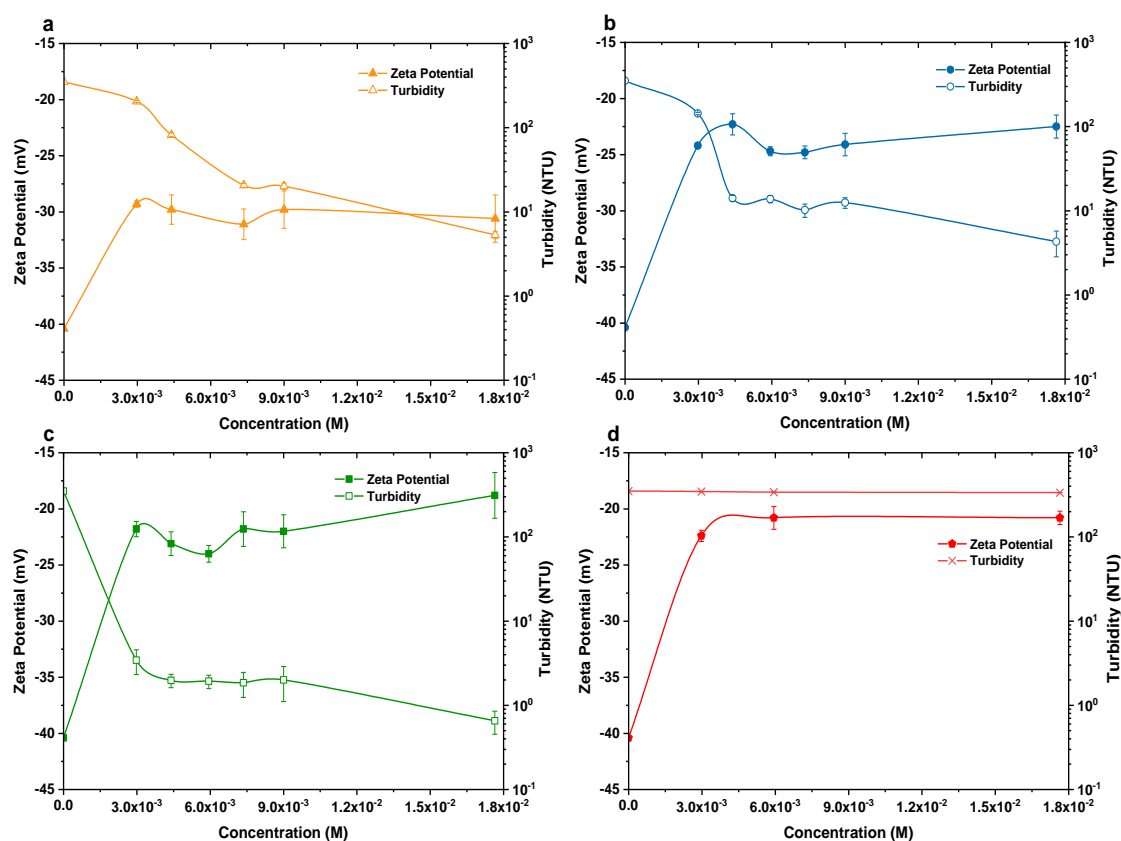


Figure 4.7: Turbidity and Zeta Potential of Bentonite Suspension as a function of (a) ChCl, (b) ChCl-LA, (c) ChCl:LA NADES, and (d) LA concentrations.

The effect of NADES on the turbidity and zeta potential of bentonite suspension is illustrated in Figure 4.7c. A reduction in the magnitude of the zeta potential to  $-18.8\text{ mV}$  at a concentration of  $1.78 \times 10^{-2}\text{ M}$  is associated with reduction in the turbidity of the supernatant to below 1 NTU resulting in achieving a 99.8% removal percentage and a clear supernatant. The high turbidity removal percentage combined with a negative zeta potential can be attributed to the electrostatic patch coagulation mechanism (EPC) where turbidity is efficiently removed without fully neutralizing the negative charges possessed by the clay's particles [106].

To explain the mechanism further, Figure 4.8 below shows the chemical structure of the cationic polyacrylamide (CPAM) and ChCl. CPAM is a cationic polymer with a high molecular weight used as a flocculant for the treatment of clay colloidal suspension. The cationic properties of the polymer come from the quaternary ammonium group giving it an advantage over anionic and amphoteric polymers [17]. Figure 6b shows the chemical structure of ChCl. The similarity in structure between the cationic PAM and ChCl especially in the presence of the quaternary ammonium group, which play a vital role in the destabilizing process, rose our attention to the potential use of choline chloride based NADES as a destabilizing agent and as an alternative for inorganic coagulants such as multivalent metal salts represented in aluminum sulfate, ferrous sulfate, ferric chloride, and ferric chloro-sulfate which have a potential environmental risk due to the presence of residual metals in the treated water. ChCl and cationic PAM have the same quaternary ammonium salt that promotes responsible for the destabilization and charge neutralization of the colloids during the flocculation process [17]. However, the number positively charged ammonium salt on the PAM surface depends on the PAM molecular weight while choline chloride has only one. Therefore, it is desired to study the similarity and differences in their mechanism and

performance as a destabilizing agent in addition to understand the role of ChCl presented in NADES during the destabilization process.

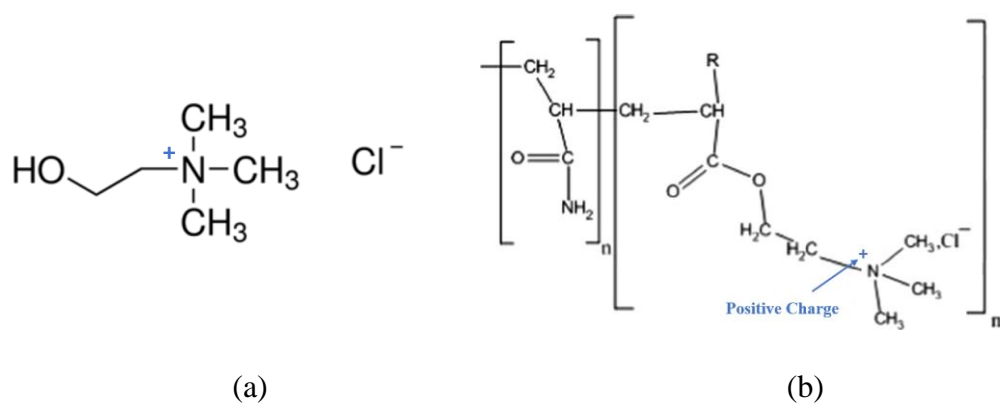


Figure 4.8: Chemical Structure of (a) Choline Chloride and (b) Cationic Polyacrylamide [67]

Flocculation of bentonite using PAM occurs through the adsorption of polyacrylamide primary amide functional groups onto the edge surface of bentonite (i.e. aluminol (Al-OH) and silanol (Si-OH) groups) via hydrogen bonding [17]. Thus, charge neutralization becomes a major mechanism, where the cationic PAM will locally reverse the particle surface charge. Collision with negative patches on another particle allows bridging (Figure 4.10) then aggregation producing big flocs [169].

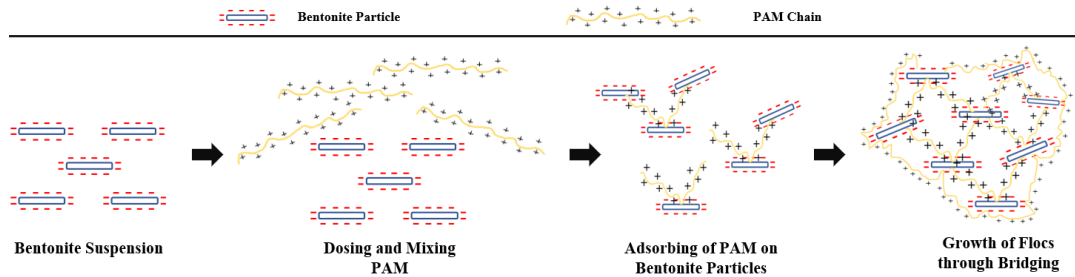


Figure 4.9: Flocculation through bridging mechanism using cationic polymer (PAM)

On the other hand, for ChCl, the coagulation process occurs through partial charge neutralization due to the attraction between the negatively charged bentonite surface and the positively charged ChCl. However, bridging is not possible as in the PAM case. Hence, coagulation occurs through the electrostatic patch (ESP) mechanism described in Figure 4.10. Consequently, the flocs grow through the electrostatic patch forces.

ESP coagulation takes place when a coagulant with low molecular weight/short-chain is utilized to destabilize colloidal and suspended particles in water. In this case, two zones will appear on the colloidal particles: the uncovered zone and the neutralized zone occurring as patches due to adsorption of an oppositely charged coagulant. As a result, particles' aggregation will occur and loose flocs will form due to the weak interaction between the particles. suspensions with high turbidity can be treated efficiently by electrostatic coagulation without the need to fully neutralize the surface charge of the particles [106]. Both coagulation through ESP and flocculation via bridging have efficient results in terms of turbidity removal and supernatant clarity, however, the main difference is the formation of larger and stronger flocs through bridging due to the longer chains of the utilized agent.

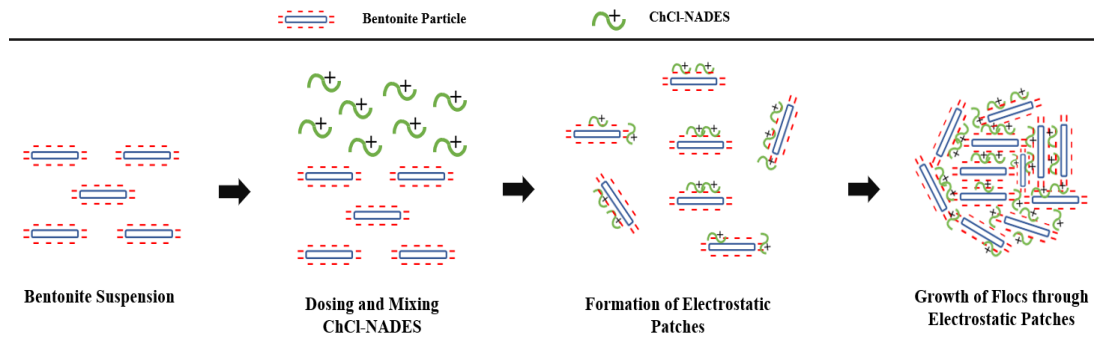


Figure 4.10: Coagulation through electrostatic patch mechanism using ChCl based NADES

Figure 4.7d represents the changes in the magnitude of zeta potential and turbidity upon the addition of LA at different concentrations to the bentonite suspension. It can be observed that in terms of turbidity reduction, LA was not efficient as the obtained turbidity at a concentration of  $1.78 \times 10^{-2} M$  was 336 NTU which is in the same range as the untreated bentonite suspension. However, a significant drop in the zeta potential magnitude to  $-22 mV$  is observed which is attributed to the positive charges gained by edges of the bentonite particles under low pH conditions [270]. At the same concentration of  $1.78 \times 10^{-2} M$ , suspensions treated with NADES, ChCl-LA, and LA exhibit the same pH value of  $\sim 3$ . Hence, the acidic environment by itself does not represent the only reason behind the high turbidity removal percentage obtained when NADES and ChCl-LA mixture were utilized for the destabilization of bentonite colloidal particles.

Destabilization and coagulation of bentonite suspension through the EPC mechanism were exhibited when NADES, ChCl, and ChCl-LA mixture were employed as destabilizing agents. At the highest analyzed concentration (i.e.,  $1.78 \times 10^{-2} M$ ), close results were obtained for the three active coagulants. Nevertheless, NADES was

the most efficient coagulant even at a very low dosage of  $2.9 \times 10^{-3} M$  (i.e., 0.25 %v/v) achieving supernatant turbidity of less than 5 NTU. While for ChCl and ChCl-LA mixture, a higher dosage was required to achieve a similar performance level as NADES. Both NADES components, ChCl and LA, affected the bentonite suspension in terms of turbidity removal and zeta potential, respectively. However, the formation of a hydrogen bond between the HBD and HBA in the NADES resulted in a coagulant with a higher molecular weight and a longer chain, therefore, a better destabilization performance

To further show the effectiveness of each proposed coagulant; turbidity of 5 NTU was set as a standard value as it represents the upper limit of the allowed turbidity for agriculture and drinking water [145,267]. Figure 4.11 and Table 4.1 show the concentration of each coagulant at which the supernatant turbidity is equal to or less than 5 NTU. Only NADES and ChCl-LA mixture were able to achieve the required target at a concentration of  $2.80 \times 10^{-3} M$  (0.23 %v/v) and  $1.69 \times 10^{-2} M$  (1.42 %v/v), respectively. However, the needed concentration to achieve the targeted value using ChCl-LA coagulant was around six times higher than the NADES concentration.

Table 4.1: Concentration of Coagulant Required to Achieve Turbidity  $\leq 5$  NTU

Coagulant	Coagulant Concentration (M)	Turbidity (NTU)
NADES	$2.80 \times 10^{-3}$	5
ChCl-LA	$1.69E \times 10^{-2}$	5
ChCl	NA	NA
LA	NA	NA



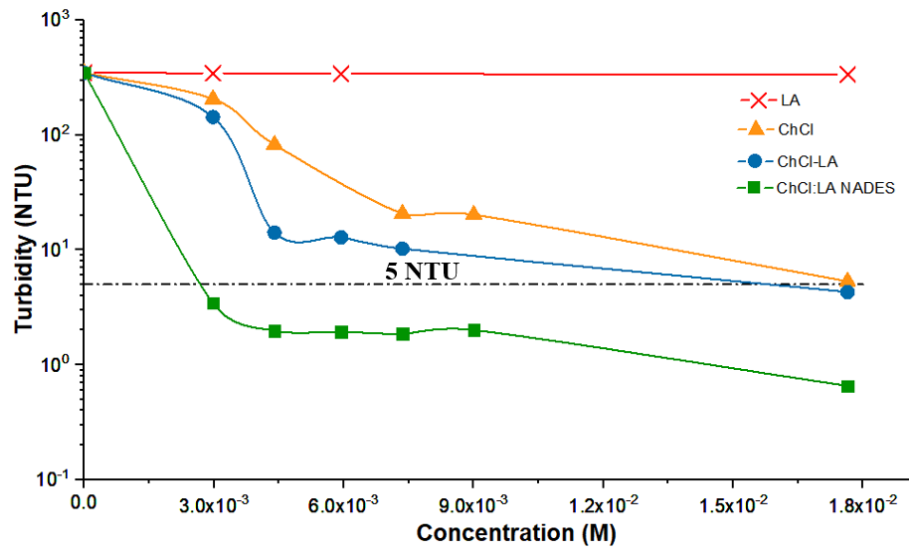


Figure 4.11: Turbidity of Bentonite suspension as a function of concentration for all tested coagulants

#### 4.2.4. Floc size distribution

The size of the produced flocs in the coagulation process can be expressed in terms of the D-values.  $D_{10}$ ,  $D_{50}$ , and  $D_{90}$  provide the floc diameter at 10%, 50%, and 90% in the cumulative floc size distribution, respectively. Commonly,  $D_{50}$  describes the median diameter of particles before and after the coagulant addition. Therefore, in the present study,  $D_{50}$  is employed to investigate the influence of coagulant type and concentration on the size and characteristics of the formed floc. The main purpose of the treatment process through destabilization of colloidal particles is represented in the turbidity reduction and formation of clear supernatant. However, the ease of the handling process of the produced sediments in further treatment stages is very crucial. Therefore, the particle size distribution was analyzed over a wider coagulant concentration range.

Table 4.2 presents the particles median diameter of both untreated and treated suspensions with concentrations of  $3.48 \times 10^{-2} M$  and  $6.76 \times 10^{-2} M$ . Untreated bentonite suspension possesses very fine particles with a median diameter of  $2.5 \mu m$ . Similar to the results obtained from the turbidity measurements, suspensions treated with LA did not show any significant changes in the floc size even at a high dosage compared to untreated suspension. For example, at a coagulant concentration of  $3.48 \times 10^{-2} M$  and  $6.76 \times 10^{-2} M$  the resultant sediment had a floc size with a  $D_{50}$  of  $2.6 \mu m$  and  $3.3 \mu m$ , respectively. Thus, the use of LA for coagulation of bentonite suspension is not efficient. Furthermore, any reduction in the turbidity is attributed to the precipitation of particles without aggregation confirming the obtained results in Figure 4.7.

Table 4.2: Coagulant Dosage with Corresponding Median Floc Diameter

Coagulant	Coagulant Concentration (Molar)	$D_{50}$ ( $\mu m$ )
-	-	2.50
NADES	$3.48 \times 10^{-2}$	21.80
	$6.76 \times 10^{-2}$	36.70
ChCl-LA	$3.48 \times 10^{-2}$	8.57
	$6.76 \times 10^{-2}$	12.30
ChCl	$3.48 \times 10^{-2}$	5.74
	$6.76 \times 10^{-2}$	10.50
LA	$3.48 \times 10^{-2}$	2.55
	$6.76 \times 10^{-2}$	3.30

Figure 4.12 illustrates a comparison between the coagulants (i.e., NADES, ChCl, and ChCl-LA) in terms of the floc size as a function of concentration. It can be observed that the floc size increases gradually with concentration upon the addition of ChCl, the mixture of ChCl-LA, or NADES. At the same coagulant dosage, it is clear that NADES forms the largest flocs with a median diameter of  $36.7 \mu\text{m}$  due to the stronger interaction between the bentonite particles and the NADES chains. Therefore, it can be concluded that ChCl:LA NADES shows the best performance as a destabilizing agent even at lower concentrations compared to ChCl, LA and the ChCl-LA mixture. Furthermore, it is worth mentioning that even though some studies showed that above 52 wt% of water the DES system will be described as an aqueous solution of DES components, however, the destabilization process of colloids and floc formation are very fast and occur within seconds. Therefore, the addition of NADES to the bentonite suspension results in better outcomes compared to the mixture of ChCl and LA (ChCl-LA). This supports the hypothesis that NADES still retain their structure within the first seconds of addition and their superior effect is clear on bentonite suspension stability.

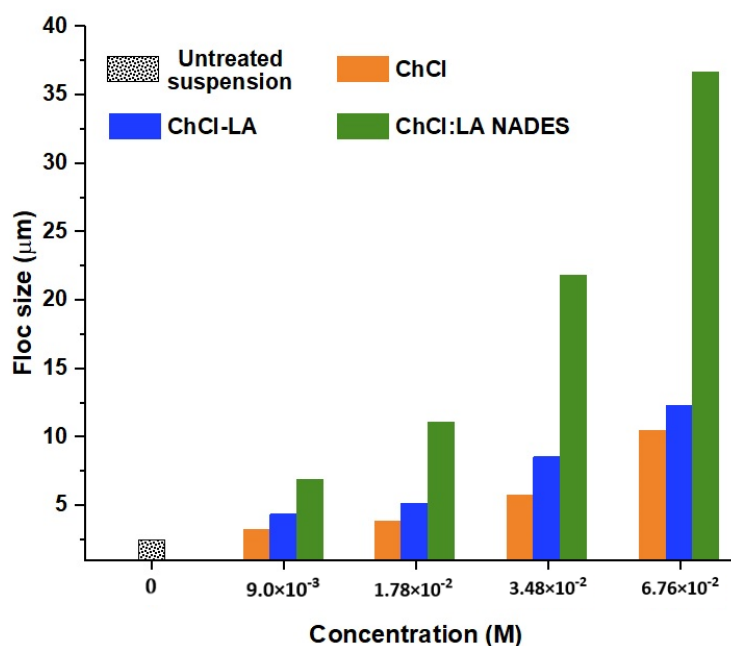


Figure 4.12: Floc size of bentonite suspension treated with ChCl, ChCl-LA, and NADES at different concentrations

Figure 4.13 represents the particle size distribution of suspensions treated with NADES, ChCl, and ChCl-LA at a constant concentration of  $6.76 \times 10^{-2} M$ . It can be observed from Figure 4.13 that when a coagulant with a greater molecular weight/ longer chain is utilized, the distribution peak shift to the right of the untreated suspension's peak indicating the formation of larger flocs [17]. Hence, NADES ( $MW = 229.70 g/mol$ ) resulted in the formation of the largest flocs with a  $D_{50}$  of  $36.7 \mu m$  followed by ChCl-LA mixture  $D_{50}$  of  $12.3 \mu m$ . Lastly, the smallest flocs with a median diameter of  $10.5 \mu m$  were formed when ChCl ( $MW = 139.6 g/mol$ ) was utilized as a coagulant. Larger flocs were formed by ChCl-LA coagulant compared to ChCl coagulant due to the effect of LA on the pH of the suspension. As a result, the edges of the clay particles became positively charged and are attracted to the negatively charged faces of the particles leading to the formation of larger flocs.

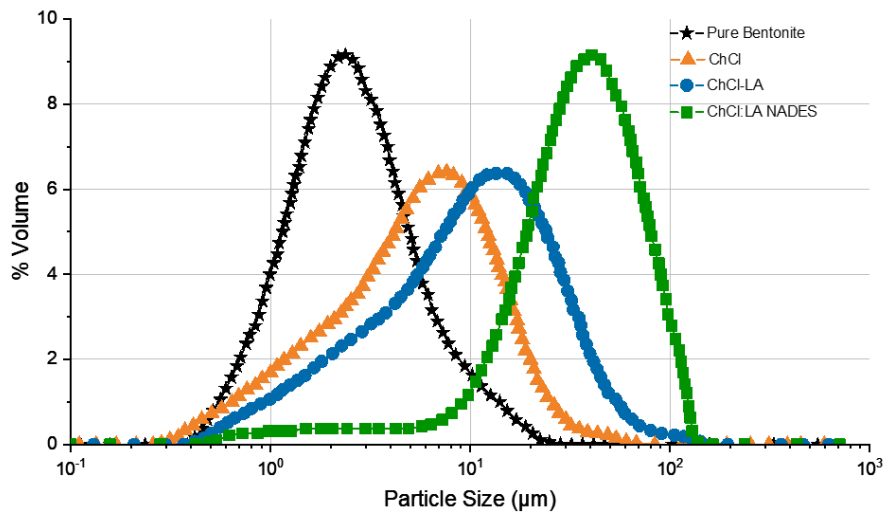


Figure 4.13: Floc size distribution of bentonite suspension treated with 3 coagulants at a concentration of  $6.76 \times 10^{-2} M$

Furthermore, the size of the formed flocs is highly influenced by the concentration of the coagulant in the suspension. Figure 4.14 represents the particle size distribution of suspensions treated with NADES as a function of concentration. Upon increasing the NADES concentration in the suspension from  $9.0 \times 10^{-3} M$  to  $6.76 \times 10^{-2} M$ , the distribution peak shift to the right of the untreated suspension peak. Thus, increasing the dosage up to a certain limit is associated with an increase in the size of the formed flocs. Similarly, ChCl and ChCl-LA mixture demonstrate the same behavior upon increasing the utilized concentration. The increase in the floc size upon increasing the coagulant concentration arises from neutralizing more patches on the particles' surface and hence, further reduction in the repulsive forces. Accordingly, more particles will move closer to each other forming larger flocs.

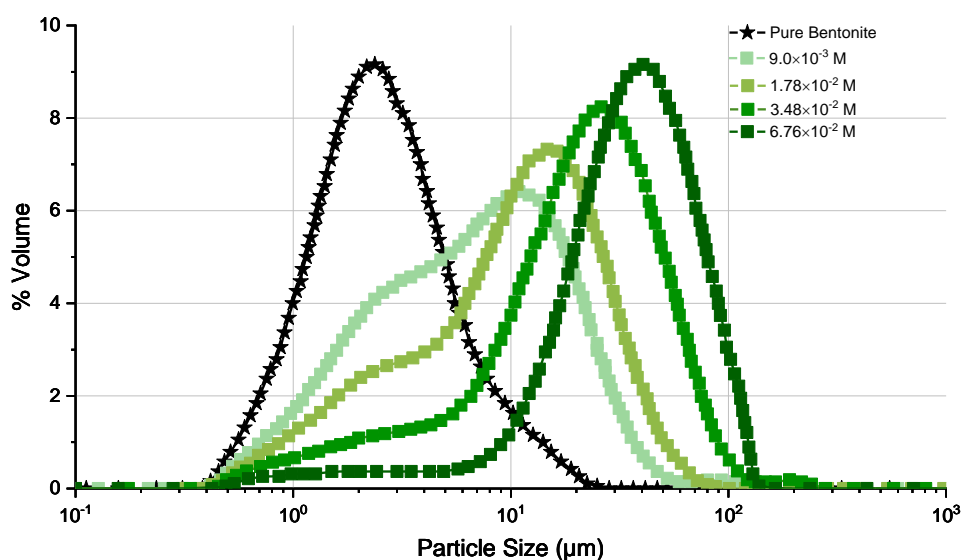
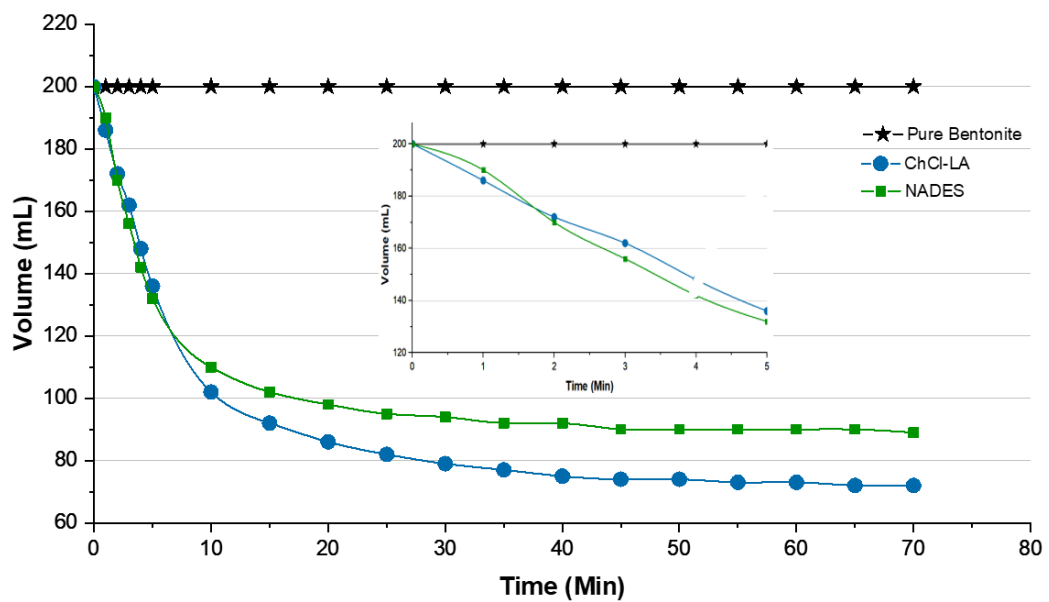


Figure 4.14: Floc size distribution of bentonite suspension treated with NADES at different concentrations.

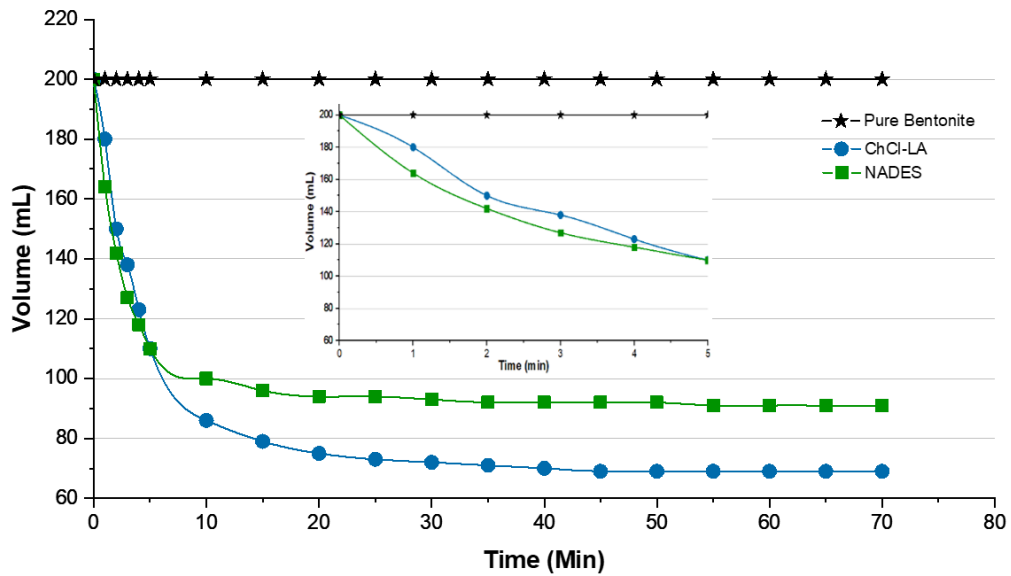
#### 4.2.5. Settling Behavior

The settling test is an analysis method to evaluate the settling ability and characteristics of the formed flocs. The settling behavior of the flocs is a function of the floc size, the coagulant type and dosage, and the ratio of solid to water. Large flocs with rapid settling rate and high compactness properties are desirable in water treatment processes [170]. The settling rate and the final sediment volume for suspensions treated with NADES and ChCl-LA at concentrations of  $3.48 \times 10^{-2} M$  and  $6.76 \times 10^{-2} M$  are illustrated in Figure 4.15. The final sediment volume of the treated bentonite is in agreement with the floc size results. From Figure 4.15, it can be observed that the final settling volume for suspensions treated with NADES is greater than that for suspensions treated with ChCl-LA mixture. Furthermore, the final volume of NADES is reached faster than ChCl-LA mixture. For instance, at a constant concentration of  $3.48 \times 10^{-2} M$ , final settling volume of 90 mL was reached after 45 min for

suspension treated with NADES. On the other hand, suspension treated with ChCl-LA mixture exhibited a final settling volume of 75 mL after 60 min. The higher settling rate and volume exhibited by suspensions treated with NADES are attributed to the formation of larger flocs, almost 2.5 times the flocs formed by ChCl-LA mixture. Moreover, increasing the applied dosage is associated with the formation of flocs with greater median diameter. Hence, a faster settling rate and larger sediment volume are expected upon increasing the dosage. For NADES, increasing the concentration from  $3.48 \times 10^{-2} M$  to  $6.76 \times 10^{-2} M$  the settling time decreased from 45 min to 30 min. Eventhough larger flocs were produced at  $6.76 \times 10^{-2} M$ , however, due to their higher compactness the settling volume remained the same (i.e., 90 mL).



(a)



(b)

Figure 4.15: Settling Behavior of Bentonite Suspension Treated with 3 coagulants at (a)  $3.48 \times 10^{-2} \text{M}$  and (b)  $6.76 \times 10^{-2} \text{M}$ . The onsets display a closer look for the first 5 minutes.

#### 4.2.6. Conclusions

NADES, ChCl, ChCl-LA, and LA were tested as destabilizing agents for stable bentonite suspension. The study was conducted to evaluate the efficiency and performance of NADES as coagulants and to determine the effect of each component on the stability of the suspension. Zeta potential, turbidity measurement, floc size distributions, and settling test were used as evaluation methods for all coagulants. From the obtained results, the following conclusions can be made:

- NADES was the most effective coagulant with almost a 100% turbidity removal associated with the highest reduction of the negative zeta potential ( $-18 \text{mV}$ ) and flocs with the largest median diameter followed by ChCl-LA mixture and ChCl.



- ChCl and ChCl-LA mixture gave relatively similar outcomes in terms of turbidity while less negative zeta potential and larger flocs were achieved using ChCl-LA mixture due to the positive charge gained by the edges of the particle under low pH conditions.
- A significantly lower dosage of NADES was required to achieve the same results obtained by of ChCl and ChCl-LA at an optimum concentration of  $1.78 \times 10^{-2} M$ .
- LA was an inefficient coagulant for bentonite suspension as the changes in the turbidity (336 *NTU*) and the floc size (3.3  $\mu m$ ) were not significant compared to the untreated suspension (350 *NTU* and 2.5  $\mu m$ ).
- Electrostatic batch coagulation mechanism (EPC) was observed in bentonite suspension treated with the three active coagulants which explain the negative zeta potential and the formation of micro-scale loose flocs with high turbidity removal percentage.
- Between NADES and ChCl-LA mixture, a higher settling rate was exhibited by suspensions treated with NADES. Moreover, increasing the coagulant dosage further enhances the flocs settling rate and reduces the sediment volume as more compacted flocs are produced.
- The difference in the coagulation efficiency of NADES and ChCl-LA mixture in terms of floc size, turbidity removal percentage, and settling rate and volume is due to the presence of a hydrogen bond connecting ChCl and LA in NADES resulting in a compound with higher molecular weight/ longer chain and hence, a better coagulant.

### **4.3. Destabilization of Stable Bentonite Colloidal Suspension Using Choline Chloride Based Deep Eutectic Solvent: Optimization Study**

#### **4.3.1. Introduction**

The appropriate implementation of the destabilization and separation process is essential to achieve the desired results of the maximum reduction in negative zeta potential and turbidity and maximizing the produced flocs size, which is important for further handling and treatment. The right execution depends mainly on the concentration of the selected coagulant, pH, and the suspended solid content (initial turbidity) [258]. In traditional practices, process optimization is achieved by optimizing each variable individually; where one variable is changing while the rest remains constant. However, such practices are very time consuming and unreliable process as they do not take into consideration the interactions between the different variables. Therefore, using a computational method to study the relation between the variables and their effect on the studied responses is necessary to find the optimum operating conditions that attain the targeted results [271].

Response surface methodology (RSM) is a statistical and mathematical method that combines experimental design, regression analysis, and optimization methods to optimize the process conditions by providing an experimental design with a specified number of experiments, Thus, reducing the required time and improving the accuracy of the obtained results [271,272]. Generally, RSM is employed for modeling and optimization of processes with a number of independent variables that influence the behavior and the performance of the system [59]. RSM can be conducted by different sampling methods such as central composite design, full factorial, and Box Behnken.

Therefore, this section further investigates the use of choline chloride based NADES as a destabilizing agent for stable colloids under different conditions. A

comparative study was performed to analyze the performance of three ChCl based NADES with different HBD which are lactic acid (LA), malic acid (MA), or citric acid (CA) as a coagulant for highly stable bentonite suspension. Furthermore, response surface methodology (RSM) and central composite design (CCD) were used to design a set of experiments to investigate the effect of the coagulant dosage and the bentonite concentration on the destabilization process of bentonite suspension using ChCl:LA NADES. The effects of these two variables were recorded in terms of the changes in zeta potential, pH, and turbidity of the suspension in addition to the variation in the size of the formed flocs. Furthermore, the experimental results in combination with the computational methods were employed to determine the optimum operating conditions for the process.

#### **4.3.2. Performance analysis**

Several factors influence the destabilization process of colloidal particles including type and dosage of the used coagulants, colloid concentration, and pH of the system [95]. Under basic conditions (i.e.,  $pH > 7$ ), colloidal suspensions are very stable due to domination of repulsive forces between the particles. On the other hand, lowering the pH values play a major role in the destabilization process by reducing the repulsive forces between the particles and hence, reducing overall negative charge and promotes further aggregation [17]. Therefore, in this study, the performance of three acidic ChCl based NADESs (i.e., ChCl:LA, ChCl:MA, and ChCl:CA) as coagulants for highly stable bentonite suspension was analyzed in terms of the reduction in negative zeta potential, the turbidity of the supernatant, and the floc size of the resultant sediment. This analysis was conducted in order to study the effect of NADES with different HBD on the destabilizing process.

#### 4.3.2.1. Turbidity and Zeta Potential

Turbidity and zeta potential measurements for the treated bentonite suspension using different ChCl based NADES coagulants (ChCl:LA, ChCl:MA, and ChCl:CA) are presented in Figure 4.17 and Figure 4.17, respectively. Untreated bentonite suspension demonstrates turbidity of 350 *NTU* and a zeta potential of  $-40.4$  *mV*. From Figure 4.17, it can be observed that for all of the investigated coagulants, the turbidity decreases with increasing the coagulant concentration. At the lowest coagulant dosage of  $2.98 \times 10^{-3}$  *M*, ChCl:LA attained a supernatant turbidity of below 5 *NTU* while suspensions coagulated with ChCl:MA and ChCl:CA achieved a reduction in the turbidity to below 100 *NTU*. The turbidity continued to gradually decrease until it reached a minimum value of less than 1 *NTU* by ChCl:LA and ChCl:CA at a concentration of  $1.78 \times 10^{-2}$  *M*. On the other hand, at the same dosage, suspensions treated with ChCl:MA exhibited turbidity of 2.5 *NTU* which is close to the final turbidity obtained when ChCl:LA was used at a concentration of  $2.9 \times 10^{-3}$  *M*. Hence, ChCl:MA is effective as a coagulant, however, a larger dosage is required to achieve better results compared to ChCl:LA and ChCl:CA.

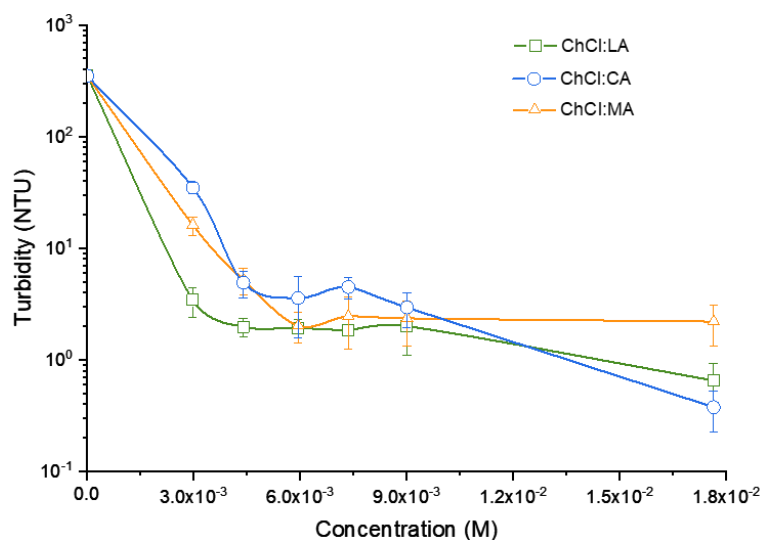


Figure 4.16: Turbidity as a function of the concentration for bentonite suspension treated with ChCl:LA, ChCl:MA, and ChCl:CA

Commonly, the reduction in the turbidity of the supernatant is associated with an increase in the corresponding zeta potential. From Figure 4.17 it is shown that the maximum increase in the magnitude of the zeta potential was achieved at a concentration of  $1.78 \times 10^{-2} \text{M}$  by ChCl:CA with a zeta potential of around  $-16 \text{ mV}$  followed by ChCl:LA and ChCl:MA with a magnitude of  $-18 \text{ mV}$  and  $-22 \text{ mV}$ , respectively. The changes displayed by the bentonite suspension upon the addition of the NADES systems are attributed to the positive charges presented in the NADESs' structure, which get attracted by the negative charges on the surface of the bentonite particles resulting in partially neutralizing some of the charges and thus reduces the surface negative zeta potential. Moreover, the negative zeta potential alongside the high reduction in turbidity is mainly due to the electrostatic patch coagulation mechanism which is observed when a coagulant with a low molecular weight is employed to destabilize suspended clay particles [106,107]. Furthermore, it is worthy to mention that the system's pH was not changed before the coagulant addition and the drop of the

pH value was a result of the organic acids in the used NADES. The final pH of all suspensions upon the coagulant addition was within the same range at all concentrations.

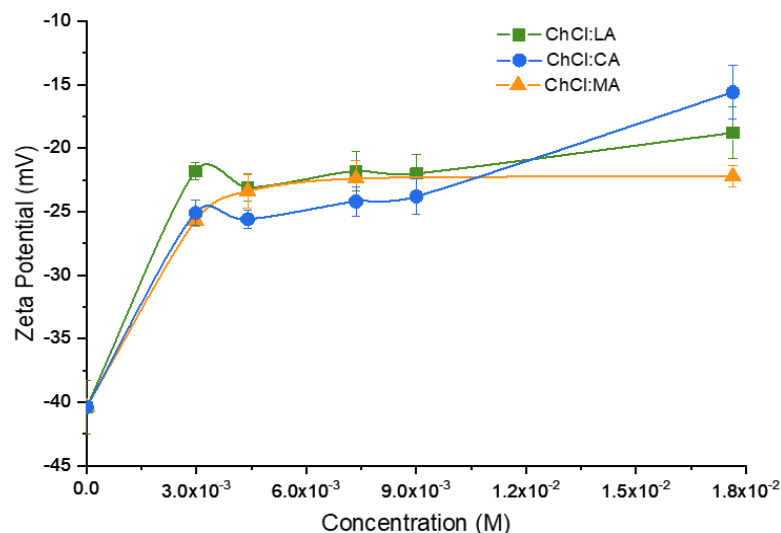


Figure 4.17: Zeta potential as a function of the concentration for bentonite suspension treated with ChCl:LA, ChCl:MA, and ChCl:CA.

#### 4.3.2.2. Particle Size Distribution

The effect of the three investigated coagulants on the destabilization and coagulation of bentonite suspension was analyzed in terms of the median diameter ( $D_{50}$ ) of the produced flocs. Figure 4.18 illustrates the effect of the coagulation process using ChCl:LA, ChCl:MA, and ChCl:CA NADESs on the floc size as a function of concentration. Untreated bentonite suspension has a median diameter of  $2.5 \mu\text{m}$  demonstrating a slight swelling in the particles upon mixing it with water. It can be observed from Figure 4.18 that upon the addition of the NADES coagulants to the

bentonite suspensions, the size of the flocs increases significantly. Increasing the concentration from  $3.48 \times 10^{-2}M$  to  $6.76 \times 10^{-2}M$  led to an increase in the floc size from 18.4  $\mu\text{m}$ , 21.8  $\mu\text{m}$ , and 29.1  $\mu\text{m}$  to 22.3  $\mu\text{m}$ , 36.7  $\mu\text{m}$ , and 36.2  $\mu\text{m}$  for ChCl:MA, ChCl:LA, and ChCl:CA, respectively. At the same coagulant concentration, the difference in the median diameter of the flocs is due to the different adsorption capacity of each coagulant on the surface of the particle [17]. The increase in the floc size as a result of the coagulant addition to the suspension is attributed to the decrease in the electrostatic repulsive forces between the particles rising from partially neutralizing some of the negative charges on the surface of the bentonite particles. Thus, the particles were allowed to come closer to each other promoting aggregation and flocs formation. Higher coagulant dosage leads to a further reduction in the repulsion forces and hence, the formation of larger flocs [17]. The produced flocs can be described as a micro-scale loose floc as their formation is a result of destabilization using a short-chain coagulant through electrostatic patch coagulation mechanism (EPC) [106,107].

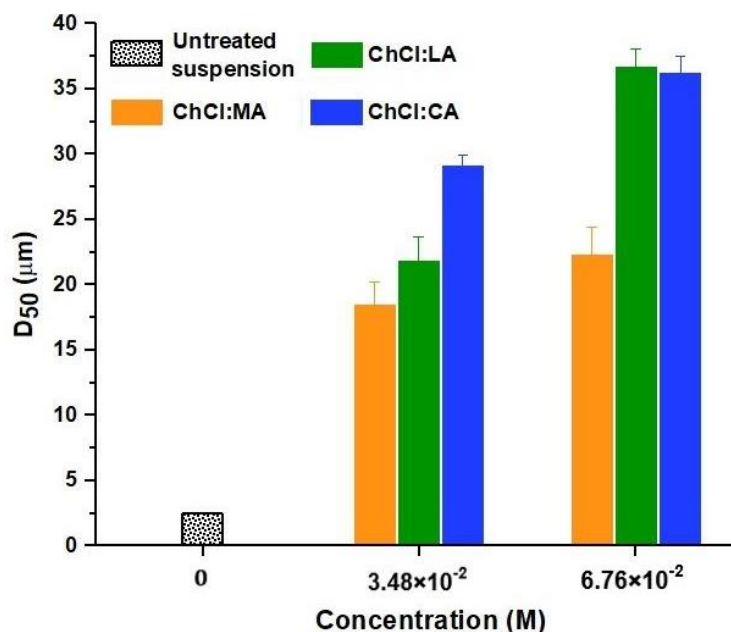


Figure 4.18: Floc size of treated suspensions using ChCl:LA, ChCl:MA, and ChCl:CA at concentrations of  $3.48 \times 10^{-2} M$  and  $6.76 \times 10^{-2} M$ .

From the conducted analysis on ChCl:LA, ChCl:MA, and ChCl:CA, it can be concluded that the performance efficiency of the three investigated coagulants is relatively similar in terms of maximizing the zeta potential and the floc size in addition to reducing the turbidity. However, both ChCl:LA and ChCl:CA have slightly better performance efficiency than ChCl:MA. Furthermore, the synthesis of ChCl:LA is simpler and more time-efficient (maximum 1 hour) compared to ChCl:CA which requires a minimum preparation time of 24 hours for both components to completely dissolve in each other. Hence, for the optimization study in the following section, the process conditions of the destabilization and separation of bentonite suspension in terms of the coagulant dosage and the bentonite concentration will be optimized using ChCl:LA NADES. ChCl:LA NADES was selected as it is efficient, easy to prepare, and remains liquid at room temperature while the other two studied NADESs are highly



viscous and require pre-heating before using them in the coagulation process.

### 4.3.3. Statistical Analysis

Experiments were conducted according to the run order from Table 3.5 and the full result of the responses for the experimental design is presented in Table 4.3.

Table 4.3: RSM Experimental results of the four studied responses

Run Order	Zeta	Turbidity	Floc size		pH
	Potential (mV)	Removal (%)	D <sub>50</sub> (μm)	D <sub>90</sub> (μm)	
1	-16.6	99.91	22.3	63.9	2.36
2	-20.7	99.80	22.7	64.8	3.50
3	-16.2	99.83	29.7	70.6	2.33
4	-15.9	99.22	20.2	48.6	2.30
5	-22.7	97.49	4.0	13.7	4.04
6	-14.1	99.89	24.1	57.9	2.37
7	-14.2	99.85	29.2	66.2	2.35
8	-7.2	99.92	31.6	67.8	2.28
9	-7.9	99.90	32.4	66.3	2.20
10	-21.7	98.78	10.2	29.1	3.50
11	-17.0	99.91	31.1	68.1	2.43
12	-17.0	99.91	30.0	68.6	2.50
13	-5.8	99.47	29.8	61.1	2.12

The relationship between the studied variables of the destabilization and separation process which are the ChCl:LA dosage and the bentonite concentration and the responses (turbidity, zeta potential, floc size, and pH) was analyzed through response surface methodology (RSM). Table 4.4 shows the significance of each developed model and the variation of the fitted data around the model through lack of fit (LOF) which was evaluated using the P-value with a confidence level of 5%. If the obtained P-value was less than 0.05 it indicates the significance of the model, otherwise, it is insignificant. From Table 4.4, it can be observed that all the models except the turbidity model are significant with a P-value below 5%. Furthermore, except for the turbidity measurement, the lack of fit of each response was insignificant (> 5%) indicating the significance of the correlation between the variables and responses [273].

Table 4.4: Significance results of the studied responses

Response	Model significance	LOF
Turbidity	0.089	0.000
Zeta potential	0.001	0.155
pH	0.000	0.098
Floc size	D <sub>50</sub>	0.002
	D <sub>90</sub>	0.003

The insignificance presented in the turbidity model is mainly due to the constant turbidity removal percentage (~99%) which leads to the absence of variation in the turbidity values and therefore, the lack of fit of the resultant model. Another

experimental study was performed by generating an experimental design using RSM and CCD with a wider range for the bentonite concentration. It was desired to investigate the effect of the ChCl:LA dosage on a highly concentrated colloidal system and the coagulation process. However, the design resulted in an insignificant model for the turbidity as well since the removal percentage varied between 97% and 99%. Thus, the turbidity as a response was excluded from the study.

#### 4.3.3.1. Optimization of the zeta potential and pH

The experimental values of zeta potential and pH for the coagulation process are presented in Table 4.3. The regression models of zeta potential and pH are described by Eq. 4.1 and Eq. 4.2, respectively.

$$Y_{ZP} = -24.53 + 0.197 x_1 + 0.17 x_2 + 0.000928 x_1^2 + 0.018 x_2^2 - 0.0102 x_1 x_2 \text{ .. Eq. 4.1}$$

$$(R^2 = 0.929, \text{ adjusted } R^2 = 0.878)$$

$$Y_{pH} = 4.392 - 0.07165x_1 - 0.0594x_2 + 0.000550x_1^2 + 0.00760x_2^2 + 0.000661x_1x_2 \text{ .. Eq. 4.2}$$

$$(R^2 = 0.995, \text{ adjusted } R^2 = 0.991)$$

Where  $x_1$  is the ChCl:LA dosage in mM and  $x_2$  is the bentonite concentration in  $\text{gL}^{-1}$ . From the above equations, variables with positive signs imply a synergistic effect while an antagonistic effect is donated by variables with negative sign [274]. For the zeta potential model, the correlation coefficient ( $R^2 = 0.929$ ) alongside the adjusted correlation coefficient (adj.  $R^2 = 0.878$ ) imply that around 12% of the experimental data deviate from the implemented model. Similar to the zeta potential model, the high correlation coefficient ( $\sim 1$ ) of the pH regression model indicates the good fit between the experimental data and the second order polynomial model [256].

Table 4.5 illustrates the significance of each term in the produced models

according to the obtained p-value. For the pH model, it can be observed that both the ChCl:LA dosage ( $x_1$ ) and the bentonite concentration ( $x_2$ ) in the system in addition to the square term ( $x_1^2$ ) are highly significant where their p-values are less than 0.05 while the remaining square and interaction terms are insignificant with a p-value higher than 5%. On the other hand, only the ChCl:LA dosage ( $x_1$ ) is significant for the zeta potential model and the remaining terms can be excluded as their effect is insignificant on the magnitude of the system electric potential [275].

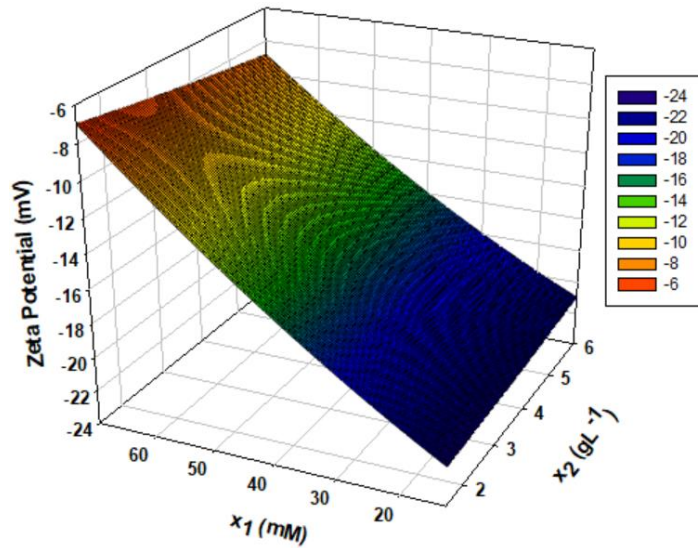
Table 4.5: Significance of the models' variables in Equations 4.1 and 4.2 for zeta potential and pH in terms of the P-value.

Model's variables	P-value	
	Zeta Potential (mV)	pH
$x_1$	0.000	0.000
$x_2$	0.713	0.031
$x_1x_1$	0.377	0.000
$x_2x_2$	0.904	0.125
$x_1x_2$	0.530	0.212

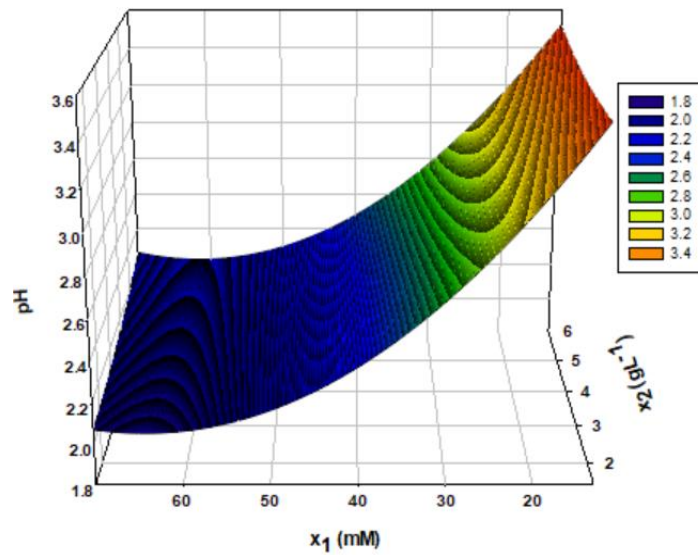
According to Equation 4.1, the optimum conditions to obtain the maximum reduction in negative zeta potential are 70.0 mM for the ChCl:LA dosage and 1.5 gL<sup>-1</sup> for the bentonite concentration in the suspension which will result in zeta potential of – 6.97 mV. On the other hand, it is desired to minimize the pH of the system as lower

pH enhances the destabilization process. Therefore, from Equation 4.2, the optimal design conditions for minimizing the pH of the system are 64.3 mM for the ChCl:LA dosage and  $1.5 \text{ gL}^{-1}$  for the bentonite concentration giving a pH of 2.05.

With zeta potential and pH as responses for the designed experiment, Figure 4.19 shows the surface plot of both responses as a function of the ChCl:LA dosage ( $x_1$ ) and the bentonite concentration ( $x_2$ ). It is noted that the optimum conditions for minimizing the pH value and maximizing the zeta potential both fall within the selected range for the study. Furthermore, it is observed that both responses are primarily affected by the variation in the ChCl:LA dosage, as increasing the dosage reduces the pH and hence increases the zeta potential [17]. The effect of the bentonite concentration on the responses is limited and unfavorable as at a constant ChCl:LA dosage. For example, at a constant ChCl:LA dosage ( $x_1$ ) of 67.72 mM a higher bentonite concentration leads to a slight decrease in the zeta potential from  $-7.67 \text{ mV}$  at  $1.5 \text{ gL}^{-1}$  to  $-9.41 \text{ mV}$  at  $6 \text{ gL}^{-1}$ . Whereas for the pH, at the same bentonite concentration of  $1.5 \text{ gL}^{-1}$  the pH decreases from 2.495 at 35.8 mM to 2.051 at 64.87 mM, while increasing the  $x_2$  in the system from  $1.5 \text{ gL}^{-1}$  to  $6 \text{ gL}^{-1}$  at a constant ChCl:LA dosage of 64.87 mM leads to increasing the pH from 2.051 to 2.233, respectively.



(a)



(b)

Figure 4.19: Surface graph of the (a) zeta potential and (b) pH as a function of the ChCl:LA dosage ( $x_1$ ) and the bentonite concentration ( $x_2$ )

To further assess the quality of the fit and the reliability of the model, the predicted values generated from the designed models should show a satisfactory result when compared to the experimental values [276]. Therefore, plots of the predicted

values from the generated models (equations 4.1 and 4.2) versus the experimental values are shown in Figure 4.20. According to the regression coefficients ( $R^2$ ), the predicted values of both the zeta potential and pH model are in good agreement with the obtained experimental results.

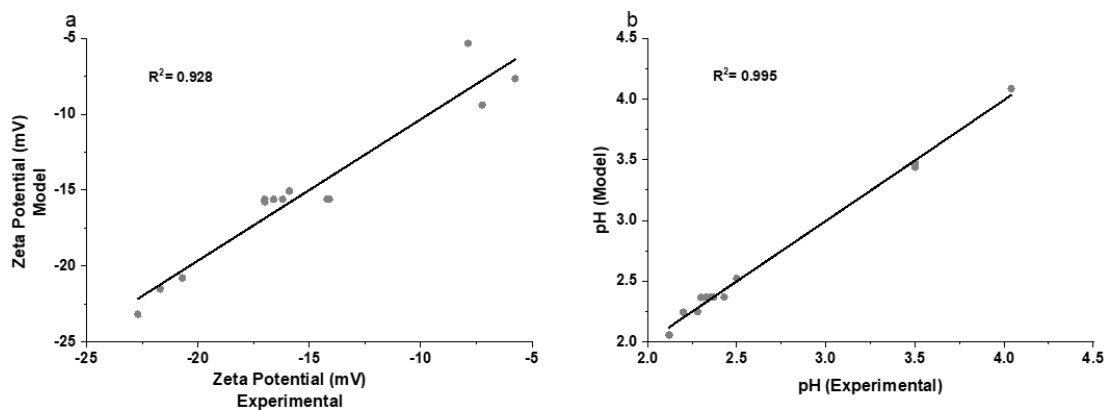


Figure 4.20: Graphical verification of the regression models for zeta potential (a) and pH (b)

#### 4.3.3.2. Optimization of the sediment floc size

The floc size of the resultant sediment was described by the particle diameter at 50% of the cumulative distribution curve where half of the flocs have a diameter below  $D_{50}$ . It is also known as the median diameter and used to describe the average floc size of the sediment. Moreover, it was described by ( $D_{90}$ ) which indicates that 10% of the produced flocs have a diameter higher than  $D_{90}$ . The experimental values of the floc size ( $D_{50}$  and  $D_{90}$ ) for the destabilization and separation process are presented in Table 4.3. The regression models of  $D_{50}$  and  $D_{90}$  are described by Eq. 4.3 and Eq. 4.4, respectively.

$$Y_{D_{50}} = -9.53 + 0.945x_1 + 4.28x_2 - 0.00562x_1^2 - 0.121x_2^2 - 0.0442 x_1x_2 \dots \text{(Eq. 4.3)}$$

$$(R^2 = 0.909, \text{adjusted } R^2 = 0.845)$$

$$Y_{D_{90}} = -19.1 + 2.210x_1 + 11.48x_2 - 0.01530x_1^2 - 0.354x_2^2 - 0.1199x_1x_2 \dots \text{(Eq. 4.4)}$$

$$(R^2 = 0.889, \text{adjusted } R^2 = 0.811)$$

The correlation coefficients and the adjusted correlation coefficient of the regression models show the accuracy of the model prediction. Eq. 4.3 describing the median floc size ( $D_{50}$ ) shows an accuracy of around 85% implying that around 15% of the experimental data variation could not be explained by the produced models. Furthermore, Equations 4.4 have lower estimation accuracy of the results and only around 19% of the predicted data deviate from the experimental values [277].

Table 4.6 demonstrates the p-values of the linear ( $x_1$  and  $x_2$ ), square ( $x_1^2$  and  $x_2^2$ ), and interaction ( $x_1x_2$ ) terms of the obtained models. From Table 4.6, both  $D_{50}$  and  $D_{90}$  models expressed by Equations 4.3 and 4.4, respectively are significant in respect of both linear terms ( $x_1$  and  $x_2$ ) in addition to the square term of the ChCl:LA dosage ( $x_1^2$ ). However, for  $x_2^2$  and  $x_1x_2$ , the models are insignificant, thus, they do not have a dominant influence on the size of the resultant flocs.



Table 4.6: Significance of the models' variables in Equations 4.3 and 4.4 for  $D_{50}$  and  $D_{90}$  in terms of the P-value

Models' variables	P-value	
	$D_{50}$ ( $\mu\text{m}$ )	$D_{90}$ ( $\mu\text{m}$ )
$x_1$	0.000	0.001
$x_2$	0.023	0.013
$x_1x_1$	0.017	0.006
$x_2x_2$	0.652	0.550
$x_1x_2$	0.164	0.095

Generally, it is desired to maximize the D-values as the larger the flocs the easier the dewatering and treatment processes of the obtained sludge. Therefore, from Equations 4.3 and 4.4, the optimum conditions for maximizing the values of  $D_{50}$  and  $D_{90}$  are as the following: 60.3 mM with  $6 \text{ gL}^{-1}$  and 48.9 mM with  $6 \text{ gL}^{-1}$ , respectively. Treating bentonite suspension systems with the stated conditions will results in flocs with  $D_{50}$  of  $32.35 \mu\text{m}$  and  $D_{90}$  of  $73.34 \mu\text{m}$ .

Figure 4.21 shows the surface plots of the floc size ( $D_{50}$  and  $D_{90}$ ) as a function of the ChCl:LA dosage and the bentonite concentration in the system. The optimum conditions that maximize the two D-values fall within the selected range for the optimization study. Furthermore, both surface plots exhibit a concavity which indicates the sensitivity of the responses to both variables: the ChCl:LA dosage ( $x_1$ ) and the bentonite concentration ( $x_2$ ) in the observed systems [257]. Nevertheless, it can be observed from Figure 4.21b that after reaching a maximum value of  $73 \mu\text{m}$  at  $x_2$  of 6

$\text{gL}^{-1}$  and  $x_1$  of almost 49 mM, the  $D_{90}$  value starts to decrease gradually with increasing the coagulant dosage to 71.1  $\mu\text{m}$  at 60.3 mM and 66.4  $\mu\text{m}$  at 70 mM. This behavior can be attributed to the fact that the bentonite particles' surface becomes saturated with the coagulant and can connect with other particles through limited sites only [17].

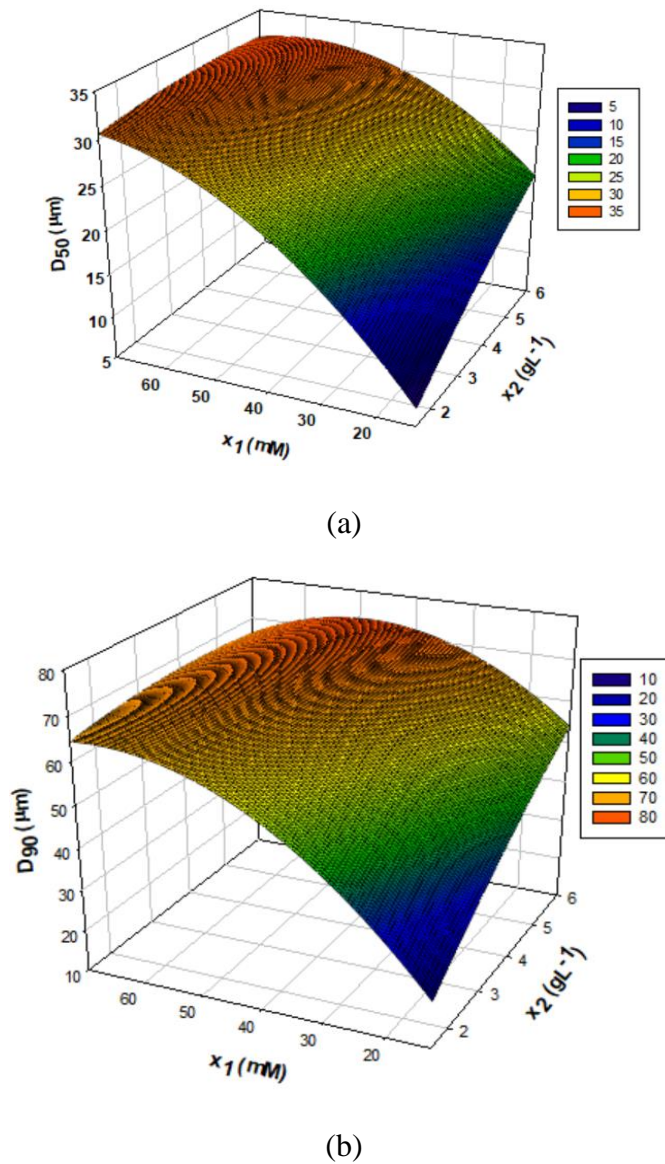


Figure 4.21: Surface graph of the floc size (a)  $D_{50}$  and (b)  $D_{90}$  as a function of the ChCl:LA dosage ( $x_1$ ) and the bentonite concentration ( $x_2$ )

For the verification of the produced models for the floc size and to check their reliability, a graphical comparison between the predicted values from the model and the experimental results are represented in Figure 4.22. It can be noticed from the regression coefficient ( $R^2$ ) for the linear fit that the relation between the predicted values from the models and the experimental results are showing similar trends with Equations 4.3 and 4.4 where  $D_{50}$  model showed a better prediction accuracy with an  $R^2$  of 0.91 followed by  $D_{90}$  and with  $R^2$  of 0.89.

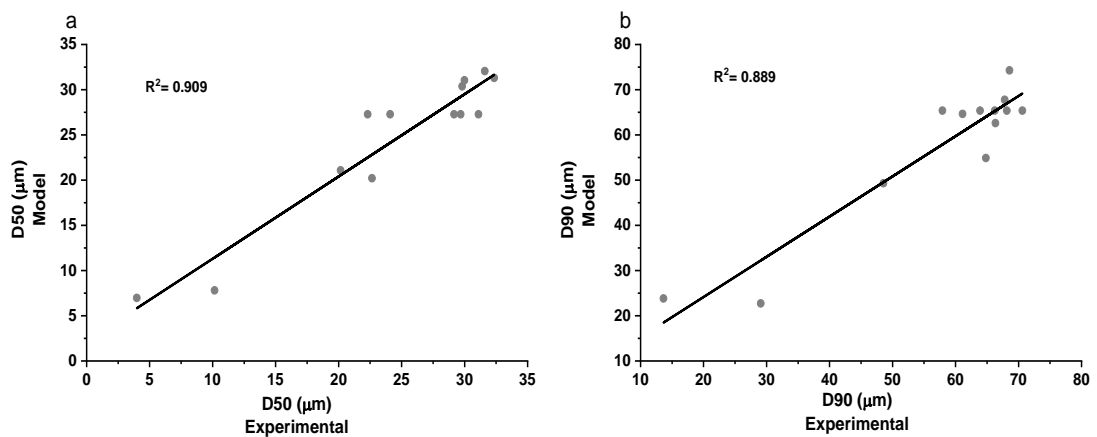


Figure 4.22: Graphical verification of the regression models for the floc size (a)  $D_{50}$  and (b)  $D_{90}$ .

#### 4.3.3.3. Multiple Response Optimization

In the previous sections, the optimum conditions were found for each response individually without taking into consideration the results of the remaining responses. Therefore, in this section, the optimization of the destabilization and coagulation process variables with respect to all responses is conducted using multiple response optimization function in Minitab.

The optimization results were evaluated using the composite desirability value. Composite desirability evaluates the ability of the designed model to satisfy the optimization conditions; its value ranges from zero to one. To be able to achieve the desired target; composite desirability close to unity is required [259,278]. By using multiple response optimization function to achieve maximum reduction in the negative zeta potential and pH in addition to maximizing the floc size the obtained composite desirability was 0.978. Therefore, the optimum condition of the destabilization and separation process of bentonite suspension was found to be as following: bentonite concentration of  $3.48 \text{ gL}^{-1}$  and a ChCl:LA dosage of 77 mM which will result in zeta potential of  $-5.8 \text{ mV}$ , floc size of  $31.5 \text{ }\mu\text{m}$  and  $63.8 \text{ }\mu\text{m}$  for  $D_{50}$  and  $D_{90}$ , respectively and a pH of 2.2. Figure 4.23 shows the overlaid contour plot of the responses as a function of the two variables. The shaded area represents the unfeasible region where the optimization of all responses together is not possible. On the other hand, the white area is the feasible region where it is possible to optimize all responses at the same time [279]. It can be noticed that the feasible region includes the optimized conditions of the process ( $3.48 \text{ gL}^{-1}$  and 77 mM) implying the validity of the results.

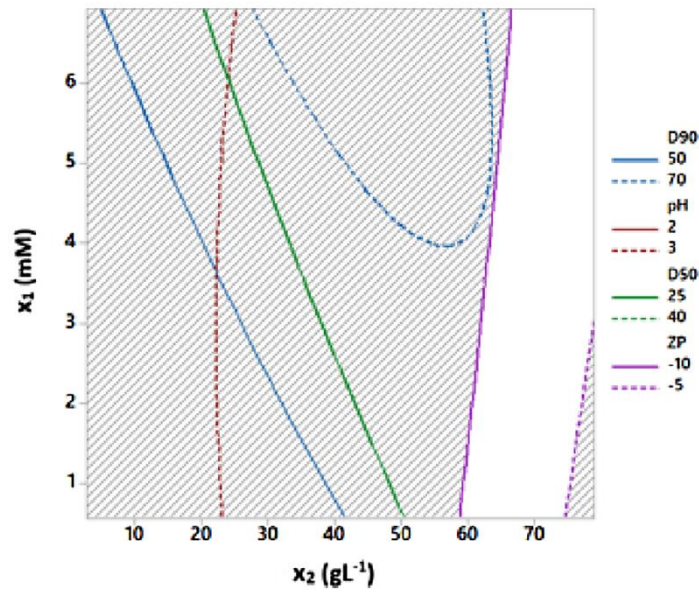


Figure 4.23: Overlaid contour plot of the optimal region

Additional three experimental runs using both ChCl:LA dosage and bentonite concentration as the independent variables with one run within the optimum region (shown in Figure 4.23) were conducted to confirm the validity of the designed experiments. Table 4.7 presents the conditions, experimental results, and the error percentage with the predicted values from the model. As shown in Table 4.7, the experimental results, of zeta potential, pH, and floc size ( $D_{50}$  and  $D_{90}$ ) are close to the predicted model with an error percentage varying from 2% to 11% with the highest percentages were due to variation in zeta potential values.

Table 4.7: Experimental confirmation of the designed models

Conditions	Response			
	Zeta Potential	pH	D <sub>50</sub>	D <sub>90</sub>
	(mV)		( $\mu\text{m}$ )	( $\mu\text{m}$ )
$x_1 = 34.8 \text{ mM}, x_2 = 3 \text{ gL}^{-1}$				
Experimental Value	-15.8	2.45	21.8	53.59
Model Response	-16.94	2.52	23.69	58.02
Error %	7.24	3.01	8.65	8.27
$x_1 = 67.6 \text{ mM}, x_2 = 1.5 \text{ gL}^{-1}$				
Experimental Value	-6.92	2.15	28.61	66.79
Model Response	-7.71	2.06	30.34	64.64
Error %	11.43	4.19	6.05	3.22
$x_1 = 17.8 \text{ mM}, x_2 = 10 \text{ gL}^{-1}$				
Experimental Value	-21.2	3.30	27.33	74.98
Model Response	-19.05	3.57	28.34	73.45
Error %	10.14	8.18	3.70	2.04

#### 4.3.4. Conclusions

Choline chloride based NADES was proved to be an effective coagulant for the destabilization and separation of stable colloidal suspension. In this study, three ChCl based NADESs with lactic acid, malic acid, and citric acid as the HBD (ChCl:LA, ChCl:MA, and ChCl:CA) were employed as a coagulant to investigate the effect of the organic acid side of the NADES. The following conclusions were drawn:

- The three NADESs were evaluated in terms of the removal percentage of the supernatant's turbidity, the reduction in the negative zeta potential, and the floc size of the resultant sediments. Both ChCl:LA and ChCl:CA showed very efficient performance as a destabilizing agent with almost similar results in all of the evaluated parameters with a reduction in the turbidity to below 1 NTU, floc size of 36  $\mu\text{m}$ , and a zeta potential of -18 mV and -16 mV, respectively.
- ChCl:LA was designated the most suitable and convenient coagulant in terms of efficiency and simplicity of the synthesis method compared to ChCl:CA, therefore, the optimization study was conducted using ChCl:LA.
- The experimental design through RSM analyzed three main parameters that are significantly affected during the destabilization of colloidal particles which are the zeta potential, pH, and the floc size ( $D_{50}$  and  $D_{90}$ ) by varying the NADES and bentonite concentration in the system.
- The optimum condition for the coagulation process of bentonite colloidal suspension using ChCl:LA NADES was found to be as following: 77 mM for the ChCl:LA dosage and 3.48  $\text{gL}^{-1}$  for the bentonite concentration in the system resulting in -5.8mV, 31.5  $\mu\text{m}$  63.8  $\mu\text{m}$ , and 2.2 for the zeta potential, floc size ( $D_{50}$  and  $D_{90}$ ), and pH, respectively.

## **4.4. Influence of Choline Chloride Based Natural Deep Eutectic Solvent on the Rheological Behavior of Bentonite Suspension**

### **4.4.1. Introduction**

At present, several researches that study the influence of inorganic and organic coagulants on the behavior of clay suspension are available in the literature [180,193]. Furthermore, researches investigating the utilization of polymeric flocculants such as polyelectrolytes and the effect of their charge density, molecular weight, and adsorption affinity are heavily conducted [17,170]. However, most of these studies analyze the coagulation/ flocculation degree in terms of the zeta potential, turbidity, and floc size only. Performing rheological analysis on coagulated/ flocculated clay suspension is an important method to understand the mechanism and evaluate the strength of the formed flocs. Yet, researches that study the relationship between the type/ structure of the coagulant/ flocculent with the destabilization degree and rheological behavior of clay suspension are still very limited. To this end, in the following sections, the kinetics of the dewatering process were investigated by zeta potential,  $\zeta$ , flocs size, and capillary suction time (CST) measurements for treated bentonite suspensions with ChCl based natural deep eutectic solvent (ChCl:LA NADES). In addition, yields stress ( $\tau_0$ ), elastic modulus ( $G'$ ), and viscous modulus ( $G''$ ) were measured for the same bentonite suspensions to study the shear sensitivity and elasticity behavior of the coagulated network. Thereby, linking these properties to the mechanical limit of the material during the dewatering process. Furthermore, the destabilization degree of bentonite suspension treated with a ChCl-LA mixture (at room temperature) will be used as a destabilizing agent for the same bentonite suspension. This assessment aims to analyze the performance difference between the synthesized NADES and the mixture of its raw constituent components to know whether NADES will have a superior performance



over ChCl-LA mixture or similar behavior will be observed due to the high level of hydration.

#### **4.4.2. Effect of the coagulant concentration on the destabilization degree**

##### **4.4.2.1. Turbidity and Zeta Potential**

Applications of NADES in aqueous media are still very rare and limited. This is attributed to the dissociation of NADESs in water to their constituent components due to their hydrophilic properties. However, several studies have shown that the dissociation degree varies depending on the type of the HBD and HBA, their molar ratio, and the bonding between them in addition to the volume ( $v\%$ ) or weight ( $wt\%$ ) percent of water in the system [268]. Hammond et. al. [269], conducted a study on ChCl based NADES with urea as the HBD to relate the degree of dissociation with the  $wt\%$  of water in the system. It was found that up to 42  $wt\%$  of water, the DES – DES interactions are still dominant, and the DES system resists hydration. Above 42  $wt\%$  of water, the DES – DES interactions' strength gradually decreases and DES – water interactions become stronger and the system can be described as aqueous DES. Therefore, the following study will investigate as will the performance difference between the NADES and the binary mixture of the constituent components (ChCl-LA) to evaluate the influence of water on the NADES interactions.

Bentonite suspension under study is a highly stable system with  $\zeta$  – potential of  $-40.4\text{ mV}$  and turbidity around 4100  $NTU$ . Figure 4.24a and Figure 4.24b demonstrate the changes in turbidity and  $\zeta$ - potential for treated bentonite suspensions with NADES and ChCl-LA mixture, respectively as a function of concentration. It is clear that for both coagulants, the increase in the applied dosage is associated with an increase in the  $\zeta$ - potential and hence, a decrease in the turbidity. This observation can be explained by the electrostatic patch coagulation mechanism (EPC) exhibited by the treated

suspensions. The coagulant will neutralize some of the negative charges on the bentonite platelets reducing the repulsive forces. Hence, the particles will be able to come closer to each other forming larger flocs that can settle under the influence of the gravitational forces on them. As a result, the turbidity of the suspension will decrease and a clear supernatant will be produced.

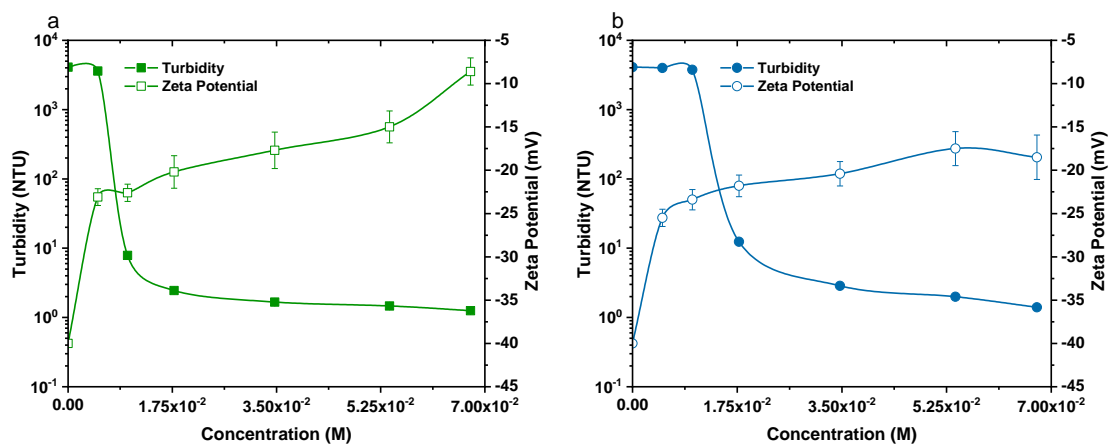


Figure 4.24: Turbidity and Zeta Potential of Bentonite Suspension as a function of the coagulant type and concentrations (a) NADES, and (b) ChCl-LA.

Table 4.8 illustrates the effect of the destabilization process of bentonite suspension in terms of turbidity, zeta potential, floc size, and CST measurements. From Figure 4.24 and Table 4.8, it can be observed that at the same coagulant dosage, NADES shows better performance as a destabilizing agent than ChCl-LA mixture. For example, at  $5.9 \times 10^{-3} M$ , treated bentonite suspension with NADES achieved a turbidity reduction of 12% while only 2% reduction was attained for ChCl-LA treated suspension which is six times less than NADES. Moreover, it is worthy to mention that at this concentration (i.e.  $5.9 \times 10^{-3} M$ ) and after allowing the treated suspension to

settle for 1 hour, almost 80% reduction in the supernatant turbidity of suspension treated with NADES. On the other hand, the turbidity of ChCl-LA treated suspension did not change. Consequently, at higher concentrations of  $1.78 \times 10^{-2} M$  and  $6.76 \times 10^{-2} M$ , NADES exhibited a higher reduction in the negative zeta potential, however, both NADES and ChCl-LA mixture showed similar turbidity removal percentage of 99% and higher.

Table 4.8: Measured parameters of the coagulated bentonite suspension

Coagulant	Concentration (M)	Turbidity (NTU)	Zeta potential (mV)	D <sub>50</sub> ( $\mu\text{m}$ )	CST (sec)
Bentonite suspension	-	4096	-40.4	2.5	37.7
ChCl:LA	$5.9 \times 10^{-3}$	3599	-23.1	3.3	59.5
NADES	$1.78 \times 10^{-2}$	2.44	-20.2	27.3	12.7
	$6.76 \times 10^{-2}$	1.25	-8.6	50.7	9.3
ChCl-LA mixture	$5.9 \times 10^{-3}$	3999	-25.5	3.6	142.6
	$1.78 \times 10^{-2}$	12.4	-21.8	7.1	20.5
	$6.76 \times 10^{-2}$	1.4	-18.5	28.8	11.1

#### 4.4.2.2. Particle size distribution

The size of the produced flocs is evaluated through  $D_{50}$  values that correspond to the median diameter of the flocs in the sediment. Figure 4.25 demonstrates the effect of the NADES dosage on the distribution of the produced flocs. It can be noticed that by increasing the applied dosage to the suspension, the distribution curves shift to the right of the untreated suspension curve. The upward shift in the curves indicates the formation of flocs with a larger diameter ( $D_{50}$ ). The increase in the  $D_{50}$  values is attributed to the greater coagulant-particle interactions at a higher dosage. Consequently, more negative patches on the surface of bentonite particles will be neutralized allowing for more particles to come closer to each other and hence, the formation of larger flocs.

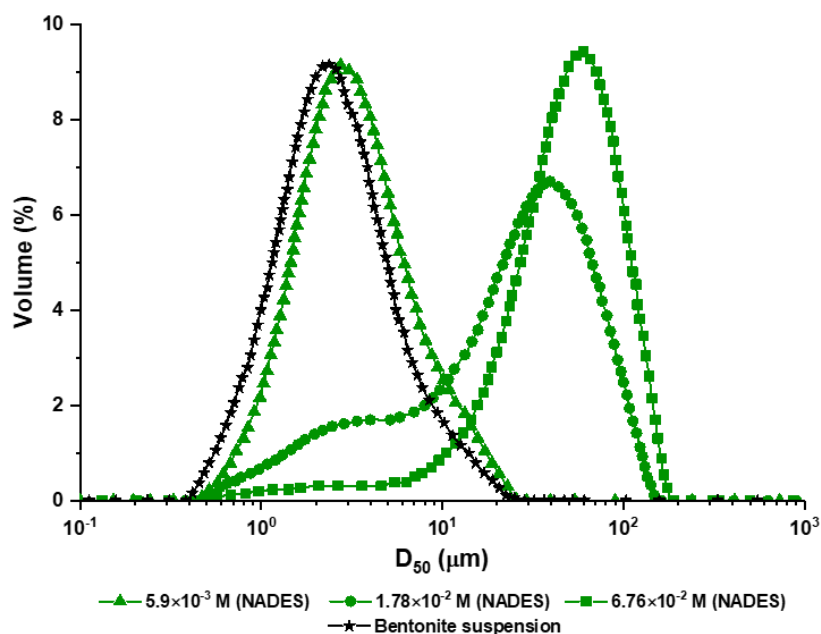


Figure 4.25: Particle size distribution for treated bentonite suspension with NADES at three different concentrations

The difference in the median diameter of the produced flocs between NADES and ChCl-LA mixture is illustrated in Figure 4.26. At the lowest concentration under study (i.e.,  $5.9 \times 10^{-3} M$ ), both coagulants produced flocs of the same  $D_{50}$ . However, when increasing the concentration, a significant difference in the  $D_{50}$  values is observed between the two coagulants. For example, at a constant concentration of  $6.76 \times 10^{-2} M$ , the flocs produced as a result of bentonite suspension treated with NADES is  $50.7 \mu m$  which is almost twice the flocs size when the suspension is treated with ChCl-LA mixture ( $28.8 \mu m$ ). The variation in the floc size between the two coagulants can be attributed mainly to their structural difference and the presence of hydrogen bonds in the NADES connecting the two components (ChCl and LA). As a result, a coagulant with a longer chain and a larger molecular weight is formed and hence, allowing for more particles connect together through EPC mechanism resulting in larger flocs.

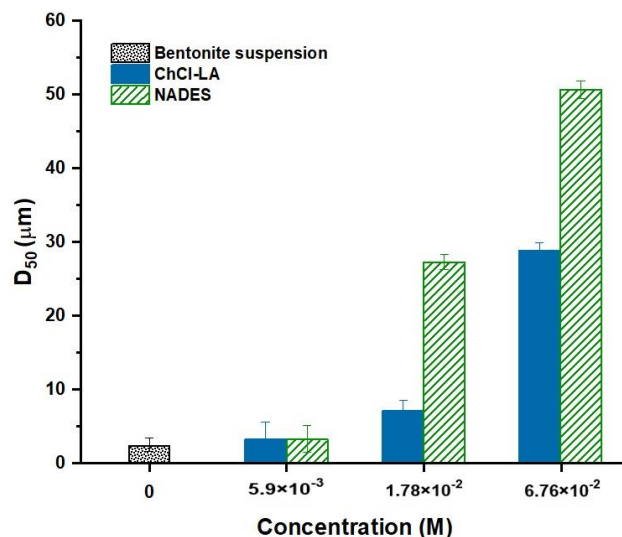


Figure 4.26: Particle size distribution for bentonite suspension treated with NADES or ChCl-LA at different concentrations

Thus, from the zeta potential, turbidity, and floc size results, it is safe to say that NADES has a better performance as a destabilizing agent for highly stable bentonite suspension over a mixture of its constituent components (ChCl-LA). Moreover, it worth mentioning that although an aqueous solution of DES components is formed at such an elevated hydration level, the time required for the destabilization process is very short and aggregation of particles occurs within seconds which justify the better outcomes of NADES compared to ChCl-LA mixture. Consequently, it supports the hypothesis that NADES still retain some of their structure within the first seconds of the addition to the suspension and their effect is clear on bentonite suspension stability.

In addition to the destabilization degree of the treated suspensions, evaluating the structural strength of the formed flocs is an essential step for further treatment processes such as filtration and separation of the cleared supernatant from the sediments. Accordingly, in the following sections, the strength of the formed flocs and the interactions between them will be examined by studying their rheological behavior in terms of viscosity, elastic modulus, and viscous modulus. In addition, the relation between the destabilization degree and the rheological behavior of the flocs will be analyzed.

#### **4.4.3. Effect of the destabilization process on the rheological behavior of bentonite suspension**

##### **4.4.3.1. Shear flow behavior**

Figure 4.27 illustrates the flow behavior of the untreated and treated bentonite suspensions with NADES or ChCl-LA. It can be observed that the untreated bentonite suspension follows Newtonian behavior as the viscosity remains constant with increasing the shear rate. Furthermore, ChCl-LA treated suspension at  $5.9 \times 10^{-2} M$  exhibits Newtonian behavior as the system does not exhibit any aggregation or

sedimentation hence, it behaves in a similar manner to the untreated suspension. On the other hand, the treated suspensions with NADES or ChCl-LA mixture exhibit a non-Newtonian behavior (except ChCl-LA at  $5.9 \times 10^{-3} M$ ) where the shear rate decreases with increasing the viscosity and increases as the shear stress increases. The obtained trends imply that the treated bentonite suspension has a shear-thinning (pseudoplastic) behavior which is observed in most of the destabilized bentonite suspensions [13,67]. Moreover, the difference between the initial and final viscosities of the treated suspensions after the shearing process is observed in Figure 4.27. The drop exhibited by the viscosity upon shearing indicates a structural breakdown in the formed flocs. However, even after high shearing of  $1000 \text{ s}^{-1}$ , the final viscosities for all treated suspension (except ChCl-LA at  $5.9 \times 10^{-3} M$ ) are still 8 times higher than the viscosity of the untreated suspension. Thus, the sheared flocs retain some of their structure and interaction and do not go back to their formal state of colloidal particles

Furthermore, from Figure 4.27 it is clear that adding NADES or ChCl-LA to the bentonite suspension leads to an increase in the viscosity of the system under study. It can be observed that with increasing the concentration of the coagulant, the initial viscosity of the suspension increases. Moreover, between suspensions treated with NADES and others treated with ChCl-LA mixture, higher viscosities are observed with NADES as the destabilizing agent. The variation in the obtained viscosity can be attributed to the differences in the structure of each coagulant. In NADES, ChCl and LA are linked together with a hydrogen bond. On the other hand, ChCl-LA coagulant is two separate components consecutively added to the suspension. Hence, the resultant coagulant from NADES possesses a longer cationic chain that attracts and neutralizes more negatively charged particles. As a result, the particles can come closer together forming larger flocs and more viscous sediment.

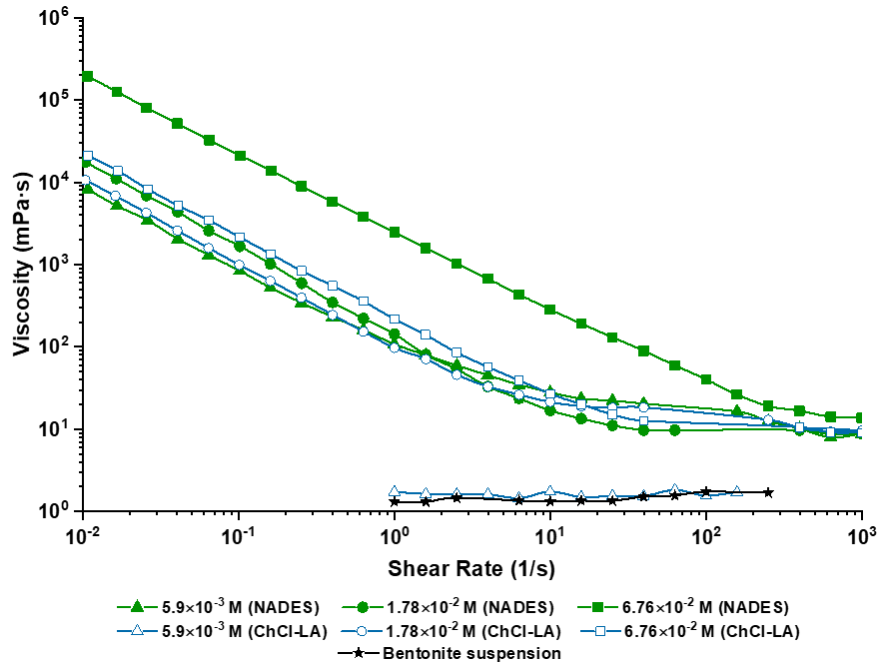


Figure 4.27: Variation in viscosity with shear rate for bentonite suspension treated with NADES and ChCl-LA at different concentrations

The relation between shear stress and shear rate for treated suspensions with NADES or ChCl-LA were fitted with a correlation coefficient ( $R^2$ ) greater than 0.9 to Bingham and Casson models defined by Eq. 4.5 and Eq. 4.6, respectively.

$$\tau = \tau_0 + n_{pl}\dot{\gamma} \dots (\text{Eq. 4.5})$$

$$\sqrt{\tau} = \sqrt{\tau_0} + \sqrt{n_{\infty}\dot{\gamma}} \dots (\text{Eq. 4.6})$$

Where,  $\tau_0$  is the yield stress ( $Pa$ ),  $n_{pl}$  is the Bingham plastic viscosity ( $Pa \cdot s$ ),  $\dot{\gamma}$  is the shear rate, and  $n_{\infty}$  is the infinite rate apparent viscosity ( $Pa \cdot s$ ). Figure 4.28 demonstrates the yield stress ( $\tau_0$ ) and the plastic/ infinite viscosity for all NADES and ChCl-LA treated bentonite suspensions as a function of concentration. The yield stress



describes the maximum stress after which the deformation of the flocs will change from elastic to plastic deformation and the flocs will not go back to their initial state. From Figure 4.28, the yield stress is observed to increase with the concentration indicating a greater ability of the flocs to reverse deformation when the applied force is removed. Higher  $\tau_0$  values were obtained in suspension treated with NADES compared to ChCl-LA. The highest achieved yield stress was around 2950 mPa when NADES was used to destabilize the bentonite suspension with a concentration of  $6.76 \times 10^{-2} M$ . This value suggests the high particle-particle interaction through NADES resulting in very strong flocs.

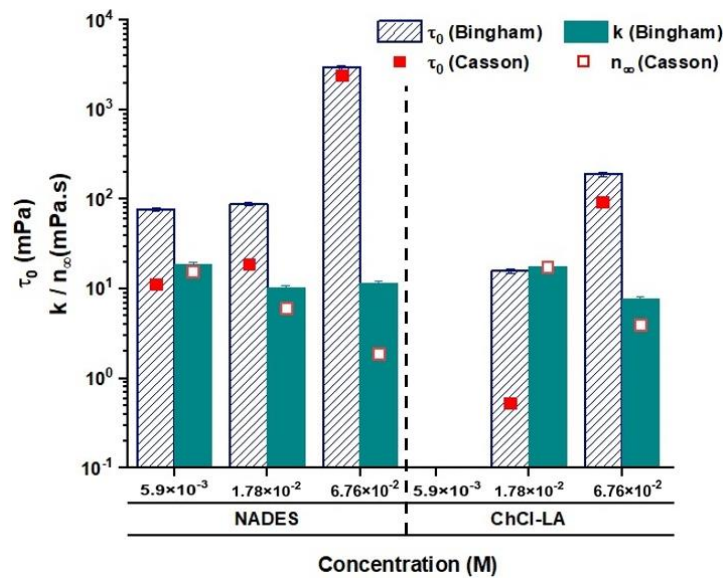
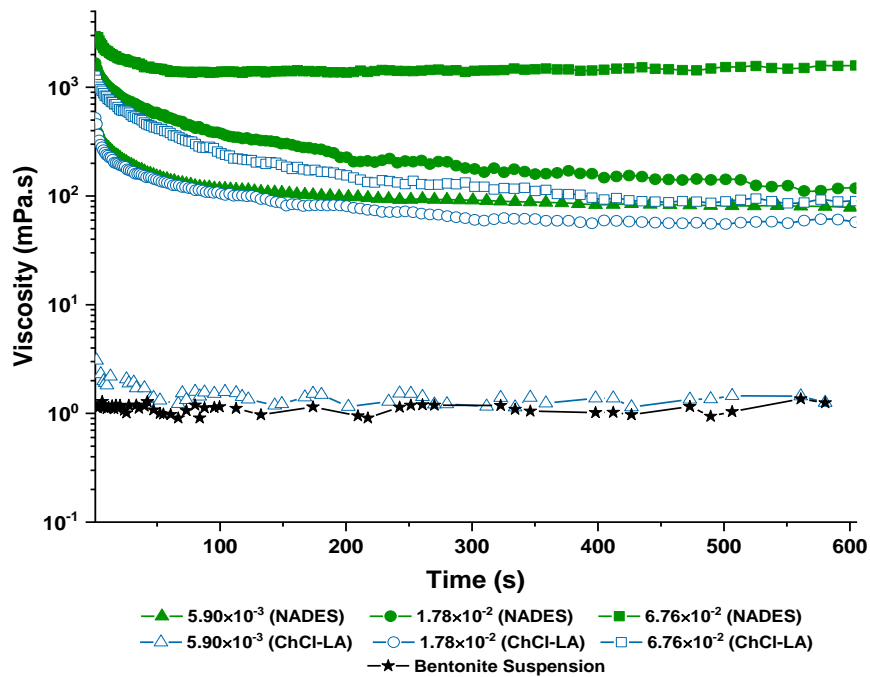
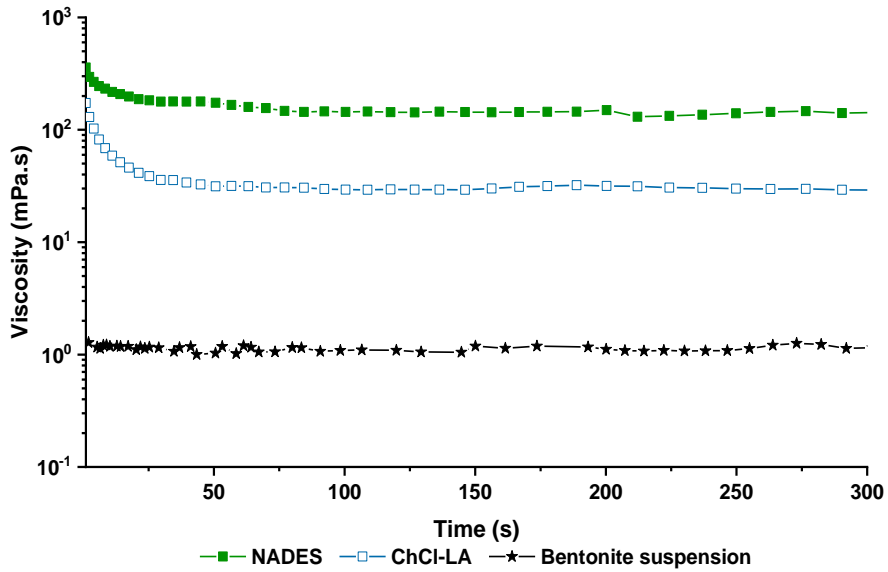


Figure 4.28: Bingham and Casson parameters for viscoelastic behavior in treated bentonite suspension.

Figure 4.29a shows the viscosity-time trends for both the untreated and treated bentonite suspensions with a constant shear rate of  $1 \text{ s}^{-1}$ . After 10 minutes of continuous shearing, the measured equilibrium viscosities are still higher than that for the untreated suspension. This suggests that the formed flocs do not completely breakdown into their constituent particles when sheared at low shear of  $1 \text{ s}^{-1}$  confirming the obtained trends from Figure 4.27. Therefore, this proves the enhancement in the flocs structure and strength of bentonite suspensions when treated with NADES or ChCl-LA.



(a)



(b)

Figure 4.29: Variation in viscosity with time for bentonite suspension treated with NADES or ChCl-LA at a constant shear rate of (a)  $1 \text{ s}^{-1}$  at different concentrations and (b)  $10 \text{ s}^{-1}$  for at  $6.76 \times 10^2 \text{ M}$ .

Moreover, Figure 4.29b illustrates the time-dependent behavior of treated suspensions using NADES and ChCl-LA at a constant concentration and shear rate of  $6.76 \times 10^{-2} \text{ M}$  and  $10 \text{ s}^{-1}$ , respectively for around 5 minutes. The purpose of the conducted analysis was to investigate the changes in the flocs interactions a higher shear rate will cause in addition to whether they will completely breakdown into their constituent particles or not. Observations from Figure 4.29b reveal that even at higher shear, bentonite suspensions treated with NADES and ChCl-LA at a concentration of  $6.76 \times 10^2 \text{ M}$  exhibit equilibrium viscosities of  $142.7 \text{ mPa}$ , and  $28.1 \text{ mPa}$ , respectively. Despite the drop in the viscosity, as manifested in the observed shear thinning behavior, the viscosity at  $10 \text{ s}^{-1}$  is still more than two orders of magnitude higher than bentonite suspension. Thus, the flocs do not completely breakdown after 5

minutes of shearing at  $10 \text{ s}^{-1}$ . Hence, the produced suspensions are stable under shearing, which facilitates the separation of these flocs in typical field applications.

Table 4.9 summarizes the initial and equilibrium viscosities for both untreated and treated suspensions with the two coagulants (i.e., NADES and ChCl-LA) at variable concentrations and two different shear rates. Depending on the concentration and the selected shear rate for the measurement, the reduction in the viscosity varied between 50% up to 95% with the lowest reduction observed in NADES treated suspension with  $6.76 \times 10^{-2} M$  at both shear rates.

Table 4.9: Initial and equilibrium viscosities of untreated and treated bentonite suspension with NADES and ChCl-LA

Coagulant	Shear Rate $s^{-1}$	Concentration $M$	Initial Viscosity	Equilibrium Viscosity $mPa.s$
-	-	-	7.0	1.1
NADES	1	$5.9 \times 10^{-3}$	507.4	80.6
		$1.78 \times 10^{-2}$	1671.1	118.5
		$6.76 \times 10^{-2}$	2956.2	1442.6
ChCl-LA	1	$5.9 \times 10^{-3}$	7.9	1.3
		$1.78 \times 10^{-2}$	522.7	58.7
		$6.76 \times 10^{-2}$	1276.0	71.9
NADES	10	$6.76 \times 10^{-2}$	358.46	142.7
ChCl-LA			173.2	28.1

#### 4.4.3.2. Viscoelastic behavior

The storage/ elastic modulus ( $G'$ ) and the loss/ viscous ( $G''$ ) modulus are properties that correspond to the amount of energy stored in or dissipated from a material during deformation.  $G'$  and  $G''$  are obtained through oscillatory measurements in order to determine the strength of the sediment produced from the destabilization of bentonite suspension. Table 4.10 shows the  $G'$  and  $G''$  values attained from the linear viscoelastic region in Figure 4.30 in addition to the critical frequency,  $\omega_c$ , ( $G' = G''$  at  $\omega_c$ ) for all NADES and ChCl-LA treated suspensions. Observations from Table 4.10 show that for all tested samples,  $G'$  values are always higher than  $G''$  which confirms the viscoelastic solid-like behavior for the treated suspension. The higher the value of  $G'$  in comparison to the  $G''$  and the positive shift in  $\omega_c$  demonstrate a higher structural strength of the formed sediments. Important factors that influence the structural strength of the studied systems are the flocs size and the interactions between them. With reference to Figure 4.26, it appears that when larger and stiffer flocs are formed, greater  $G'$  values are achieved. This observation is a result of the better interactions between the positively charged coagulant and the negatively charged bentonite particles at higher concentrations. Therefore, resulting in larger and stronger flocs with higher resistivity to breakage upon increasing the angular frequency in oscillatory shear. The obtained findings show similar trends to other studies on the treatment of bentonite suspension using polyelectrolytes as a destabilizing agent [67,94].

Table 4.10: Elastic/ storage modulus and loss modulus for untreated and treated bentonite suspension with NADES and ChCl-LA at three different concentrations

Coagulant	Concentration	$G'$	$G''$	Critical frequency, $\omega_c$
	$M$	$mPa$	$mPa$	rad/s
NADES	$5.9 \times 10^{-3}$	4856.3	467.9	29.2
	$1.78 \times 10^{-2}$	9406	723.1	46.9
	$6.76 \times 10^{-2}$	17286.0	1448.5	> 200
ChCl-LA	$5.9 \times 10^{-3}$	639.4	57.1	18.2
	$1.78 \times 10^{-2}$	4050.5	342.1	29.2
	$6.76 \times 10^{-2}$	8579.8	607.3	75.3

Figure 4.30 represents the viscoelastic behavior of the treated bentonite suspension with NADES and ChCl-LA by means of elastic moduli ( $G'$ ) and viscous moduli ( $G''$ ) as a function of the oscillatory frequency at a constant strain of 0.3%. As  $G'$  represents the amount of mechanical energy stored in the systems under study, systems treated with NADES appear to have higher storage capacity than those treated with ChCl-LA. Whereas, at a unified dosage, the attained  $G'$  and  $G''$  values for suspensions treated with NADES are higher by around twice the magnitude compared with ChCl-LA treated system. The obtained results follow the same trend as the floc size distribution and viscosity trends. Thus, it confirms that better interactions between the coagulant and bentonite particles contribute to the formation of larger, stronger, and more compacted and stable flocs, which are desired for further treatment and separation processes.

On the other hand, the  $G''$  values demonstrate the simultaneous energy loss with increasing the oscillatory frequency by the viscoelastic systems. The sharp decrease in the values of  $G'$  at higher angular frequency is associated with a sharp increase in the  $G''$  values implying the transition of the treated bentonite suspension behavior from solid-like to liquid-like behavior. The point after which the material starts exhibiting a behavior shift is known as the transition point or the critical frequency. Figure 4.30 shows that for the treated suspensions with a concentration  $\leq 1.78 \times 10^{-2}M$ ,  $G'$  remains steady under an oscillatory frequency of 30 rads/sec or less. Furthermore, when comparing both coagulants at similar concentrations, it appears that NADES exhibits solid-like behavior over a wider frequency range. For example, at  $6.76 \times 10^{-2}M$ , the  $G'$  values remain steady under oscillations of frequency as high as 100 rads/sec for NADES treated suspension indicating the formation of strong flocs with high breakage resistance. While flocs breakage starts at an oscillatory frequency of 50 rads/sec for systems treated with ChCl-LA at the same concentration. In addition, the treated bentonite suspension with the highest yield stress ( $\tau_0$ ) showed stronger and stiffer flocs with higher elastic properties.

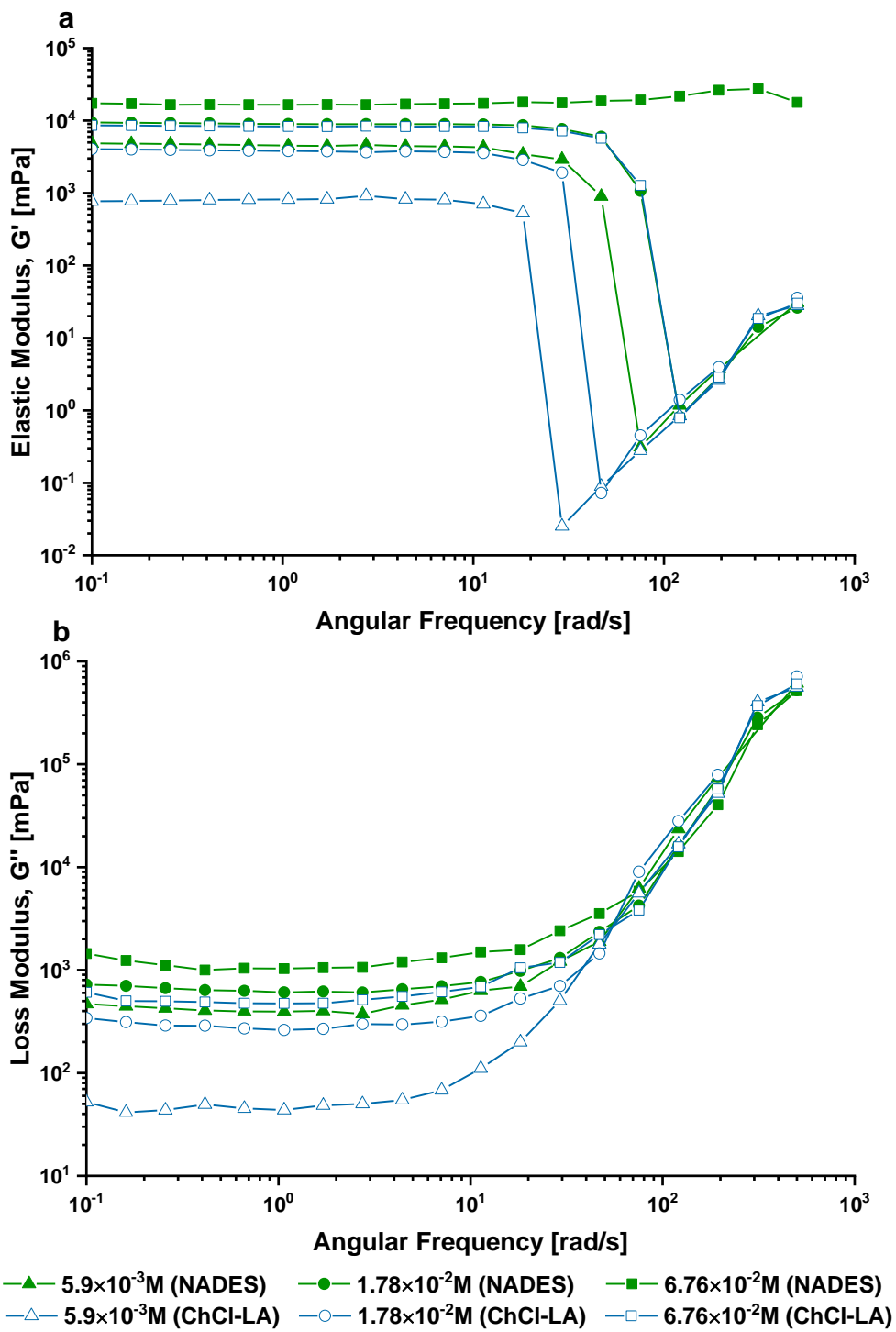


Figure 4.30: (a) Elastic modulus and (b) viscous modulus for treated bentonite suspension with NADES and ChCl-LA at three different concentrations



#### **4.4.4. Destabilization degree vs. rheological behavior of treated bentonite suspension**

##### **4.4.4.1. Zeta potential**

Zeta potential ( $\zeta$  – potential) is a physical property exhibited by the particles in any solid-liquid systems [280]. It is known as the difference in the potential between the suspension media and the stationary layer surrounding the particle. In other words, it is the total net surface charge of the particles in a system. Zeta potential has a significant role in determining the stability of the suspension. High  $\zeta$  – potential values indicate the domination of repulsive forces between the particles over attractive forces and hence, resulting in highly stable system [1,84]. Consequently, the dispersed system will have low viscosity and will begin to flow under the application of low stress [23]. On the other hand, when the system is destabilized using a flocculant or a coagulant such as NADES or ChCl-LA mixture, the negative charges on the particles attract the positive charges on the coagulant promoting the formation of flocs through electrostatic patch coagulation mechanism (EPC). Therefore, the viscosity of the system increases and higher stress magnitudes will be required to breakdown the formed flocs and initiate the flow. Figure 4.31 demonstrates the relation between the zeta potential and three other parameters which are: the viscosity, the yield stress, and the elastic modulus for bentonite suspensions treated with NADES and ChCl-LA mixture at different concentrations.

From Table 4.8, untreated bentonite suspension has the lowest zeta potential of  $-40.4$  mV with a floc size of  $2.5$   $\mu\text{m}$  and is described as a Newtonian fluid where the viscosity is independent of the shear rate. This is attributed to the high stability of the system due to the domination of the repulsive forces between the bentonite particles. From Figure 4.31, it can be seen that the addition of NADES or ChCl-LA to the

bentonite suspension aggregates the system and reduces its stability by reducing the negative  $\zeta$ . By increasing the concentration of the coagulant (NADES or ChCl-LA), the systems under study exhibit a further reduction in the negative zeta potential. This reduction is associated in all cases with an increase in the viscosity, elastic modulus, and yield stress. The increase in the rheological parameters is mainly attributed to the formation of larger, stronger, and stiffer flocs that can withstand higher stress before breaking.

Furthermore, in addition to the concentration effect on the zeta potential, the type of the used coagulant influences the rheological behavior of the system. For treated bentonite suspension with NADES and ChCl-LA at a concentration of  $1.78 \times 10^{-2}$  M, the obtained  $\zeta$  values are similar ( $-20.2$  mV and  $-21.8$  mV, respectively). However, the rheological parameters for the NADES treated bentonite suspension is almost double the values of the system coagulated with ChCl-LA. The observed behavior is mainly due to the difference in structure between the two coagulants.

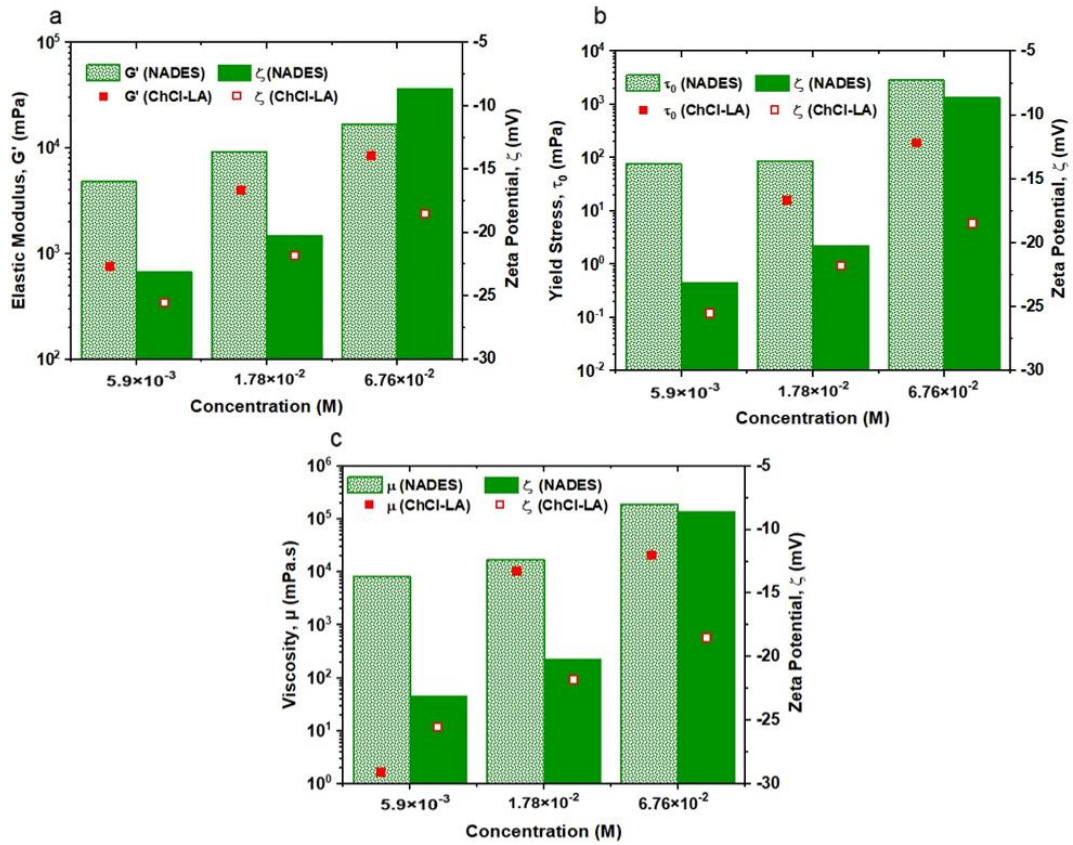


Figure 4.31: (a) Elastic modulus, (b) Bingham yield stress, and (c) viscosity of treated bentonite suspension as a function of zeta potential at different concentrations.

#### 4.4.4.2. Flocs size and CST

Floc size is commonly determined through particle size distribution (PDS) which is a method used to determine the average size of particles presented in a system. Showing the relationship between the results of the particle size distribution represented in the median diameter ( $D_{50}$ ) and the rheological behavior of the treated bentonite suspension is an important step as it supports the obtained trend correlating the zeta potential results to the rheological parameters.

Figure 4.32 reveals the relation between the floc size ( $D_{50}$ ) and the elastic

modulus, the Bingham yield stress, and the initial viscosity of the treated bentonite suspension with NADES or ChCl-LA. In addition, they show the effect of the coagulant type and concentration on the floc size and the rheological parameters. Observations from

Figure 4.32 demonstrates that an increase in coagulant concentration leads to the formation of larger flocs which is associated with higher elastic modulus, yield stress, and viscosity. Furthermore, the type of the used coagulant has an influence on the floc size and rheological parameters. By comparing the performance of the NADES and ChCl-LA at a constant concentration of  $1.78 \times 10^{-2}$  M, it is clear that NADES results in a better characteristic. Moreover, at a concentration of  $5.9 \times 10^{-2}$  M, the resultant flocs have approximately similar median diameters, however, all three rheological parameters (i.e., elastic modulus, yield stress, and initial viscosity) are higher for NADES treated suspension. The difference in the rheological behavior between the two coagulants is mainly attributed to their structural difference and the hydrogen bonding connecting the two components in NADES which results in a longer coagulant chain where more particles can get attached forming larger flocs. Nevertheless, the obtained trends are in good agreement with the zeta potential results as less negative zeta potential values were associated with larger and stronger flocs giving higher elastic modulus, yield stress, and viscosity.

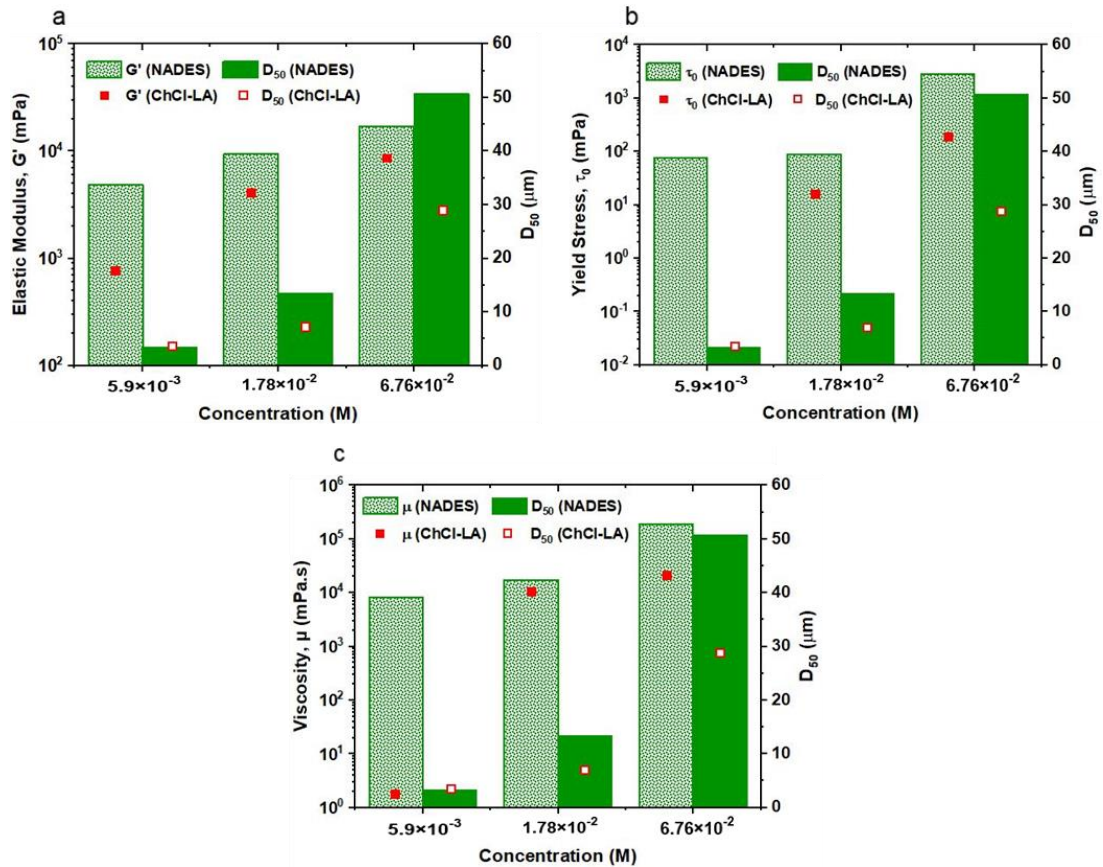


Figure 4.32: (a) Elastic modulus, (b) Bingham yield stress, and (c) viscosity of treated bentonite suspension as a function of  $D_{50}$  at different concentrations.

Furthermore, capillary suction time (CST) was conducted to analyze the effect of the coagulant's concentration on the filterability of bentonite suspension. CST is known as the time needed for free water to filtrate from the solid layer (flocs) through porous media such as filter papers as a result of capillary suction pressure [149]. Generally, flocs with smaller median diameter exhibit larger CST values than that of larger diameter as the water flow more easily and at higher rates in wider capillaries [152,153]. Figure 4.33 illustrates the variation in CST with the elastic modulus, the yield stress, and the initial viscosity for bentonite suspension treated with NADES and ChCl-LA as a function of the concentration. It can be seen that as the studied rheological

parameters increase with concentration, the CST values decrease as a result of the formation of larger flocs and hence, wider capillaries and higher filtration rates. When NADES was used as a coagulant, the CST of bentonite sediments decreased from almost 60 sec at a concentration of  $5.90 \times 10^{-3}$  to 9 sec at a concentration of  $6.76 \times 10^{-2}$ . Furthermore, as it was observed previously with zeta potential and floc size, NADES showed a higher filtration rate (lower CST values) compared to  $\text{ChCl-LA}$ . Therefore, it can be concluded that all six parameters are directly related to each other's as when larger flocs with a less negative zeta potential are formed, greater elastic modulus, yield stress, and viscosity with lower CST are obtained. Thus, NADES has a better performance as a destabilizing agent for bentonite suspension.

The obtained results show comparable trends with other well-known destabilizing agents. For example, polyDADMAC (FL 4440) was used as a coagulant for the conditioning of industrial MBR sludge [23]. At an optimum dosage of 50 mg/L, the conditioned sludge had flocs with a median diameter of 52  $\mu\text{m}$  and CST of 8 sec [23]. Furthermore, the CST of synthetic clay suspension coagulated with traditional coagulants such as aluminum sulfate and ferric chloride were 55.5 sec and 75.7 sec, respectively [152]. Therefore, it is clear from the obtained results that NADES as a novel coagulant is compatible with traditional coagulants in terms of performance and environmental properties.

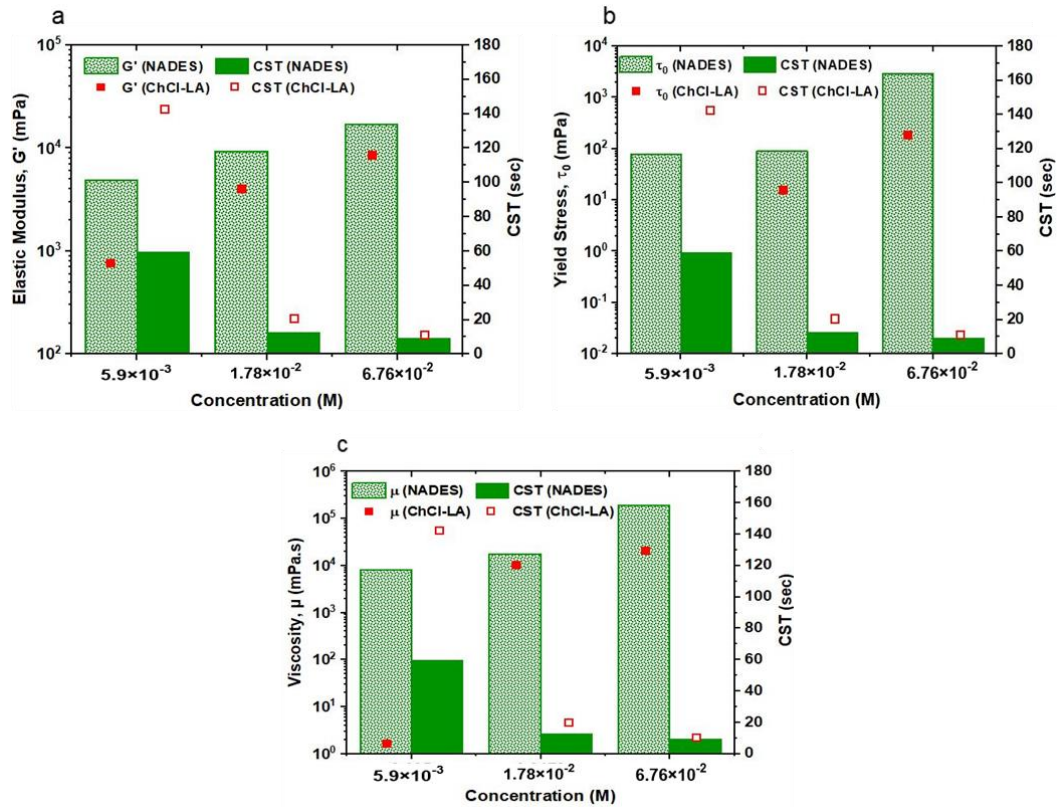


Figure 4.33: (a) Elastic modulus, (b) Bingham yield stress, and (c) viscosity of treated bentonite suspension as a function of CST at different concentrations.

#### 4.4.5. Conclusions

The main purpose of this study was to investigate the effect of the destabilization process using NADES and a combination of its constituent components (ChCl-LA) on the destabilization degree and the rheological behavior of bentonite suspension. Furthermore, a correlation between the rheological parameters (i.e., elastic modulus, yield stress, and initial viscosity) and the destabilization degree of the treated suspension was performed. The achieved results provided the following conclusions:

- Untreated bentonite suspension exhibited a Newtonian behavior where the viscosity remained constant with increasing the shear rate.

- Treated suspensions showed a non-Newtonian shear thinning behavior as the viscosity decreased upon shearing and they were described by the Bingham model. In addition, time-dependent (thixotropic) behavior was detected in bentonite suspensions treated with NADES and ChCl-LA.
- The destabilization process with NADES and ChCl-LA was found to enhance the rheological parameters of bentonite suspension such as yield stress ( $\tau_0$ ), elastic modulus ( $G'$ ) in addition to the initial and equilibrium viscosities. This enhancement is mainly attributed to interactions between the coagulant and the bentonite particles allowing the formation of larger particles and hence, more viscous and stronger systems.
- A higher destabilization degree was accompanied by an enhancement in the rheological behavior of the treated suspensions. Thus, increasing the coagulant dosage was found to be advantageous as it further aggregates the system and enhances the studied rheological parameters.
- The use of NADES as the destabilizing agent demonstrates better performance compared to ChCl-LA which is mainly due to the presence of the hydrogen bond connecting choline chloride and lactic acid in NADES resulting in coagulant with better properties.
- At a concentration of  $6.76 \times 10^{-2}$  M, suspension treated with NADES achieved high reduction in turbidity (99.97%) and the negative zeta potential with a  $D_{50}$  of  $50.7 \mu\text{m}$  and short CST of 9.3 sec. As a result the system exhibited relatively high viscosity and yield stress of 194,110 mPa.s and 2959.3 mPa, respectively.



## 5. CONCLUSIONS AND FUTURE PROSPECTS

### 5.1. Conclusions

The ultimate objective of this study is to understand the influence of choline chloride (ChCl) based natural deep eutectic solvents (NADESs) on the destabilization and separation processes of clay minerals specifically bentonite and to determine the optimum operating conditions of the process. To accomplish the aim of the study, comprehensive knowledge of the bentonite-NADES systems in both the free settling region and the networked region of the suspension is required. Knowledge of the suspension's free settling region and the networked region is obtained from the electrokinetics (settling behavior, zeta potential, turbidity, and floc size measurements) and rheological measurements of the formed sediments, respectively. Furthermore, a correlation between the electrokinetic and rheological properties of the treated suspensions is conducted to achieve the targeted objective.

In aqueous media, bentonite forms a highly stable suspension which raises the complexity of the treatment process. The stability of bentonite suspensions arises from the colloidal nature of the particles possessing a negative surface charge. Therefore, the selection of choline chloride based NADES as a destabilizing agent for bentonite suspensions is attributed to the presence of a cationic functional group in the ChCl structure. The utilized NADESs were synthesized with a 1:1 molar ratio of ChCl as the hydrogen bond acceptor (HBA) and three carboxylic acids i.e., lactic acid (LA), malic acid (MA), and citric acid (CA) as the hydrogen bond donors (HBD). The destabilization degree of bentonite suspension was evaluated through the changes in the electrokinetic parameters of the suspension including zeta potential, the residual turbidity of the supernatant, and the floc size of the produced sediments. Additionally, the influence of ChCl, LA, and a mixture of both (ChCl-LA) on the electrokinetic of

bentonite suspension was investigated to determine the role of each component in the destabilization process and the influence of water on the efficiency of NADES as a destabilizing agent.

In the absence of any destabilizing agent, bentonite suspension exhibits a negative zeta potential of  $-40$  mV and have particles with a median diameter ( $D_{50}$ ) of  $2.5$   $\mu\text{m}$ . The turbidity of the suspension varies depending on the amount of bentonite in the system from 350 NTU up to 4100 NTU. The coagulants' efficiency was determined according to the obtained results from minimizing the required dosage, maximizing the reduction in the residual turbidity and negative zeta potential of the supernatant, and achieving larger and stronger floc with a faster settling rate. With a turbidity reduction of 2% and particle size of  $3.3$   $\mu\text{m}$ , bentonite suspensions treated with LA by itself did not exhibit any significant changes in the turbidity or the floc size. ChCl on its own demonstrated a good reduction in the residual turbidity. Nevertheless, the obtained results in terms of the zeta potential and a floc size of less than  $10\mu\text{m}$  even at higher dosage lowered its performance efficiency as a coagulant. The observed electrokinetic parameters for bentonite suspensions treated with ChCl-LA mixture indicate its effectiveness in the coagulation process. However, similar results were observed by the three NADES systems under study with one-sixth of the dosage utilized by ChCl-LA mixture. The variation in the coagulation efficiency between the ChCl-LA mixture and the three NADES systems is attributed to the structural difference between them represented in the presence of hydrogen bonds between ChCl and the carboxylic acids in the NADES structure. As a result, coagulants with longer chains and higher molecular weight are formed bringing more particles together and hence, giving more desirable outcomes at a lower dosage. ChCl:LA and ChCl:CA showed similar performance with a 99.8% and 99.9% turbidity reduction, zeta potential of  $-18.8$  mV

and  $-15.6$  mV, and floc size of  $36.7$   $\mu\text{m}$  and  $36.2$   $\mu\text{m}$ , respectively. However, the simplicity and time efficiency in addition to the lower dosage requirement of ChCl:LA made it a more efficient and more economical coagulant for bentonite suspension. Accordingly, the most efficient coagulant was ChCl:LA followed by ChCl:CA, ChCl:MA, ChCl-LA mixture, ChCl, and lastly LA with the lowest coagulation efficiency.

Destabilization of bentonite suspension using ChCl based NADESs, ChCl-LA mixture, or ChCl occurs through electrostatic patch coagulation (EPC) mechanism where the coagulant gets absorbed on patches of the negatively charges surface. As a result, electrostatic attraction is exhibited between the particles permitting them to come closer forming larger and more settable flocs. The exhibited coagulation mechanism explains the high reduction achieved in the turbidity. The influence of the coagulant dosage and the bentonite concentration on the destabilization process with CHCl:LA NADES was investigated by conducting an optimization study using the response surface methodology (RSM) function in Minitab. The performance efficiency of the destabilization process was found to be mainly a function of the applied coagulant dosage to the bentonite suspension. More desirable results of minimizing the residual turbidity to below 5 NTU and maximizing the zeta potential and floc size were accomplished by increasing the coagulant dosage. According to the performed optimization study, the optimum operating conditions for the destabilization process with ChCl:LA NADES are  $77$  mM and  $3.48$   $\text{gL}^{-1}$  for the ChCl:LA dosage and the bentonite concentration in the system, respectively. Under these conditions, a supernatant with a turbidity removal of 99.9%, a zeta potential of  $-5.8$  mV, and a pH of 2.2, and sediment with a median floc size of 31.5 were obtained.

The influence of ChCl:LA NADES and ChCl-LA mixture on the coagulation

efficiency of bentonite suspension was assessed through measurements of the rheological parameters. Bentonite suspension in the absence of any coagulant/flocculent demonstrates a Newtonian fluid while a non-Newtonian shear thinning behavior is attained from coagulated suspension with ChC:LA NADES. On the other hand, coagulated suspension with ChCl-LA exhibit a Newtonian behavior at low coagulant dosage and a non-Newtonian shear thinning behavior at moderate and high dosage. Viscoelastic measurements through elastic ( $G'$ ) and viscous ( $G''$ ) modulus of the coagulated suspensions illustrated a solid-like behavior as  $G'$  was always greater in value than  $G''$ .

In spite of the coagulant type, the viscosity along with the Bingham yield stress and the elastic modulus of the coagulated suspensions were found to increase with increasing the coagulant dosage indicating the formation of stronger particle-particle interactions. Furthermore, coagulated suspensions with ChCl:LA NADES demonstrated higher rheological parameters compared to ChCh-LA mixture as larger flocs and stronger networks were formed. Overall, ChCl:LA NADES demonstrates better rheological performance. Hence, it can be concluded that ChCl:LA NADES results in a stronger and more compacted network with a rapid filtration rate of the water within the produced sediment.

## 5.2. Future Prospects

The presented research study investigates for the first time, novel application of ChCl based NADES as a destabilizing agent for colloidal clay suspension. Hence, there is tremendous work that can be conducted to develop and improve the treatment process of colloidal suspensions using the emerging coagulant.

- i. The performance of ChCl:LA NADES in destabilization and separation of different types of colloidal suspension such as kaolinite and precipitated calcium carbonate (PCC) in suspension should be investigated to determine its treatment efficiency of clay suspensions with different complexities.
- ii. The influence of NADES with different combinations and molar ratios of the hydrogen bond donor and acceptor on the coagulation performance of clay suspensions could be examined. For example, conducting a study on the treatment efficiency of NADES synthesized from ChCl with sugars or amines such as fructose and urea, respectively.
- iii. ChCl based NADES is highly efficient in the reduction of the supernatant residual turbidity, however, the formed flocs are relatively small and loose. On the other hand, flocculation with polyelectrolytes is characterized by the formation of large and strong flocs with a moderate turbidity reduction. Therefore, it is beneficial to test the performance of the hybrid coagulation/flocculation process using ChCl based NADES as a coagulant with polyelectrolytes as a flocculant.
- iv. Pilot-scale testing of the coagulation process using ChCl based NADES could be performed at advanced stages. Furthermore, an examination of the coagulation performance on real industrial wastewater could be conducted.

## REFERENCES

- [1] S.M.R. Shaikh, M.S. Nasser, I. Hussein, A. Benamor, S.A. Onaizi, H. Qiblawey, Influence of polyelectrolytes and other polymer complexes on the flocculation and rheological behaviors of clay minerals: A comprehensive review, *Sep. Purif. Technol.* 187 (2017) 137–161. <https://doi.org/10.1016/j.seppur.2017.06.050>.
- [2] S.O. Obaje, J.I. Omada, U.A. Dambatta, Clays and their Industrial Applications : Synoptic Review, *Int. J. Sci. Technol.* 3 (2013) 264–270.
- [3] J.D.D. Moraes, S.R.A. Bertolino, S.L. Cuffini, D.F. Ducart, P.E. Bretzke, G.R. Leonardi, Clay minerals: Properties and applications to dermocosmetic products and perspectives of natural raw materials for therapeutic purposes—A review, *Int. J. Pharm.* 534 (2017) 213–219. <https://doi.org/10.1016/j.ijpharm.2017.10.031>.
- [4] Z. Huang, Y. Li, W. Chen, J. Shi, N. Zhang, X. Wang, Z. Li, L. Gao, Y. Zhang, Modified bentonite adsorption of organic pollutants of dye wastewater, *Mater. Chem. Phys.* 202 (2017) 266–276. <https://doi.org/10.1016/j.matchemphys.2017.09.028>.
- [5] M. Magzoub, M. Mahmoud, M. Nasser, I. Hussein, S. Elkatatny, A. Sultan, Thermochemical Upgrading of Calcium Bentonite for Drilling Fluid Applications, *J. Energy Resour. Technol. Trans. ASME.* 141 (2019). <https://doi.org/10.1115/1.4041843>.
- [6] S.A. Memon, R. Arsalan, S. Khan, T.Y. Lo, Utilization of Pakistani bentonite as partial replacement of cement in concrete, *Constr. Build. Mater.* 30 (2012) 237–242. <https://doi.org/10.1016/j.conbuildmat.2011.11.021>.
- [7] Y. Sun, Y. Li, Y. Xu, X. Liang, L. Wang, In situ stabilization remediation of cadmium (Cd) and lead (Pb) co-contaminated paddy soil using bentonite, *Appl.*

- Clay Sci. 105–106 (2015) 200–206. <https://doi.org/10.1016/j.clay.2014.12.031>.
- [8] Q. Tang, T. Katsumi, T. Inui, Z. Li, Membrane behavior of bentonite-amended compacted clay, *Soils Found.* 54 (2014) 329–344. <https://doi.org/10.1016/j.sandf.2014.04.019>.
- [9] M.S. Nasser, F.A. Twaiq, S.A. Onaizi, Effect of polyelectrolytes on the degree of flocculation of papermaking suspensions, *Sep. Purif. Technol.* 103 (2013) 43–52. <https://doi.org/10.1016/j.seppur.2012.10.024>.
- [10] C. Viseras, P. Cerezo, R. Sanchez, I. Salcedo, C. Aguzzi, Current challenges in clay minerals for drug delivery, *Appl. Clay Sci.* 48 (2010) 291–295. <https://doi.org/10.1016/j.clay.2010.01.007>.
- [11] J. Nones, H.G. Riella, A.G. Trentin, J. Nones, Effects of bentonite on different cell types: A brief review, *Appl. Clay Sci.* 105–106 (2015) 225–230. <https://doi.org/10.1016/j.clay.2014.12.036>.
- [12] X. Wang, L. Yang, J. Zhang, C. Wang, Q. Li, Preparation and characterization of chitosan-poly(vinyl alcohol)/bentonite nanocomposites for adsorption of Hg(II) ions, *Chem. Eng. J.* 251 (2014) 404–412. <https://doi.org/10.1016/j.cej.2014.04.089>.
- [13] B. Abu-Jdayil, Rheology of sodium and calcium bentonite-water dispersions: Effect of electrolytes and aging time, *Int. J. Miner. Process.* 98 (2011) 208–213. <https://doi.org/10.1016/j.minpro.2011.01.001>.
- [14] O. Karnland, Chemical and Mineralogical Characterization of the Bentonite Buffer for the Acceptance Control Procedure in a KBS-3 Repository, Stockholm, 2010.
- [15] O. Duman, S. Tunç, Electrokinetic and rheological properties of Na-bentonite in some electrolyte solutions, *Microporous Mesoporous Mater.* 117 (2009) 331–

338. <https://doi.org/10.1016/j.micromeso.2008.07.007>.
- [16] G. Tchobanoglous, F.L. Burton, H.D. Stensel, *Metcalf & Eddy wastewater engineering: treatment and reuse*, 2003.
- [17] S.M.R. Shaikh, M.S. Nasser, I.A. Hussein, A. Benamor, Investigation of the effect of polyelectrolyte structure and type on the electrokinetics and flocculation behavior of bentonite dispersions, *Chem. Eng. J.* 311 (2017) 265–276. <https://doi.org/10.1016/j.cej.2016.11.098>.
- [18] U.C. Ugochukwu, Characteristics of clay minerals relevant to bioremediation of environmental contaminated systems, in: *Modif. Clay Zeolite Nanocomposite Mater. Environ. Pharm. Appl.*, Elsevier Inc., 2018: pp. 219–242. <https://doi.org/10.1016/B978-0-12-814617-0.00006-2>.
- [19] D.T. Moussa, M.H. El-Naas, M. Nasser, M.J. Al-Marri, A comprehensive review of electrocoagulation for water treatment: Potentials and challenges, *J. Environ. Manage.* 186 (2017) 24–41. <https://doi.org/10.1016/j.jenvman.2016.10.032>.
- [20] B. Zhang, H. Su, X. Gu, X. Huang, H. Wang, Effect of structure and charge of polysaccharide flocculants on their flocculation performance for bentonite suspensions, *Colloids Surfaces A Physicochem. Eng. Asp.* 436 (2013) 443–449. <https://doi.org/10.1016/j.colsurfa.2013.07.017>.
- [21] L. Carlson, *Bentonite Mineralogy Part 1 : Methods of Investigation-a literature Review Part 2 : Mineralogical Research of Selected Bentonites*, POSIVA Rep. (2004).
- [22] L. Karimi, A. Salem, The role of bentonite particle size distribution on kinetic of cation exchange capacity, *J. Ind. Eng. Chem.* 17 (2011) 90–95. <https://doi.org/10.1016/j.jiec.2010.12.002>.
- [23] S.A. Yousefi, M.S. Nasser, I.A. Hussein, A. Benamor, M.H. El-Naas, Influence



- of polyelectrolyte structure and type on the degree of flocculation and rheological behavior of industrial MBR sludge, *Sep. Purif. Technol.* 233 (2020). <https://doi.org/10.1016/j.seppur.2019.116001>.
- [24] T. Chatterjee, S. Chatterjee, S.H. Woo, Enhanced coagulation of bentonite particles in water by a modified chitosan biopolymer, *Chem. Eng. J.* 148 (2009) 414–419. <https://doi.org/10.1016/j.cej.2008.09.016>.
- [25] D. Ghernaout, B. Ghernaout, A. Boucherit, Effect of pH on electrocoagulation of bentonite suspensions in batch using iron electrodes, *J. Dispers. Sci. Technol.* 29 (2008) 1272–1275. <https://doi.org/10.1080/01932690701857483>.
- [26] N. Hilal, O.O. Ogunbiyi, M. Al-Abri, Neural network modeling for separation of bentonite in tubular ceramic membranes, *Desalination.* 228 (2008) 175–182. <https://doi.org/10.1016/j.desal.2007.10.006>.
- [27] S. Ju, M.E. Weber, A.S. Mujumdar, Electroosmotic dewatering of bentonite suspensions, *Sep. Technol.* 1 (1991) 214–221. [https://doi.org/10.1016/0956-9618\(91\)80016-S](https://doi.org/10.1016/0956-9618(91)80016-S).
- [28] A. Mahmoud, A. Fernandez, T.M. Chituchi, P. Arlabosse, Thermally assisted mechanical dewatering (TAMD) of suspensions of fine particles: Analysis of the influence of the operating conditions using the response surface methodology, *Chemosphere.* 72 (2008) 1765–1773. <https://doi.org/10.1016/j.chemosphere.2008.04.075>.
- [29] S.M.R. Shaikh, M.S. Nasser, M. Magzoub, A. Benamor, I.A. Hussein, M.H. El-Naas, H. Qiblawey, Effect of electrolytes on electrokinetics and flocculation behavior of bentonite-polyacrylamide dispersions, *Appl. Clay Sci.* 158 (2018) 46–54. <https://doi.org/10.1016/j.clay.2018.03.017>.
- [30] C.S. Lee, J. Robinson, M.F. Chong, A review on application of flocculants in

- wastewater treatment, *Process Saf. Environ. Prot.* 92 (2014) 489–508.  
<https://doi.org/10.1016/j.psep.2014.04.010>.
- [31] J.L. Lin, C. Huang, C.J.M. Chin, J.R. Pan, Coagulation dynamics of fractal flocs induced by enmeshment and electrostatic patch mechanisms, *Water Res.* 42 (2008) 4457–4466. <https://doi.org/10.1016/j.watres.2008.07.043>.
- [32] E. Barbot, P. Dussouillez, J.Y. Bottero, P. Moulin, Coagulation of bentonite suspension by polyelectrolytes or ferric chloride: Floc breakage and reformation, *Chem. Eng. J.* 156 (2010) 83–91. <https://doi.org/10.1016/j.cej.2009.10.001>.
- [33] M. Daifa, E. Shmoeli, A.J. Domb, Enhanced flocculation activity of polyacrylamide-based flocculant for purification of industrial wastewater, *Polym. Adv. Technol.* 30 (2019) 2636–2646. <https://doi.org/10.1002/pat.4730>.
- [34] J. Ma, J. Shi, L. Ding, H. Zhang, S. Zhou, Q. Wang, X. Fu, L. Jiang, K. Fu, Removal of emulsified oil from water using hydrophobic modified cationic polyacrylamide flocculants synthesized from low-pressure UV initiation, *Sep. Purif. Technol.* 197 (2018) 407–417. <https://doi.org/10.1016/j.seppur.2018.01.036>.
- [35] T. Liu, E. Ding, F. Xue, Polyacrylamide and poly(N,N-dimethylacrylamide) grafted cellulose nanocrystals as efficient flocculants for kaolin suspension, *Int. J. Biol. Macromol.* 103 (2017) 1107–1112. <https://doi.org/10.1016/j.ijbiomac.2017.05.098>.
- [36] M.S. Nasser, A.E. James, The effect of polyacrylamide charge density and molecular weight on the flocculation and sedimentation behaviour of kaolinite suspensions, *Sep. Purif. Technol.* 52 (2006) 241–252. <https://doi.org/10.1016/j.seppur.2006.04.005>.
- [37] E.L. Smith, A.P. Abbott, K.S. Ryder, Deep Eutectic Solvents (DESs) and Their

- Applications, *Chem. Rev.* 114 (2014) 11060–11082.  
<https://doi.org/10.1021/cr300162p>.
- [38] Q. Zhang, K. De Oliveira Vigier, S. Royer, F. Jérôme, Deep eutectic solvents: Syntheses, properties and applications, *Chem. Soc. Rev.* 41 (2012) 7108–7146.  
<https://doi.org/10.1039/c2cs35178a>.
- [39] A.P. Abbott, G. Capper, D.L. Davies, R.K. Rasheed, V. Tambyrajah, Novel solvent properties of choline chloride/urea mixtures, *Chem. Commun.* 9 (2003) 70–71. <https://doi.org/10.1039/b210714g>.
- [40] Y.A. Elhamarnah, M. Nasser, H. Qiblawey, A. Benamor, M. Atilhan, S. Aparicio, A comprehensive review on the rheological behavior of imidazolium based ionic liquids and natural deep eutectic solvents, *J. Mol. Liq.* 277 (2019) 932–958. <https://doi.org/10.1016/j.molliq.2019.01.002>.
- [41] T. Altamash, M.S. Nasser, Y. Elhamarnah, M. Magzoub, R. Ullah, B. Anaya, S. Aparicio, M. Atilhan, Gas Solubility and Rheological Behavior of Natural Deep Eutectic Solvents (NADES) via Combined Experimental and Molecular Simulation Techniques, *ChemistrySelect.* 2 (2017) 7278–7295.  
<https://doi.org/10.1002/slct.201701223>.
- [42] Y. Elhamarnah, H. Qiblawey, M.S. Nasser, A. Benamor, Thermo-rheological characterization of Malic Acid based Natural Deep Eutectic Solvents, *Sci. Total Environ.* 708 (2020) 134848. <https://doi.org/10.1016/j.scitotenv.2019.134848>.
- [43] P.W. Stott, A.C. Williams, B.W. Barry, Transdermal delivery from eutectic systems: Enhanced permeation of a model drug, ibuprofen, *J. Control. Release.* 50 (1998) 297–308. [https://doi.org/10.1016/S0168-3659\(97\)00153-3](https://doi.org/10.1016/S0168-3659(97)00153-3).
- [44] I.M. Aroso, A. Paiva, R.L. Reis, A.R.C. Duarte, Natural deep eutectic solvents from choline chloride and betaine – Physicochemical properties, *J. Mol. Liq.* 241

- (2017) 654–661. <https://doi.org/10.1016/j.molliq.2017.06.051>.
- [45] Y. Hao, M.-N. Chen, Z.-H. Zhang, W.-H. Zhang, X. Jiang, X.-L. Zhou, Choline chloride and lactic acid: A natural deep eutectic solvent for one-pot rapid construction of spiro[indoline-3,4'-pyrazolo[3,4-b]pyridines], *J. Mol. Liq.* 278 (2019) 124–129. <https://doi.org/10.1016/j.molliq.2019.01.065>.
- [46] Y. Dai, G.J. Witkamp, R. Verpoorte, Y.H. Choi, Tailoring properties of natural deep eutectic solvents with water to facilitate their applications, *Food Chem.* 187 (2015) 14–19. <https://doi.org/10.1016/j.foodchem.2015.03.123>.
- [47] G. García, S. Aparicio, R. Ullah, M. Atilhan, Deep eutectic solvents: Physicochemical properties and gas separation applications, *Energy and Fuels.* 29 (2015) 2616–2644. <https://doi.org/10.1021/ef5028873>.
- [48] Y. Zhang, X. Ji, X. Lu, Choline-based deep eutectic solvents for CO<sub>2</sub> separation: Review and thermodynamic analysis, *Renew. Sustain. Energy Rev.* 97 (2018) 436–455. <https://doi.org/10.1016/j.rser.2018.08.007>.
- [49] D. Yang, M. Hou, H. Ning, J. Zhang, J. Ma, G. Yang, B. Han, Efficient SO<sub>2</sub> absorption by renewable choline chloride-glycerol deep eutectic solvents, *Green Chem.* 15 (2013) 2261–2265. <https://doi.org/10.1039/c3gc40815a>.
- [50] S. Mukhopadhyay, S. Mukherjee, N. Farihah, A. Hayyan, F. Des, Ammonium-based deep eutectic solvents as novel soil washing agent for lead removal, *Chem. Eng. J.* 294 (2016) 316–322. <https://doi.org/10.1016/j.cej.2016.02.030>.
- [51] D. Chandran, M. Khalid, R. Walvekar, N.M. Mubarak, S. Dharaskar, W.Y. Wong, T.C.S.M. Gupta, Deep eutectic solvents for extraction-desulphurization: A review, *J. Mol. Liq.* 275 (2019) 312–322. <https://doi.org/10.1016/j.molliq.2018.11.051>.
- [52] A. Abo-Hamad, M. Hayyan, M.A.H. AlSaadi, M.A. Hashim, Potential

- applications of deep eutectic solvents in nanotechnology, *Chem. Eng. J.* 273 (2015) 551–567. <https://doi.org/10.1016/j.cej.2015.03.091>.
- [53] E. Bağda, H. Altundağ, M. Soylak, Highly Simple Deep Eutectic Solvent Extraction of Manganese in Vegetable Samples Prior to Its ICP-OES Analysis, *Biol. Trace Elem. Res.* 179 (2017) 334–339. <https://doi.org/10.1007/s12011-017-0967-5>.
- [54] M.B. Arain, E. Yilmaz, M. Soylak, Deep eutectic solvent based ultrasonic assisted liquid phase microextraction for the FAAS determination of cobalt, *J. Mol. Liq.* 224 (2016) 538–543. <https://doi.org/10.1016/j.molliq.2016.10.005>.
- [55] L. Gu, W. Huang, S. Tang, S. Tian, X. Zhang, A novel deep eutectic solvent for biodiesel preparation using a homogeneous base catalyst, *Chem. Eng. J.* 259 (2015) 647–652. <https://doi.org/10.1016/j.cej.2014.08.026>.
- [56] A.P. Abbott, G. Capper, D.L. Davies, R.K. Rasheed, P. Shikotra, Selective extraction of metals from mixed oxide matrixes using choline-based ionic liquids, *Inorg. Chem.* 44 (2005) 6497–6499. <https://doi.org/10.1021/ic0505450>.
- [57] W. Huang, S. Tang, H. Zhao, S. Tian, Activation of commercial CaO for biodiesel production from rapeseed oil using a novel deep eutectic solvent, *Ind. Eng. Chem. Res.* 52 (2013) 11943–11947. <https://doi.org/10.1021/ie401292w>.
- [58] T. Altamash, M. Atilhan, A. Aliyan, R. Ullah, M. Nasser, S. Aparicio, Rheological, Thermodynamic, and Gas Solubility Properties of Phenylacetic Acid-Based Deep Eutectic Solvents, *Chem. Eng. Technol.* 40 (2017) 778–790. <https://doi.org/10.1002/ceat.201600475>.
- [59] M. Racar, D. Dolar, A. Špehar, A. Kraš, K. Košutić, Optimization of coagulation with ferric chloride as a pretreatment for fouling reduction during nanofiltration of rendering plant secondary effluent, *Chemosphere.* 181 (2017) 485–491.

<https://doi.org/10.1016/j.chemosphere.2017.04.108>.

- [60] K.A. Carrado, A. Decarreau, S. Petit, F. Bergaya, G. Lagaly, Synthetic Clay Minerals and Purification of Natural Clays, in: *Dev. Clay Sci.*, 2006: pp. 115–139. [https://doi.org/10.1016/S1572-4352\(05\)01004-4](https://doi.org/10.1016/S1572-4352(05)01004-4).
- [61] R.A. Schoonheydt, C.T. Johnston, F. Bergaya, Clay minerals and their surfaces, in: *Dev. Clay Sci.*, 2018: pp. 1–21. <https://doi.org/10.1016/B978-0-08-102432-4.00001-9>.
- [62] C.D. Barton, A.D. Karathanasis, Clay minerals, *Encycl. Soil Sci.* (2002) 187–192. <https://doi.org/10.1081/E-ESS-120001688>.
- [63] S.W. Bailey, Summary of recommendations of AIPEA nomenclature committee on clay minerals, *Am. Mineral.* 65 (1980) 1–7.
- [64] S. Farrokhpay, D. Bradshaw, Effect of clay minerals on froth stability in mineral flotation: A review, in: *26th Int. Miner. Process. Congr. IMPC 2012 Innov. Process. Sustain. Growth - Conf. Proc.*, 2012: pp. 4601–4611. <https://doi.org/10.13140/2.1.2025.0567>.
- [65] C. Volzone, J. Ortiga, Influence of the exchangeable cations of montmorillonite on gas adsorptions, *Process Saf. Environ. Prot.* 82 (2004) 170–174. <https://doi.org/10.1205/095758204322972807>.
- [66] M.S. Nasser, S.A. Onaizi, I.A. Hussein, M.A. Saad, M.J. Al-Marri, A. Benamor, Intercalation of ionic liquids into bentonite: Swelling and rheological behaviors, *Colloids Surfaces A Physicochem. Eng. Asp.* 507 (2016) 141–151. <https://doi.org/10.1016/j.colsurfa.2016.08.006>.
- [67] S.M.R. Shaikh, INVESTIGATION OF ELECTROKINETIC AND RHEOLOGICAL BEHAVIORS OF FLOCCULATED POLYELECTROLYTES-BENTONITE DISPERSIONS, (2017).

- [68] F. Civan, MINERALOGY AND MINERAL SENSITIVITY OF PETROLEUM-BEARING FORMATIONS, in: *Reserv. Form. Damage*, second, 2007: pp. 13–77.
- [69] S.L. Abdullahi, A.A. Audu, Comparative analysis on chemical composition of bentonite clays obtained from Ashaka and tango deposits in Gombe State, Nigeria, *ChemSearch J.* 8 (2017) 35-40–40.
- [70] M.K. Uddin, A review on the adsorption of heavy metals by clay minerals, with special focus on the past decade, *Chem. Eng. J.* 308 (2017) 438–462. <https://doi.org/10.1016/j.cej.2016.09.029>.
- [71] A. Zoltán, J. Fodor, R.B. Williams, Bentonite, kaolin, and selected clay minerals, *Environ. Heal. Criteria.* 231 (2005) 196.
- [72] I. Kobayashi, H. Owada, T. Ishii, A. Iizuka, Evaluation of specific surface area of bentonite-engineered barriers for Kozeny-Carman law Evaluation of specific surface area of bentonite-engineered barriers, *Soils Found.* 57 (2017) 683–697. <https://doi.org/10.1016/j.sandf.2017.08.001>.
- [73] S.H. Ismaeel, K.A.-E. M.S. Mabrouk, A.A.A. Ali, Synthesis and Characterization of Bentonite Nanocomposites from Egyptian Bentonite Clay, *Nanotechnol. Allied Sci.* 1 (2017) 16–29.
- [74] B. Karpiński, M. Szkodo, Clay Minerals – Mineralogy and Phenomenon of Clay Swelling in Oil & Gas Industry, *Adv. Mater. Sci.* 15 (2015) 37–55. <https://doi.org/10.1515/adms-2015-0006>.
- [75] M. Diab, D. Curtil, N. El-shinnawy, M.L. Hassan, I.F. Zeid, E. Mauret, Biobased polymers and cationic microfibrillated cellulose as retention and drainage aids in papermaking: Comparison between softwood and bagasse pulps, *Ind. Crops Prod.* 72 (2015) 34–45. <https://doi.org/10.1016/j.indcrop.2015.01.072>.

- [76] J. Shen, Z. Song, X. Qian, W. Liu, Modification of papermaking grade fillers: A brief review, *BioResources*. 4 (2009) 1190–1209. <https://doi.org/10.15376/biores.4.3.1190-1209>.
- [77] R. Saboori, S. Sabbaghi, A. Kalantariasl, Improvement of rheological, filtration and thermal conductivity of bentonite drilling fluid using copper oxide/polyacrylamide nanocomposite, *Powder Technol.* 353 (2019) 257–266. <https://doi.org/10.1016/j.powtec.2019.05.038>.
- [78] J.H. Park, H.J. Shin, M.H. Kim, J.S. Kim, N. Kang, J.Y. Lee, K.T. Kim, J.I. Lee, D.D. Kim, Application of montmorillonite in bentonite as a pharmaceutical excipient in drug delivery systems, *J. Pharm. Investig.* 46 (2016) 363–375. <https://doi.org/10.1007/s40005-016-0258-8>.
- [79] H. Masihi, G. Badalians Gholikandi, Using acidic-modified bentonite for anaerobically digested sludge conditioning and dewatering, *Chemosphere*. 241 (2020) 125096. <https://doi.org/10.1016/j.chemosphere.2019.125096>.
- [80] S. Kakaei, E.S. Khameneh, F. Rezazadeh, M.H. Hosseini, Heavy metal removing by modified bentonite and study of catalytic activity, *J. Mol. Struct.* 1199 (2020) 126989. <https://doi.org/10.1016/j.molstruc.2019.126989>.
- [81] Y. Fu, D.D.L. Chung, Coagulation of oil in water using sawdust, bentonite and calcium hydroxide to form floating sheets, *Appl. Clay Sci.* 53 (2011) 634–641. <https://doi.org/10.1016/j.clay.2011.05.014>.
- [82] S. Abdelkrim, A. Mokhtar, A. Djelad, F. Bennabi, A. Souna, A. Bengueddach, M. Sassi, Chitosan/Ag-Bentonite Nanocomposites: Preparation, Characterization, Swelling and Biological Properties, *J. Inorg. Organomet. Polym. Mater.* 30 (2020) 831–840. <https://doi.org/10.1007/s10904-019-01219-8>.



- [83] W.K.M.B. Salameh, H. Ahmad, W. Mhairat, Comparison of Electrocoagulation and Coagulation, 1 (2016) 176–181.
- [84] D.T. Moussa, M.H. El-Naas, M. Nasser, M.J. Al-Marri, A comprehensive review of electrocoagulation for water treatment: Potentials and challenges, *J. Environ. Manage.* 186 (2017) 24–41. <https://doi.org/10.1016/j.jenvman.2016.10.032>.
- [85] G.M. Kontogeorgis, S. Kiil, *Introduction to Applied Colloid and Surface Chemistry*, 2016. <https://doi.org/10.1002/9781118881194>.
- [86] H.P.C.R. Raj, *Principles of Colloid and Surface Chemistry, Revised and Expanded*, 1997. [https://doi.org/10.1016/0021-9797\(79\)90045-6](https://doi.org/10.1016/0021-9797(79)90045-6).
- [87] P. Taylor, D. Ghernaout, M. Naceur, B. Ghernaout, A review of electrocoagulation as a promising coagulation process for improved organic and inorganic matters removal by electrophoresis and electroflotation, *Desalin. Water Treat.* 28 (2011) 287–320.
- [88] D. Ghernaout, Controlling Coagulation Process: From Zeta Potential to Streaming Potential, *Am. J. Environ. Prot.* 4 (2015) 16. <https://doi.org/10.11648/j.ajeps.s.2015040501.12>.
- [89] N.K. Shamma, Coagulation and Flocculation, in: *Physicochem. Treat. Process.*, Humana Press, New Jersey, 2005: pp. 103–140. <https://doi.org/10.1385/1-59259-820-x:315>.
- [90] P.F. Luckham, S. Rossi, Colloidal and rheological properties of bentonite suspensions, *Adv. Colloid Interface Sci.* 82 (1999) 43–92. [https://doi.org/10.1016/S0001-8686\(99\)00005-6](https://doi.org/10.1016/S0001-8686(99)00005-6).
- [91] Y.-S. Peng, *Electrokinetics and Settling Characteristics of Paper Industry Suspension*, University of Manchester, Institution of Science and Technology, 2000.

- [92] M. Elimelech, J. Gregory, X. Jia, R.A. Williams, Colloidal hydrodynamics and transport, in: Part. Depos. Aggreg., 1995: pp. 68–109. <https://doi.org/10.1016/b978-0-7506-0743-8.50008-x>.
- [93] M. Elimelech, J. Gregory, X. Jia, R.A. Williams, Surface interaction potentials, in: Part. Depos. Aggreg., 1995: pp. 33–67. <https://doi.org/10.1016/b978-0-7506-0743-8.50007-8>.
- [94] M. Shamlooh, A. Rimeh, M.S. Nasser, M.A. Al-Ghouti, M.H. El-Naas, H. Qiblawey, Enhancement of flocculation and shear resistivity of bentonite suspension using a hybrid system of organic coagulants and anionic polyelectrolytes, Sep. Purif. Technol. 237 (2020) 116462. <https://doi.org/10.1016/j.seppur.2019.116462>.
- [95] C.Y. Teh, P.M. Budiman, K.P.Y. Shak, T.Y. Wu, Recent Advancement of Coagulation-Flocculation and Its Application in Wastewater Treatment, Ind. Eng. Chem. Res. 55 (2016) 4363–4389. <https://doi.org/10.1021/acs.iecr.5b04703>.
- [96] J.F. Carstens, J. Bachmann, I. Neuweiler, A new approach to determine the relative importance of DLVO and non-DLVO colloid retention mechanisms in porous media, Colloids Surfaces A Physicochem. Eng. Asp. 560 (2019) 330–335. <https://doi.org/10.1016/j.colsurfa.2018.10.013>.
- [97] T. Okubo, Fundamentals of Colloid and Surface Chemistry, 2015. <https://doi.org/10.1016/b978-0-12-802163-7.00002-7>.
- [98] A.I. Zouboulis, P.A. Moussas, F. Vasilakou, Polyferric sulphate: Preparation, characterisation and application in coagulation experiments, J. Hazard. Mater. 155 (2008) 459–468. <https://doi.org/10.1016/j.jhazmat.2007.11.108>.
- [99] O. Sahu, P. Chaudhari, Review on Chemical treatment of Industrial Waste

- Water, J. Appl. Sci. Environ. Manag. 17 (2013).  
<https://doi.org/10.4314/jasem.v17i2.8>.
- [100] D.H. Bache, C. Johnson, E. Papavasiliopoulos, E. Rasool, F.J. McGilligan, Sweep coagulation: Structures, mechanisms and practice, J. Water Supply Res. Technol. - AQUA. 48 (1999) 201–210.
- [101] T. Suopajarvi, Functionalized nanocelluloses in wastewater treatment applications, University of Oulo, 2015.
- [102] B. Ersoy, I. Tosun, A. Günay, S. Dikmen, Turbidity removal from wastewaters of natural stone processing by coagulation/flocculation methods, Clean - Soil, Air, Water. 37 (2009) 225–232. <https://doi.org/10.1002/clen.200800209>.
- [103] T. Li, Z. Zhu, D. Wang, C. Yao, H. Tang, Characterization of floc size, strength and structure under various coagulation mechanisms, Powder Technol. 168 (2006) 104–110. <https://doi.org/10.1016/j.powtec.2006.07.003>.
- [104] J. Nan, M. Yao, T. Chen, S. Li, Z. Wang, G. Feng, Breakage and regrowth of flocs formed by sweep coagulation using additional coagulant of poly aluminium chloride and non-ionic polyacrylamide, Environ. Sci. Pollut. Res. 23 (2016) 16336–16348. <https://doi.org/10.1007/s11356-016-6805-z>.
- [105] T. Suopajarvi, Functionalized nanocelluloses in wastewater treatment applications, 2015. [https://doi.org/0006-3223\(90\)90442-5](https://doi.org/0006-3223(90)90442-5) [pii].
- [106] Y.L. Cheng, R.J. Wong, J.C. Te Lin, C. Huang, D.J. Lee, A.S. Mujumdar, Water coagulation using electrostatic patch coagulation (EPC) mechanism, Dry. Technol. 28 (2010) 850–857. <https://doi.org/10.1080/07373937.2010.490492>.
- [107] C. Ye, D. Wang, B. Shi, J. Yu, J. Qu, M. Edwards, H. Tang, Alkalinity effect of coagulation with polyaluminum chlorides: Role of electrostatic patch, Colloids Surfaces A Physicochem. Eng. Asp. 294 (2007) 163–173.

<https://doi.org/10.1016/j.colsurfa.2006.08.005>.

- [108] J. Gregory, Rates of flocculation of latex particles by cationic polymers, *J. Colloid Interface Sci.* 42 (1973) 448–456. [https://doi.org/10.1016/0021-9797\(73\)90311-1](https://doi.org/10.1016/0021-9797(73)90311-1).
- [109] D. Wang, H. Tang, J. Gregory, Relative importance of charge neutralization and precipitation on coagulation of kaolin with PACI: Effect of sulfate ion, *Environ. Sci. Technol.* 36 (2002) 1815–1820. <https://doi.org/10.1021/es001936a>.
- [110] B. Bolto, J. Gregory, Organic polyelectrolytes in water treatment., *Water Res.* 41 (2007) 2301–24. <https://doi.org/10.1016/j.watres.2007.03.012>.
- [111] R. Hogg, Bridging flocculation by polymers, *KONA Powder Part. J.* 30 (2012) 3–14. <https://doi.org/10.14356/kona.2013005>.
- [112] J. Swenson, M. V. Smalley, H.L.M. Hatharasinghe, Mechanism and strength of polymer bridging flocculation, *Phys. Rev. Lett.* 81 (1998) 5840–5843. <https://doi.org/10.1103/PhysRevLett.81.5840>.
- [113] H. Burkert, J. Hartmann, G. Herth, Coagulants and flocculants, *Ullmann's Encycl. Ind. Chem.* (2016).
- [114] J. Bartby, *Coagulation and Flocculation in Water and Wastewater Treatment*, Second edi, 2006.
- [115] P.A. Lara, D.. Rodríguez, G.A. Peñuela, Application of coagulation by sweep for removal of metals in natural water used in dairy cattle, (2016) 299–304.
- [116] A. Matilainen, M. Vepsäläinen, M. Sillanpää, Natural organic matter removal by coagulation during drinking water treatment: A review, *Adv. Colloid Interface Sci.* 159 (2010) 189–197. <https://doi.org/10.1016/j.cis.2010.06.007>.
- [117] M.A. Martín, I. González, M. Berrios, J.A. Siles, A. Martín, Optimization of coagulation-flocculation process for wastewater derived from sauce

- manufacturing using factorial design of experiments, *Chem. Eng. J.* 172 (2011) 771–782. <https://doi.org/10.1016/j.cej.2011.06.060>.
- [118] F.M. Pang, P. Kumar, T.T. Teng, A.K. Mohd Omar, K.L. Wasewar, Removal of lead, zinc and iron by coagulation-flocculation, *J. Taiwan Inst. Chem. Eng.* 42 (2011) 809–815. <https://doi.org/10.1016/j.jtice.2011.01.009>.
- [119] M.J. Brandt, K.M. Johnson, A.J. Elphinston, D.D. Ratnayaka, Storage, Clarification and Chemical Treatment, in: *Twort's Water Supply*, 2017: pp. 323–366. <https://doi.org/10.1016/b978-0-08-100025-0.00008-9>.
- [120] E. Fosso-Kankeu, A. Webster, I.O. Ntwampe, F.B. Waanders, Coagulation/Flocculation Potential of Polyaluminium Chloride and Bentonite Clay Tested in the Removal of Methyl Red and Crystal Violet, *Arab. J. Sci. Eng.* 42 (2017) 1389–1397. <https://doi.org/10.1007/s13369-016-2244-x>.
- [121] N.D. Tzoupanos, a I. Zouboulis, Coagulation-Flocculation Processes in Water / Wastewater Treatment: the Application of New Generation of Chemical Reagents, 6th IASME/WSEAS Int. Conf. HEAT Transf. Therm. Eng. Environ. (2008) 309–317.
- [122] Z. He, H. Lan, W. Gong, R. Liu, Y. Gao, H. Liu, J. Qu, Coagulation behaviors of aluminum salts towards fluoride: Significance of aluminum speciation and transformation, *Sep. Purif. Technol.* 165 (2016) 137–144. <https://doi.org/10.1016/j.seppur.2016.01.017>.
- [123] A.I. Zouboulis, N. Tzoupanos, Alternative cost-effective preparation method of polyaluminium chloride (PAC) coagulant agent: Characterization and comparative application for water/wastewater treatment, *Desalination*. 250 (2010) 339–344. <https://doi.org/10.1016/j.desal.2009.09.053>.
- [124] S. Syafalni, I. Abustan, S.N.F. Zakaria, M.H. Zawawi, R.A. Rahim, Raw water

- treatment using bentonite-chitosan as a coagulant, *Water Sci. Technol. Water Supply*. 12 (2012) 480–488. <https://doi.org/10.2166/ws.2012.016>.
- [125] M. Ferhat, S. Kadouche, N. Drouiche, K. Messaoudi, B. Messaoudi, H. Lounici, Competitive adsorption of toxic metals on bentonite and use of chitosan as flocculent coagulant to speed up the settling of generated clay suspensions, *Chemosphere*. 165 (2016) 87–93. <https://doi.org/10.1016/j.chemosphere.2016.08.125>.
- [126] P.N. Dave, A. Gor, *Natural polysaccharide-based hydrogels and nanomaterials: Recent trends and their applications*, Elsevier Inc., 2018. <https://doi.org/10.1016/B978-0-12-813351-4.00003-1>.
- [127] M.A. Aizat, F. Aziz, 12 -Chitosan Nanocomposite Application in Wastewater Treatments, in: *Nanotechnol. Water Wastewater Treat. Theory Appl.*, Elsevier Inc., 2018: pp. 243–265. <https://doi.org/10.1016/B978-0-12-813902-8.00012-5>.
- [128] H.K. Jun, J.S. Kim, H.K. No, S.P. Meyers, Chitosan as a Coagulant for Recovery of Proteinaceous Solids from Tofu Wastewater, *J. Agric. Food Chem.* 42 (1994) 1834–1838. <https://doi.org/10.1021/jf00044a050>.
- [129] M. Thanou, J.C. Verhoef, H.E. Junginger, Oral drug absorption enhancement by chitosan and its derivatives, *Adv. Drug Deliv. Rev.* 52 (2001) 117–126. [https://doi.org/10.1016/S0169-409X\(01\)00231-9](https://doi.org/10.1016/S0169-409X(01)00231-9).
- [130] M.A.A. Razali, Z. Ahmad, M.S.B. Ahmad, A. Ariffin, Treatment of pulp and paper mill wastewater with various molecular weight of polyDADMAC induced flocculation, *Chem. Eng. J.* 166 (2011) 529–535. <https://doi.org/10.1016/j.cej.2010.11.011>.
- [131] W. John, *Synthesis, properties and analysis of polydadmac for water purification*, (2008). <http://hdl.handle.net/10019.1/19531>.

- [132] A. Ariffin, M.A.A. Razali, Z. Ahmad, PolyDADMAC and polyacrylamide as a hybrid flocculation system in the treatment of pulp and paper mills waste water, *Chem. Eng. J.* 179 (2012) 107–111. <https://doi.org/10.1016/j.cej.2011.10.067>.
- [133] W. Sun, G. Zhang, L. Pan, H. Li, A. Shi, Synthesis, characterization, and flocculation properties of branched cationic polyacrylamide, *Int. J. Polym. Sci.* 2013 (2013). <https://doi.org/10.1155/2013/397027>.
- [134] V. Grumezescu, A.M. Holban, I. Barbu, R.C. Popescu, A.E. Oprea, V. Lazar, A.M. Grumezescu, M.C. Chifiriuc, Nanoarchitectonics Used in Antiinfective Therapy, in: *Antibiot. Resist. Mech. New Antimicrob. Approaches*, Elsevier Inc., 2016: pp. 145–166. <https://doi.org/10.1016/B978-0-12-803642-6.00007-1>.
- [135] Y. Wang, B. Gao, Q. Yue, X. Zhan, X. Si, C. Li, Flocculation performance of epichlorohydrin-dimethylamine polyamine in treating dyeing wastewater, *J. Environ. Manage.* 91 (2009) 423–431. <https://doi.org/10.1016/j.jenvman.2009.09.012>.
- [136] Y. Niu, Z. Ding, B. Chen, Y. Chen, The application of epichlorohydrin-dimethylamine polymer flocculant for tannery wastewater treatment, *Adv. Mater. Res.* 610–613 (2013) 480–484. <https://doi.org/10.4028/www.scientific.net/AMR.610-613.480>.
- [137] W. Brostow, H.E. Hagg Lobland, S. Pal, R.P. Singh, Polymeric Flocculants for Wastewater and Industrial Effluent Treatment, *J. Mater. Educ. Pal Singh J. Mater. Educ.* 31 (2009) 3–4. <http://www.unt.edu/LAPOM/>;
- [138] H. Zheng, J. Ma, F. Ji, X. Tang, W. Chen, J. Zhu, Y. Liao, M. Tan, Synthesis and application of anionic polyacrylamide in water treatment, *Asian J. Chem.* 25 (2013) 7071–7074. <https://doi.org/10.14233/ajchem.2013.15144>.
- [139] C.C. Shen, S. Petit, C.J. Li, C.S. Li, N. Khatoon, C.H. Zhou, Interactions between

- smectites and polyelectrolytes, *Appl. Clay Sci.* 198 (2020) 105778.  
<https://doi.org/10.1016/j.clay.2020.105778>.
- [140] J. Song, T. Yamagushi, D.J. Silva, M.A. Hubbe, O.J. Rojas, Effect of charge asymmetry on adsorption and phase separation of polyampholytes on silica and cellulose surfaces, *J. Phys. Chem. B.* 114 (2010) 719–727.  
<https://doi.org/10.1021/jp909047t>.
- [141] A. Rabiee, A. Ershad-Langroudi, H. Jamshidi, Polyacrylamide-based polyampholytes and their applications, *Rev. Chem. Eng.* 30 (2014) 501–519.  
<https://doi.org/10.1515/revce-2014-0004>.
- [142] H. Patel, R.T. Vashi, Use of Naturally Prepared Coagulants for the Treatment of Wastewater from Dyeing Mills, in: *Charact. Treat. Text. Wastewater*, 2015: pp. 147–158. <https://doi.org/10.1016/b978-0-12-802326-6.00006-x>.
- [143] I. Woodard & Curran, Waste characterization, in: *Theory Appl. Transp. Porous Media*, second, 2006: pp. 83–126. [https://doi.org/10.1007/978-94-024-0996-3\\_7](https://doi.org/10.1007/978-94-024-0996-3_7).
- [144] A. Soros, J.E. Amburgey, C.E. Stauber, M.D. Sobsey, L.M. Casanova, Turbidity reduction in drinking water by coagulation-flocculation with chitosan polymers, *J. Water Health.* 17 (2019) 204–218. <https://doi.org/10.2166/wh.2019.114>.
- [145] Guidelines for Drinking-water Quality, *Society.* 20 (1994) 1591–1603.  
<https://doi.org/10.1111/j.1462-2920.2010.02199.x>.
- [146] R.W. Herschy, *Water quality for drinking: WHO guidelines*, 2011.  
[https://doi.org/10.1007/978-1-4020-4410-6\\_184](https://doi.org/10.1007/978-1-4020-4410-6_184).
- [147] D. Al-Risheq, M.S. Nasser, H. Qiblawey, A. Benamor, I.A. Hussein, Destabilization and Separation of High Stable Colloidal Dispersions Using Choline Chloride Based Natural Deep Eutectic Solvent, *Sep. Purif. Technol.* 255



- (2021). <https://doi.org/10.1016/j.seppur.2020.117737>.
- [148] Y. Zhou, G. V. Franks, Flocculation mechanism induced by cationic polymers investigated by light scattering, *Langmuir*. 22 (2006) 6775–6786. <https://doi.org/10.1021/la060281+>.
- [149] N. Gray, Capillary Suction Time (CST), in: *Prog. Filtr. Sep.*, 1st ed., 2015: pp. 659–670. <https://doi.org/10.1016/B978-0-12-384746-1.00017-3>.
- [150] A. Mahmoud, J. Olivier, J. Vaxelaire, A.F.A. Hoadley, Advances in Mechanical Dewatering of Wastewater Sludge Treatment, in: *Wastewater Reuse Manag.*, 2013: pp. 1–500. <https://doi.org/10.1007/978-94-007-4942-9>.
- [151] D. Fitria, Impact of coagulation mixing and time on CST values, *Lect. Notes Eng. Comput. Sci.* 2 (2015) 899–901.
- [152] C. Turchiuli, C. Fargues, Influence of structural properties of alum and ferric flocs on sludge dewaterability, *Chem. Eng. J.* 103 (2004) 123–131. <https://doi.org/10.1016/j.cej.2004.05.013>.
- [153] O. Sawalha, M. Scholz, Assessment of capillary suction time (CST) test methodologies, *Environ. Technol.* 28 (2007) 1377–1386. <https://doi.org/10.1080/09593332808618898>.
- [154] H.F. Wang, H. Hu, H.J. Wang, R.J. Zeng, Impact of dosing order of the coagulant and flocculant on sludge dewatering performance during the conditioning process, *Sci. Total Environ.* 643 (2018) 1065–1073. <https://doi.org/10.1016/j.scitotenv.2018.06.161>.
- [155] Y.B. Pambou, L. Fraikin, T. Salmon, M. Crine, A. Léonard, Enhanced sludge dewatering and drying comparison of two linear polyelectrolytes co-conditioning with polyaluminum chloride, *Desalin. Water Treat.* 57 (2016) 27989–28006. <https://doi.org/10.1080/19443994.2016.1178602>.

- [156] A. Taguet, Rheological characterization of compatibilized polymer blends, in: *Compat. Polym. Blends Micro Nano Scale Phase Morphol. Interphase Charact. Prop.*, Elsevier Inc., 2019: pp. 453–487. <https://doi.org/10.1016/B978-0-12-816006-0.00016-5>.
- [157] M. Sonebi, A. Yahia, Mix design procedure, tests, and standards, in: *Self-Compacting Concr. Mater. Prop. Appl.*, Elsevier Inc., 2019: pp. 1–30. <https://doi.org/10.1016/B978-0-12-817369-5.00001-5>.
- [158] G. Stack, Viscosity of Newtonian and Non-Newtonian Fluids, RheoSense. (2019). <https://www.rheosense.com/applications/viscosity/newtonian-non-newtonian>.
- [159] P.F. Luckham, S. Rossi, The colloidal and rheological properties of bentonite suspension, *Adv. Colloid Interface Sci.* 82 (1999) 43–92. [https://doi.org/10.1016/S0001-8686\(99\)00005-6](https://doi.org/10.1016/S0001-8686(99)00005-6).
- [160] M.J. Pearse, Historical use and future development of chemicals for solid-liquid separation in the mineral processing industry, *Miner. Eng.* 16 (2003) 103–108. [https://doi.org/10.1016/S0892-6875\(02\)00288-1](https://doi.org/10.1016/S0892-6875(02)00288-1).
- [161] N. Ratkovich, W. Horn, F.P. Helmus, S. Rosenberger, W. Naessens, I. Nopens, T.R. Bentzen, Activated sludge rheology: A critical review on data collection and modelling, *Water Res.* 47 (2013) 463–482. <https://doi.org/10.1016/j.watres.2012.11.021>.
- [162] N.P. Chafe, J.R. de Bruyn, Drag and relaxation in a bentonite clay suspension, *J. Nonnewton. Fluid Mech.* 131 (2005) 44–52. <https://doi.org/10.1016/j.jnnfm.2005.08.010>.
- [163] M.S. Nasser, M.J. Al-Marri, A. Benamor, S.A. Onaizi, M. Khraisheh, M.A. Saad, Flocculation and viscoelastic behavior of industrial papermaking

- suspensions, *Korean J. Chem. Eng.* 33 (2016) 448–455.  
<https://doi.org/10.1007/s11814-015-0167-y>.
- [164] N. Cruz, Y. Peng, Rheology measurements for flotation slurries with high clay contents – A critical review, *Miner. Eng.* 98 (2016) 137–150.  
<https://doi.org/10.1016/j.mineng.2016.08.011>.
- [165] A.E. James, D.J.A. Williams, Particle interactions and rheological effects in kaolinite suspensions, *Adv. Colloid Interface Sci.* 17 (1982) 219–232.  
[https://doi.org/10.1016/0001-8686\(82\)80021-3](https://doi.org/10.1016/0001-8686(82)80021-3).
- [166] T. Chen, *Rheological Techniques for Yield Stress Analysis*, 2000.  
<http://www.tainstruments.com/pdf/literature/RH025.pdf>.
- [167] M.I. Magzoub, M.S. Nasser, I.A. Hussein, A. Benamor, S.A. Onaizi, A.S. Sultan, M.A. Mahmoud, Effects of sodium carbonate addition, heat and agitation on swelling and rheological behavior of Ca-bentonite colloidal dispersions, *Appl. Clay Sci.* 147 (2017) 176–183. <https://doi.org/10.1016/j.clay.2017.07.032>.
- [168] H. Van Olphen, FORCES BETWEEN SUSPENDED BENTONITE PARTICLES PART II-CALCIUM BENTONITE, *Clays Clay Miner.* 6 (1957) 196–206.
- [169] M.S. Nasser, A.E. James, Effect of polyacrylamide polymers on floc size and rheological behaviour of kaolinite suspensions, *Colloids Surfaces A Physicochem. Eng. Asp.* 301 (2007).  
<https://doi.org/10.1016/j.colsurfa.2006.12.080>.
- [170] M.S. Nasser, A.E. James, Settling and sediment bed behaviour of kaolinite in aqueous media, *Sep. Purif. Technol.* 51 (2006) 10–17.  
<https://doi.org/10.1016/j.seppur.2005.12.017>.
- [171] M.S. Nasser, A.E. James, Degree of flocculation and viscoelastic behaviour of

- kaolinite-sodium chloride dispersions, *Colloids Surfaces A Physicochem. Eng. Asp.* 315 (2008) 165–175. <https://doi.org/10.1016/j.colsurfa.2007.07.030>.
- [172] R.K. Khandal, T.F. Tadros, Application of viscoelastic measurements to the investigation of the swelling of sodium montmorillonite suspensions, *J. Colloid Interface Sci.* 125 (1988) 122–128. [https://doi.org/10.1016/0021-9797\(88\)90060-4](https://doi.org/10.1016/0021-9797(88)90060-4).
- [173] R. Sohm, T.F. Tadros, Viscoelastic properties of sodium montmorillonite (Gelwhite H) suspensions, *J. Colloid Interface Sci.* 132 (1989) 62–71. [https://doi.org/10.1016/0021-9797\(89\)90216-6](https://doi.org/10.1016/0021-9797(89)90216-6).
- [174] E. Bazrafshan, F.K. Mostafapour, M. Ahmadabadi, A.H. Mahvi, Turbidity removal from aqueous environments by *Pistacia atlantica* (Baneh) seed extract as a natural organic coagulant aid, *Desalin. Water Treat.* 56 (2015) 977–983. <https://doi.org/10.1080/19443994.2014.942704>.
- [175] L. Smoczyński, K.T. Muńska, M. Kosobucka, B. Pierozyński, R. Wardzyńska, B. Załęska-Chróst, Destabilization of model wastewater in the chemical coagulation process, *Ecol. Chem. Eng. S.* 21 (2014) 269–279. <https://doi.org/10.2478/eces-2014-0021>.
- [176] S.M. Mohan, Use of naturalized coagulants in removing laundry waste surfactant using various unit processes in lab-scale, *J. Environ. Manage.* 136 (2014) 103–111. <https://doi.org/10.1016/j.jenvman.2014.02.004>.
- [177] J. Bratby, *Coagulation and Flocculation in Water and Wastewater Treatment*, Third, IWA Publishing, 2016.
- [178] S. Hussain, J. van Leeuwen, C. Chow, S. Beecham, M. Kamruzzaman, D. Wang, M. Drikas, R. Aryal, Removal of organic contaminants from river and reservoir waters by three different aluminum-based metal salts: Coagulation adsorption

- and kinetics studies, *Chem. Eng. J.* 225 (2013) 394–405.  
<https://doi.org/10.1016/j.cej.2013.03.119>.
- [179] W. Yu, J. Gregory, L.C. Campos, N. Graham, Dependence of floc properties on coagulant type, dosing mode and nature of particles, *Water Res.* 68 (2015) 119–126. <https://doi.org/10.1016/j.watres.2014.09.045>.
- [180] N. Wei, Z. Zhang, D. Liu, Y. Wu, J. Wang, Q. Wang, Coagulation behavior of polyaluminum chloride: Effects of pH and coagulant dosage, *Chinese J. Chem. Eng.* 23 (2015) 1041–1046. <https://doi.org/10.1016/j.cjche.2015.02.003>.
- [181] J. Duan, J. Gregory, Coagulation by hydrolysing metal salts, *Adv. Colloid Interface Sci.* 100–102 (2003) 475–502. [https://doi.org/10.1016/S0001-8686\(02\)00067-2](https://doi.org/10.1016/S0001-8686(02)00067-2).
- [182] S. BinAhmed, G. Ayoub, M. Al-Hindi, F. Azizi, The effect of fast mixing conditions on the coagulation–flocculation process of highly turbid suspensions using liquid bittern coagulant, *Desalin. Water Treat.* 53 (2015) 3388–3396. <https://doi.org/10.1080/19443994.2014.933043>.
- [183] W. zheng Yu, J. Gregory, L. Campos, G. Li, The role of mixing conditions on floc growth, breakage and re-growth, *Chem. Eng. J.* 171 (2011) 425–430. <https://doi.org/10.1016/j.cej.2011.03.098>.
- [184] G.M. Ayoub, A. Hamzeh, L. Semerjian, Post treatment of tannery wastewater using lime/bittern coagulation and activated carbon adsorption, *Desalination.* 273 (2011) 359–365. <https://doi.org/10.1016/j.desal.2011.01.045>.
- [185] W. Subramonian, T.Y. Wu, S.P. Chai, A comprehensive study on coagulant performance and floc characterization of natural *Cassia obtusifolia* seed gum in treatment of raw pulp and paper mill effluent, *Ind. Crops Prod.* 61 (2014) 317–324. <https://doi.org/10.1016/j.indcrop.2014.06.055>.

- [186] Z.L. Yang, B.Y. Gao, Q.Y. Yue, Y. Wang, Effect of pH on the coagulation performance of Al-based coagulants and residual aluminum speciation during the treatment of humic acid-kaolin synthetic water, *J. Hazard. Mater.* 178 (2010) 596–603. <https://doi.org/10.1016/j.jhazmat.2010.01.127>.
- [187] D. Hendricks, *Fundamentals of Water Treatment Unit Processes, Physical, Chemical, and Biological*, CRC Press, 2010.
- [188] Y. Matsui, A. Yuasa, Y. Furuya, T. Kamei, Dynamic analysis of coagulation with alum and PACl, *J. / Am. Water Work. Assoc.* 90 (1998) 96–106. <https://doi.org/10.1002/j.1551-8833.1998.tb08522.x>.
- [189] M. V. Jadhav, Y.S. Mahajan, Assessment of feasibility of natural coagulants in turbidity removal and modeling of coagulation process, *Desalin. Water Treat.* 52 (2014) 5812–5821. <https://doi.org/10.1080/19443994.2013.816875>.
- [190] M. V. Jadhav, Y.S. Mahajan, Investigation of the performance of chitosan as a coagulant for flocculation of local clay suspensions of different turbidities, *KSCE J. Civ. Eng.* 17 (2013) 328–334. <https://doi.org/10.1007/s12205-013-2021-2>.
- [191] Z. Zhu, T. Li, J. Lu, D. Wang, C. Yao, Characterization of kaolin flocs formed by polyacrylamide as flocculation aids, *Int. J. Miner. Process.* 91 (2009) 94–99. <https://doi.org/10.1016/j.minpro.2009.01.003>.
- [192] S.Y. Choy, K.N. Prasad, T.Y. Wu, M.E. Raghunandan, R.N. Ramanan, Performance of conventional starches as natural coagulants for turbidity removal, *Ecol. Eng.* 94 (2016) 352–364. <https://doi.org/10.1016/j.ecoleng.2016.05.082>.
- [193] W. John, C.A. Buckley, E.P. Jacobs, R.D. Sanderson, Synthesis and Use of Polyadmac for Water Purification, *Water Res. Comm. (WRC), Bienn. Conf.*

- Water Inst. South. Africa (WISA), Durban, South Africa. (2002) 19–23.
- [194] A.K. Tolkou, A.I. Zouboulis, Synthesis and coagulation performance of composite poly-aluminum-ferric-silicate-chloride coagulants in water and wastewater, *Desalin. Water Treat.* 53 (2015) 3309–3318. <https://doi.org/10.1080/19443994.2014.933614>.
- [195] J. Płotka-Wasyłka, M. de la Guardia, V. Andruch, M. Vilková, Deep eutectic solvents vs ionic liquids: Similarities and differences, *Microchem. J.* 159 (2020). <https://doi.org/10.1016/j.microc.2020.105539>.
- [196] Y.T. Lo, SYNTHESIS AND CHARACTERIZATION OF DEEP EUTECTIC SOLVENTS (DES) WITH MULTIFUNCTIONAL BUILDING BLOCKS, 2019.
- [197] Y. Cui, Investigation of Structure and Dynamics of Deep Eutectic Solvent Using Infrared Spectroscopy, (2018).
- [198] A.S.B. González, M.C. Kroon, W. Weggemans, M. Francisco, S.L. García de Dios, Comparison of a low transition temperature mixture (LTTM) formed by lactic acid and choline chloride with choline lactate ionic liquid and the choline chloride salt: physical properties and vapour–liquid equilibria of mixtures containing water and ethanol, *RSC Adv.* 3 (2013) 23553. <https://doi.org/10.1039/c3ra40303c>.
- [199] G. Imperato, E. Eibler, J. Niedermaier, B. König, Low-melting sugar-urea-salt mixtures as solvents for Diels-Alder reactions, *Chem. Commun.* (2005) 1170–1172. <https://doi.org/10.1039/b414515a>.
- [200] L.I.N. Tomé, V. Baião, W. da Silva, C.M.A. Brett, Deep eutectic solvents for the production and application of new materials, *Appl. Mater. Today.* 10 (2018) 30–50. <https://doi.org/10.1016/j.apmt.2017.11.005>.

- [201] Q. Zhang, K. De Oliveira Vigier, S. Royer, F. Jérôme, Deep eutectic solvents: syntheses, properties and applications., *Chem. Soc. Rev.* 41 (2012) 7108–46. <https://doi.org/10.1039/c2cs35178a>.
- [202] A.P. Abbott, J.C. Barron, K.S. Ryder, D. Wilson, Eutectic-based ionic liquids with metal-containing anions and cations, *Chem. - A Eur. J.* 13 (2007) 6495–6501. <https://doi.org/10.1002/chem.200601738>.
- [203] B. Kudłak, K. Owczarek, J. Namieśnik, Selected issues related to the toxicity of ionic liquids and deep eutectic solvents—a review, *Environ. Sci. Pollut. Res.* 22 (2015) 11975–11992. <https://doi.org/10.1007/s11356-015-4794-y>.
- [204] X. Li, K.H. Row, Development of deep eutectic solvents applied in extraction and separation, *J. Sep. Sci.* 39 (2016) 3505–3520. <https://doi.org/10.1002/jssc.201600633>.
- [205] T. Altamash, M.S. Nasser, Y. Elhamarnah, M. Magzoub, R. Ullah, H. Qiblawey, S. Aparicio, M. Atilhan, Gas solubility and rheological behavior study of betaine and alanine based natural deep eutectic solvents (NADES), *J. Mol. Liq.* 256 (2018) 286–295. <https://doi.org/10.1016/j.molliq.2018.02.049>.
- [206] F. Hollmann, Y. Dai, I.W.C.E. Arends, M. Verberne, R. Verpoorte, Y.H. Choi, J. van Spronsen, G.-J. Witkamp, Are Natural Deep Eutectic Solvents the Missing Link in Understanding Cellular Metabolism and Physiology?, *Plant Physiol.* 156 (2011) 1701–1705. <https://doi.org/10.1104/pp.111.178426>.
- [207] I. Igwe, C. Okonkwo, U. Uzoukwu, C. Onyenegecha, The Effect of Choline Chloride on the Performance of Broiler Chickens, *Annu. Res. Rev. Biol.* 8 (2015) 1–8. <https://doi.org/10.9734/arrb/2015/19372>.
- [208] Chaudhari, K.I. Prajapati, D.C. Lunagariya, P.M. Sorathiya, S.N. Patel, R.P. Patel, N. A.L., An importance of choline chloride for poultry and cattle: an



- overview, *Int. J. Sci. Environ. Technol.* 6 (2017) 2804–2810.  
<http://www.ijset.net/journal/1895.pdf>.
- [209] A.P. Abbott, P.M. Cullis, M.J. Gibson, R.C. Harris, E. Raven, Extraction of glycerol from biodiesel into a eutectic based ionic liquid, *Green Chem.* 9 (2007) 868–872. <https://doi.org/10.1039/b702833d>.
- [210] A.P. Abbott, T.J. Bell, S. Handa, B. Stoddart, Cationic functionalisation of cellulose using a choline based ionic liquid analogue, *Green Chem.* 8 (2006) 784–786. <https://doi.org/10.1039/b605258d>.
- [211] S. Sun, Y. Niu, Q. Xu, Z. Sun, X. Wei, Efficient SO<sub>2</sub> absorptions by four kinds of deep eutectic solvents based on choline chloride, *Ind. Eng. Chem. Res.* 54 (2015) 8019–8024. <https://doi.org/10.1021/acs.iecr.5b01789>.
- [212] N. Osowska, L. Ruzik, New potentials in the extraction of trace metal using natural deep eutectic solvents (NADES), *Food Anal. Methods.* 12 (2019) 926–935. <https://doi.org/10.1007/s12161-018-01426-y>.
- [213] C. D’Agostino, R.C. Harris, A.P. Abbott, L.F. Gladden, M.D. Mantle, Molecular motion and ion diffusion in choline chloride based deep eutectic solvents studied by <sup>1</sup>H pulsed field gradient NMR spectroscopy, *Phys. Chem. Chem. Phys.* 13 (2011) 21383–21391. <https://doi.org/10.1039/c1cp22554e>.
- [214] A.P. Abbott, G. Capper, S. Gray, Design of improved deep eutectic solvents using hole theory, *ChemPhysChem.* 7 (2006) 803–806. <https://doi.org/10.1002/cphc.200500489>.
- [215] A.P. Abbott, D. Boothby, G. Capper, D.L. Davies, R. Rasheed, Deep Eutectic Solvents Formed Between Choline Chloride and Carboxylic Acids, *J. Am. Chem. Soc.* 126 (2004) 9142–9147.
- [216] K. Shahbaz, S. Baroutian, F.S. Mjalli, M.A. Hashim, I.M. Alnashef, Densities of

- ammonium and phosphonium based deep eutectic solvents: Prediction using artificial intelligence and group contribution techniques, *Thermochim. Acta.* 527 (2012) 59–66. <https://doi.org/10.1016/j.tca.2011.10.010>.
- [217] A.P. Abbott, R.C. Harris, K.S. Ryder, Application of hole theory to define ionic liquids by their transport properties, *J. Phys. Chem. B.* 111 (2007) 4910–4913. <https://doi.org/10.1021/jp0671998>.
- [218] W. Guo, Y. Hou, S. Ren, S. Tian, W. Wu, Formation of deep eutectic solvents by phenols and choline chloride and their physical properties, *J. Chem. Eng. Data.* 58 (2013) 866–872. <https://doi.org/10.1021/je300997v>.
- [219] G. Niu, S. Yang, H. Li, J. Yi, M. Wang, X. Lv, J. Zhong, Electrodeposition of Cu-Ga Precursor Layer from Deep Eutectic Solvent for CuGaS<sub>2</sub> Solar Energy Thin Film, *J. Electrochem. Soc.* 161 (2014) D333–D338. <https://doi.org/10.1149/2.050406jes>.
- [220] N.M. Pereira, P.M. V. Fernandes, C.M. Pereira, A. Fernando Silva, Electrodeposition of Zinc from Choline Chloride-Ethylene Glycol Deep Eutectic Solvent: Effect of the Tartrate Ion, *J. Electrochem. Soc.* 159 (2012) D501–D506. <https://doi.org/10.1149/2.004209jes>.
- [221] M. Rostom Ali, M.Z. Rahman, S. Sankar Saha, Electroless and electrolytic deposition of nickel from deep eutectic solvents based on choline chloride, *Indian J. Chem. Technol.* 21 (2014) 127–133.
- [222] T. Yanai, K. Shiraishi, T. Shimokawa, Y. Watanabe, T. Ohgai, M. Nakano, K. Suzuki, H. Fukunaga, Electroplated Fe films prepared from a deep eutectic solvent, *J. Appl. Phys.* 115 (2014) 1–4. <https://doi.org/10.1063/1.4870319>.
- [223] C.D. Gu, Y.H. You, Y.L. Yu, S.X. Qu, J.P. Tu, Microstructure, nanoindentation, and electrochemical properties of the nanocrystalline nickel film, *Surf. Coatings*

Technol. 205 (2011) 4928–4933.

- [224] C. Gu, J. Tu, One-step fabrication of nanostructured ni film with lotus effect from deep eutectic solvent, *Langmuir*. 27 (2011) 10132–10140. <https://doi.org/10.1021/la200778a>.
- [225] J.H. Liao, P.C. Wu, Y.H. Bai, Eutectic mixture of choline chloride/urea as a green solvent in synthesis of a coordination polymer: [Zn(O<sub>3</sub>PCH<sub>2</sub>CO<sub>2</sub>)<sub>2</sub>].NH<sub>4</sub>, *Inorg. Chem. Commun.* 8 (2005) 390–392. <https://doi.org/10.1016/j.inoche.2005.01.025>.
- [226] M.C. Serrano, M.C. Gutiérrez, R. Jiménez, M.L. Ferrer, F. Del Monte, Synthesis of novel lidocaine-releasing poly(diols-co-citrate) elastomers by using deep eutectic solvents, *Chem. Commun.* 48 (2012) 579–581. <https://doi.org/10.1039/c1cc15284j>.
- [227] B.N. Borse, S.R. Shukla, Y.A. Sonawane, G.S. Shankerling, Synthesis of some novel pyrimidinedione and pyrimidinetrione derivatives by a greener method: Study of their antimicrobial activity and photophysical properties, *Synth. Commun.* 43 (2013) 865–876. <https://doi.org/10.1080/00397911.2011.611324>.
- [228] D.Y. Dai, L. Wang, Q. Chen, M.Y. He, Selective oxidation of sulfides to sulfoxides catalysed by deep eutectic solvent with H<sub>2</sub>O<sub>2</sub>, *J. Chem. Res.* 38 (2014) 183–185. <https://doi.org/10.3184/174751914X13923144871332>.
- [229] D.A. Alonso, A. Baeza, R. Chinchilla, G. Guillena, I.M. Pastor, D.J. Ramón, Deep Eutectic Solvents: The Organic Reaction Medium of the Century, *European J. Org. Chem.* 2016 (2016) 612–632. <https://doi.org/10.1002/ejoc.201501197>.
- [230] K. El ttaib, The electrodeposition of composite materials using deep eutectic solvents, 2011.

<http://scholar.google.com/scholar?hl=en&btnG=Search&q=intitle:The+Electro+deposition+of+Composite+Materials+using+Deep+Eutectic+Solvents#0>.

- [231] M.C. Gutiérrez, F. Rubio, F. Del Monte, Resorcinol-formaldehyde polycondensation in deep eutectic solvents for the preparation of carbons and carbon - Carbon nanotube composites, *Chem. Mater.* 22 (2010) 2711–2719. <https://doi.org/10.1021/cm9023502>.
- [232] A.P. Abbott, O. Alaysuy, A.P.M. Antunes, A.C. Douglas, J. Guthrie-Strachan, W.R. Wise, Processing of Leather Using Deep Eutectic Solvents, *ACS Sustain. Chem. Eng.* 3 (2015) 1241–1247.
- [233] J.A. Sirviö, M. Visanko, H. Liimatainen, Deep eutectic solvent system based on choline chloride-urea as a pre-treatment for nanofibrillation of wood cellulose, *Green Chem.* 17 (2015) 3401–3406. <https://doi.org/10.1039/c5gc00398a>.
- [234] H.G. Morrison, C.C. Sun, S. Neervannan, Characterization of thermal behavior of deep eutectic solvents and their potential as drug solubilization vehicles, *Int. J. Pharm.* 378 (2009) 136–139. <https://doi.org/10.1016/j.ijpharm.2009.05.039>.
- [235] M. Francisco, A. van den Bruinhorst, L.F. Zubeir, C.J. Peters, M.C. Kroon, A new low transition temperature mixture (LTTM) formed by choline chloride+lactic acid: Characterization as solvent for CO<sub>2</sub> capture, *Fluid Phase Equilib.* 340 (2013) 77–84. <https://doi.org/10.1016/j.fluid.2012.12.001>.
- [236] K. Mulia, S. Putri, E. Krisanti, Nasruddin, Natural deep eutectic solvents (NADES) as green solvents for carbon dioxide capture, *AIP Conf. Proc.* 1823 (2017). <https://doi.org/10.1063/1.4978095>.
- [237] A. Kamgar, S. Mohsenpour, F. Esmailzadeh, Solubility prediction of CO<sub>2</sub>, CH<sub>4</sub>, H<sub>2</sub>, CO and N<sub>2</sub> in Choline Chloride/Urea as a eutectic solvent using NRTL and COSMO-RS models, *J. Mol. Liq.* 247 (2017) 70–74.

<https://doi.org/10.1016/j.molliq.2017.09.101>.

- [238] I. Adeyemi, M.R.M. Abu-zahra, Solubility of CO<sub>2</sub> in Choline Chloride-Amine Based Deep, IRES Int. Conf. (2017) 22–25.
- [239] E. Ali, M.K. Hadj-Kali, S. Mulyono, I. Alnashef, A. Fakeeha, F. Mjalli, A. Hayyan, Solubility of CO<sub>2</sub> in deep eutectic solvents: Experiments and modelling using the Peng-Robinson equation of state, Chem. Eng. Res. Des. 92 (2014) 1898–1906. <https://doi.org/10.1016/j.cherd.2014.02.004>.
- [240] R.B. Leron, M.H. Li, Solubility of carbon dioxide in a choline chloride-ethylene glycol based deep eutectic solvent, Thermochim. Acta. 551 (2013) 14–19. <https://doi.org/10.1016/j.tca.2012.09.041>.
- [241] N. Ra, N.J. Nicholas, Y. Wu, K.A. Mumford, S.E. Kentish, W. Stevens, Experiments and Thermodynamic Modeling of the Solubility of Carbon Dioxide in Three Different Deep Eutectic Solvents (DESs), (2015). <https://doi.org/10.1021/acs.jced.5b00492>.
- [242] A. Tatar, A. Barati-Harooni, A. Najafi-Marghmaleki, A. Bahadori, Accurate prediction of CO<sub>2</sub> solubility in eutectic mixture of levulinic acid (or furfuryl alcohol) and choline chloride, Int. J. Greenh. Gas Control. 58 (2017) 212–222. <https://doi.org/10.1016/j.ijggc.2017.01.013>.
- [243] X. Liu, B. Gao, D. Deng, SO<sub>2</sub> absorption/desorption performance of renewable phenol-based deep eutectic solvents, Sep. Sci. Technol. 53 (2018) 2150–2158. <https://doi.org/10.1080/01496395.2018.1446026>.
- [244] D. Deng, X. Liu, B. Gao, Physicochemical Properties and Investigation of Azole-Based Deep Eutectic Solvents as Efficient and Reversible SO<sub>2</sub> Absorbents, Ind. Eng. Chem. Res. 56 (2017) 13850–13856. <https://doi.org/10.1021/acs.iecr.7b02478>.

- [245] M. Rogošić, K.Z. Kučan, Deep eutectic solvents based on choline chloride and ethylene glycol as media for extractive denitrification/desulfurization/dearomatization of motor fuels, *J. Ind. Eng. Chem.* 72 (2019) 87–99. <https://doi.org/10.1016/j.jiec.2018.12.006>.
- [246] H.F. Hizaddin, A. Ramalingam, M.A. Hashim, M.K.O. Hadj-Kali, Evaluating the performance of deep eutectic solvents for use in extractive denitrification of liquid fuels by the conductor-like screening model for real solvents, *J. Chem. Eng. Data.* 59 (2014) 3470–3487. <https://doi.org/10.1021/je5004302>.
- [247] C. Bakirtzi, K. Triantafyllidou, D.P. Makris, common native Greek medicinal plants, *J. Dermatol. Sci.* (2016). <https://doi.org/10.1016/j.jarmap.2016.03.003>.
- [248] J.H. Oh, J.S. Lee, Synthesis of gold microstructures with surface nanoroughness using a deep eutectic solvent for catalytic and diagnostic applications, *J. Nanosci. Nanotechnol.* 14 (2014) 3753–3757. <https://doi.org/10.1166/jnn.2014.8658>.
- [249] Y. Zhao, Y. Zhao, H. Feng, J. Shen, Synthesis of nickel phosphide nano-particles in a eutectic mixture for hydrotreating reactions, *J. Mater. Chem.* 21 (2011) 8137–8145. <https://doi.org/10.1039/c1jm10230c>.
- [250] Y. Zheng, L. Ye, L. Yan, Y. Gao, The electrochemical behavior and determination of quercetin in choline chloride/urea deep eutectic solvent electrolyte based on abrasively immobilized multi-wall carbon nanotubes modified electrode, *Int. J. Electrochem. Sci.* 9 (2014) 238–248.
- [251] V.S. Raghuwanshi, M. Ochmann, A. Hoell, F. Polzer, K. Rademann, Deep eutectic solvents for the self-assembly of gold nanoparticles: A SAXS, UV-Vis, and TEM investigation, *Langmuir.* 30 (2014) 6038–6046. <https://doi.org/10.1021/la500979p>.
- [252] M. Arshad, A. Easa, H. Qiblawey, M. Nasser, A. Benamor, R. Bhosale, M. Al-

- Ghouthi, Experimental measurements and modelling of viscosity and density of calcium and potassium chlorides ternary solutions, *Sci. Rep.* 10 (2020) 1–19. <https://doi.org/10.1038/s41598-020-73484-4>.
- [253] A. Dutta, *Fourier Transform Infrared Spectroscopy*, in: *Spectrosc. Methods Nanomater. Charact.*, Elsevier Inc., 2017: pp. 73–93. <https://doi.org/10.1016/B978-0-323-46140-5.00004-2>.
- [254] E.A. López-Maldonado, M.T. Oropeza-Guzman, J.L. Jurado-Baizaval, A. Ochoa-Terán, Coagulation-flocculation mechanisms in wastewater treatment plants through zeta potential measurements, *J. Hazard. Mater.* 279 (2014) 1–10. <https://doi.org/10.1016/j.jhazmat.2014.06.025>.
- [255] Elsevier and Shanghai Jiao Tong University Press Aerospace Series, B. Wu, Chapter 2 - Technical Background, in: *Reliab. Anal. Dyn. Syst.* Shanghai Jiao Tong Univ. Press Aerosp. Ser., 2013: pp. 25–41. <https://doi.org/10.1016/B978-0-12-407711-9.00002-9>.
- [256] A.L. Ahmad, S.S. Wong, T.T. Teng, A. Zuhairi, Optimization of coagulation-flocculation process for pulp and paper mill effluent by response surface methodological analysis, *J. Hazard. Mater.* 145 (2007) 162–168. <https://doi.org/10.1016/j.jhazmat.2006.11.008>.
- [257] J.P. Wang, Y.Z. Chen, X.W. Ge, H.Q. Yu, Optimization of coagulation-flocculation process for a paper-recycling wastewater treatment using response surface methodology, *Colloids Surfaces A Physicochem. Eng. Asp.* 302 (2007) 204–210. <https://doi.org/10.1016/j.colsurfa.2007.02.023>.
- [258] S. Ghafari, H.A. Aziz, M.H. Isa, A.A. Zinatizadeh, Application of response surface methodology (RSM) to optimize coagulation-flocculation treatment of leachate using poly-aluminum chloride (PAC) and alum, *J. Hazard. Mater.* 163

- (2009) 650–656. <https://doi.org/10.1016/j.jhazmat.2008.07.090>.
- [259] S.C. Kim, Application of response surface method as an experimental design to optimize coagulation-flocculation process for pre-treating paper wastewater, *J. Ind. Eng. Chem.* 38 (2016) 93–102. <https://doi.org/10.1016/j.jiec.2016.04.010>.
- [260] M. Scholz, Review of recent trends in Capillary Suction Time (CST) dewaterability testing research, *Ind. Eng. Chem. Res.* 44 (2005) 8157–8163. <https://doi.org/10.1021/ie058011u>.
- [261] G. Degam, Deep Eutectic Solvents Synthesis , Characterization and Applications in Pretreatment of Lignocellulosic Biomass, Theses Diss. (2017) 195. 1156.
- [262] N. Delgado-Mellado, M. Larriba, P. Navarro, V. Rigual, M. Ayuso, J. García, F. Rodríguez, Thermal stability of choline chloride deep eutectic solvents by TGA/FTIR-ATR analysis, *J. Mol. Liq.* 260 (2018) 37–43. <https://doi.org/10.1016/j.molliq.2018.03.076>.
- [263] S. Zullaikah, O. Rachmaniah, A.T. Utomo, H. Niawanti, Y.H. Ju, Green Separation of Bioactive Natural Products Using Liquefied Mixture of Solids, *Green Chem.* (2018). <https://doi.org/10.5772/intechopen.71755>.
- [264] Y. Dai, G.J. Witkamp, R. Verpoorte, Y.H. Choi, Tailoring properties of natural deep eutectic solvents with water to facilitate their applications, *Food Chem.* 187 (2015) 14–19. <https://doi.org/10.1016/j.foodchem.2015.03.123>.
- [265] J. Xu, C.L. Toh, X. Liu, S. Wang, C. He, X. Lu, Synthesis and self-assembly of donor - Spacer - Acceptor molecules. Liquid crystals formed by single-component “complexes” via Intermolecular hydrogen-bonding interaction, *Macromolecules.* 38 (2005) 1684–1690. <https://doi.org/10.1021/ma0479991>.
- [266] M. Francisco, A. Van Den Bruinhorst, M.C. Kroon, Low-transition-temperature mixtures (LTTMs): A new generation of designer solvents, *Angew. Chemie -*



- Int. Ed. 52 (2013) 3074–3085. <https://doi.org/10.1002/anie.201207548>.
- [267] S.Y. Soifer, Irrigation water quality requirements, *Water Int.* 12 (1987) 15–18. <https://doi.org/10.1080/02508068708686548>.
- [268] C. D’Agostino, L.F. Gladden, M.D. Mantle, A.P. Abbott, E.I. Ahmed, A.Y.M. Al-Murshedi, R.C. Harris, Molecular and ionic diffusion in aqueous-deep eutectic solvent mixtures: Probing inter-molecular interactions using PFG NMR, *Phys. Chem. Chem. Phys.* 17 (2015) 15297–15304. <https://doi.org/10.1039/c5cp01493j>.
- [269] O.S. Hammond, D.T. Bowron, K.J. Edler, The Effect of Water upon Deep Eutectic Solvent Nanostructure: An Unusual Transition from Ionic Mixture to Aqueous Solution, *Angew. Chemie.* 129 (2017) 9914–9917. <https://doi.org/10.1002/ange.201702486>.
- [270] L.A.L.I. Shah, INDUSTRIAL APPLICATION SUITABILITY OF INDIGENOUS BENTONITE CLAY IN, (2013).
- [271] H. Abdul Aziz, S. Syed Zainal, M. Alazaiza, Optimization of Coagulation-Flocculation Process of Landfill Leachate by Tin (IV) Chloride Using Response Surface Methodology, *Avicenna J. Environ. Heal. Eng.* 6 (2019) 1–8. <https://doi.org/10.15171/ajehe.2019.01>.
- [272] R.R. Barton, Responce Surface Methodology, 2013. <https://doi.org/10.1007/978-1-4419-1153-7>.
- [273] Y. Wang, K. Chen, L. Mo, J. Li, J. Xu, Optimization of coagulation-flocculation process for papermaking-reconstituted tobacco slice wastewater treatment using response surface methodology, *J. Ind. Eng. Chem.* 20 (2014) 391–396. <https://doi.org/10.1016/j.jiec.2013.04.033>.
- [274] S. Sadri Moghaddam, M.R. Alavi Moghaddam, M. Arami,

- Coagulation/flocculation process for dye removal using sludge from water treatment plant: Optimization through response surface methodology, *J. Hazard. Mater.* 175 (2010) 651–657. <https://doi.org/10.1016/j.jhazmat.2009.10.058>.
- [275] M.A.M. Al-Alwani, N.A. Ludin, A.B. Mohamad, A.A.H. Kadhum, M.M. Baabbad, K. Sopian, Optimization of dye extraction from *Cordyline fruticosa* via response surface methodology to produce a natural sensitizer for dye-sensitized solar cells, *Results Phys.* 6 (2016) 520–529. <https://doi.org/10.1016/j.rinp.2016.08.013>.
- [276] M. Sinaei Nobandegani, M.R. Sardashti Birjandi, T. Darbandi, M.M. Khalilipour, F. Shahraki, D. Mohebbi-Kalhari, An industrial Steam Methane Reformer optimization using response surface methodology, *J. Nat. Gas Sci. Eng.* 36 (2016) 540–549. <https://doi.org/10.1016/j.jngse.2016.10.031>.
- [277] K. Folens, S. Huysman, S. Van Hulle, G. Du Laing, Chemical and economic optimization of the coagulation-flocculation process for silver removal and recovery from industrial wastewater, *Sep. Purif. Technol.* 179 (2017) 145–151. <https://doi.org/10.1016/j.seppur.2017.02.013>.
- [278] J.P. Wang, Y.Z. Chen, Y. Wang, S.J. Yuan, H.Q. Yu, Optimization of the coagulation-flocculation process for pulp mill wastewater treatment using a combination of uniform design and response surface methodology, *Water Res.* 45 (2011) 5633–5640. <https://doi.org/10.1016/j.watres.2011.08.023>.
- [279] R.L. Mason, R.F. Gunst, J.L. Hess, *Statistical Design and Analysis of Experiments: With Applications to Engineering and Science*, Second, New York, 2003.
- [280] M.R. Shah, M. Imran, S. Ullah, Liposomes, in: *Lipid-Based Nanocarriers Drug Deliv. Diagnosis*, 2017: pp. 63–110. <https://doi.org/10.1016/B978-0-323-52729->

3.00003-2.